

Copyright
by
Apostolos Drolias
2007

**Experiments on Link-to-Column Connections in Steel Eccentrically
Braced Frames**

by

Apostolos Drolias, DCE

Thesis

Presented to the Faculty of the Graduate School of

The University of Texas at Austin

in Partial Fulfillment

of the Requirements

for the Degree of

Master of Science in Engineering

The University of Texas at Austin

August 2007

**Experiments on Link-to-Column Connections in Steel Eccentrically
Braced Frames**

**Approved by
Supervising Committee:**

Michael D. Engelhardt

Karl H. Frank

Dedication

To my family and my friends

Acknowledgements

I would like to express my gratitude to Dr. Michael Engelhardt for his guidance and support throughout my graduate career, especially during this research project. I am thankful to Eric Schell for his invaluable assistance throughout the construction and testing of the specimens, and for using the data acquisition system during all experiments. Also, I am thankful to Dr. Taichiro Okazaki for conducting the first two experiments of this research, and for providing many reports and data necessary for the completion of this project.

I am grateful to David Braley, welder of the Facilities Services of the University of Texas at Austin, for fabricating great part of the specimens tested in this project. Also, I would like to thank the staff at Ferguson Structural Engineering Laboratory, in particular Dennis Phillip, Blake Stasney, and Gregory Harris for their great assistance in completing my work.

Finally, I would like to thank all my friends and especially Akshay Prabhakar and Chanseok Jeong for their great support and friendship throughout my graduate studies.

This thesis is dedicated to my parents, Ioannis and Theodora Drolas, and my sister, Maria Drolas, for their unconditional love and support.

August 2007

Abstract

Experiments on Link-to-Column Connections in Steel Eccentrically Braced Frames

Apostolos Drolias, MSE

The University of Texas at Austin, 2007

Supervisor: Michael D. Engelhardt

This thesis describes the results of an experimental project on the seismic performance of link-to-column connections in steel eccentrically braced frames (EBFs). Previous research in this area has highlighted the very large force and deformation demands on link-to-column connections and the difficulty in identifying economical and practical details that can provide satisfactory performance. Therefore, the main objective of this experimental project, which has built upon recent work in this area by others, was to conduct pilot tests on two proposed link-to-column connection details to evaluate their potential to satisfy the connection performance requirements of the 2005 AISC *Seismic Provisions*. A total of eight specimens were tested in this program. In the first link-to-column connection detail, the link was welded to the face of the column using either double-sided fillet welds, or a combination of PJP groove welds and fillet welds. This

detail is envisioned to be most appropriate as a shop welded link-to-column connection. The second detail was constructed with reinforcement, in the form of two supplemental stiffeners in the first panel of the link adjacent to the column. This detail is expected to be suitable for field welding, and was developed in a joint study with Hong and Uang (2005, 2006) at the University of California at San Diego (UCSD). The results from both the experimental program and the analytical studies conducted at UCSD identified these two link-to-column connections as very promising details. Both details showed the potential for outstanding performance, with the capability of developing the link's full plastic rotation capacity without connection failure, and the capability of satisfying the link-to-column connection performance requirements of the 2005 AISC *Seismic Provisions*. Despite the fact that only a small number of tests were conducted in this pilot program, the excellent performance of the connections in these tests justifies further work on these details. Additional analytical and large-scale experimental studies are recommended to further confirm the performance of these connections, identify appropriate limits of application for these details, and to further refine the preliminary design approaches that have been developed for these connections.

Table of Contents

List of Tables	xi
List of Figures	xi
CHAPTER 1 INTRODUCTION.....	1
1.1 General.....	1
1.2 Background on EBFs	2
1.3 Background on Link-To-Column Connections	10
1.3.1 General.....	10
1.3.2 Differences of link-to-column connections in EBFs and beam-to-column connections in MRFs	11
1.4 Previous Research on Link-To-Column Connections	11
1.4.1 Pre-Northridge research on link-to-column connections.....	11
1.4.2 Post-Northridge research on link-to-column connections	12
1.5 Research Motivation.....	15
1.6 Research Objectives.....	16
CHAPTER 2 EXPERIMENTAL SETUP AND TEST SPECIMENS.....	17
2.1 Introduction.....	17
2.2 Test Setup.....	17
2.1.1 Loading System	18
2.1.2 Lateral Bracing System.....	21
2.3 Test Specimens	23

2.3.1 General.....	23
2.3.2 Connection Concept Development	27
2.3.2.1 Phase I.....	27
2.3.2.2 Phase II.....	28
2.3.3 Section Dimensions & Material Properties.....	28
2.3.3.1 Tensile Coupon Tests.....	31
2.3.4 Test Specimen Parameters and Details.....	36
2.3.4.1 Phase I (Specimens AISC-1 to AISC-4).....	36
2.3.4.2 Phase II (Specimens AISC-5 to AISC-8).....	48
2.4 Instrumentation	72
2.5 Test procedure.....	73
2.5.1 Loading Protocol.....	73
2.5.2 Data Reduction Procedure	75
CHAPTER 3 TEST RESULTS.....	79
3.1 General.....	79
3.2 Link Response Parameters.....	79
3.3 Description of Test Specimen Performance	80
3.3.1 Specimen AISC-1	80
3.3.2 Specimen AISC-2	82
3.3.3 Specimen AISC-3	84
3.3.4 Specimen AISC-4	85
3.3.5 Specimen AISC-5	86
3.3.6 Specimen AISC-6	88

3.3.7 Specimen AISC-7	90
3.3.8 Specimen AISC-8	92
3.4 Summary and Discussion of Test Results.....	94
CHAPTER 4 ADDITIONAL EXPERIMENTAL DATA.....	130
4.1 General.....	130
4.2 Link Overstrength Data.....	130
4.3 Link End Moments	137
CHAPTER 5 SUMMARY AND CONCLUSIONS.....	146
5.1 Summary	146
5.2 Results and Conclusions	148
APPENDIX A WELDING/FABRICATION SEQUENCE AND WELDING PROCEDURES.....	152
A.1 General.....	152
A.2 Specified Procedures.....	152
REFERENCES.....	178
VITA.....	181

List of Tables

Table 2.1: Dimensions of link and column sections	30
Table 2.2: Nominal Cross-Section Properties.....	30
Table 2.3: Calculated Cross-section Properties based on Measured Yield Stresses and Dimensions.....	31
Table 2.4: Tensile coupon data for W10x68 (Arce 2002)	32
Table 2.5: Average yield stresses used for W10x68.....	33
Table 2.6: Tensile coupon data for W18x40 (Okazaki 2004).....	35
Table 2.7: Average yield stresses used for W18x40.....	35
Table 2.8: Link Sections used for test specimens (Phase I).....	39
Table 2.9: Specimen connection and welding details (Phase I).....	39
Table 2.10: Link Sections used for test specimens (Phase II)	51
Table 2.11: Specimen connection and welding details (Phase II)	52
Table 2.12: AISC Seismic Loading Protocol.....	74
Table 3.1: Summary of Test Results (Phase I)	98
Table 3.2: Summary of Test Results (Phase II)	99
Table 4.1: Overstrength Factors for Specimens of Phase I.....	135
Table 4.2: Overstrength Factors for Specimens of Phase II	136

List of Figures

Figure 1.1: Typical bracing arrangements for EBFs.....	3
Figure 1.2: Typical force distribution in EBFs (Okazaki 2004)	4
Figure 1.3: Free body diagram of the link (Okazaki 2004)	4
Figure 1.4: Link rotation angle (<i>Seismic Provisions</i>)	8
Figure 1.5: Link Inelastic Rotation Requirements	9
Figure 2.1: Loading system details (dimensions in inches).....	19
Figure 2.2: Link force distributions (Okazaki 2004)	20
Figure 2.3: Lateral Bracing System (Galvez 2004)	22
Figure 2.4: Concept of “Column-Tree” Link-to-Column Connection Detail (Phase I)	26
Figure 2.5: Concept of the “Reinforced” Link-to-Column Connection Detail (Phase II).....	27
Figure 2.6: Location of tensile coupon tests for W10x68 (a = 1-3/8 inches) (Arce 2002)	32
Figure 2.7: Location of tensile coupon tests for W18x40 (Okazaki 2004).....	34
Figure 2.8: Specimens AISC 1 to 3 – Overall Layout	41
Figure 2.9: Specimens AISC 1 and 2 – Connection Detail.....	41
Figure 2.10: Specimen AISC 3 – Connection Detail.....	42
Figure 2.11: Overall details of specimens AISC 1 to 3	42
Figure 2.12: Link-to-Column connection detail for Specimens AISC 1 to 3	43
Figure 2.13: Link top flange welding detail for Specimens AISC 1 to 3	43
Figure 2.14: Fillet welds of the link flange and web to the column flange in AISC-1	44

Figure 2.15: Fillet weld between link flange and column flange in Specimen AISC-2	44
Figure 2.16: Fillet weld between link top flange and column flange in specimen AISC-2	45
Figure 2.17: Specimen AISC-4 – Overall Layout	45
Figure 2.18: Specimen AISC-4 – Connection Detail.....	46
Figure 2.19: Specimen AISC-4 – Link End Preparations and Welds.....	46
Figure 2.20: Overall Layout - Specimen AISC-4	47
Figure 2.21: Partial penetration groove weld of the link top flange – Specimen AISC-4	47
Figure 2.22: Fillet welds of the link web and the inside face of the flanges – Specimen AISC-4	48
Figure 2.23: Supplemental Stiffener’s Configuration (Hong, Uang; 2006)	53
Figure 2.24: Shear Force and Moment Diagrams for Specimen AISC-5	54
Figure 2.25: Shear Force and Moment Diagrams for Specimen AISC-6.....	56
Figure 2.26: Specimen AISC-5 – Overall Layout	62
Figure 2.27: Specimen AISC-8 – Overall Layout	62
Figure 2.28: Specimens AISC-5 & 8 – Connection Details	63
Figure 2.29: Specimens AISC-5 & 8 – Secondary Stiffener Detail	63
Figure 2.30: Overall View of Specimen AISC-5 after Completion of Fabrication.....	64
Figure 2.31: Specimen AISC-5 – Link-to-Column Connection Region – Frontside of Link.....	64
Figure 2.32: Specimen AISC-5 after Completion of Fabrication – Backside of Link	65

Figure 2.33: Overall View of Specimen AISC-8 after Completion of Fabrication.....	65
Figure 2.34: Specimen AISC-8 – Link-to-Column Connection Region – Frontside of Link.....	66
Figure 2.35: Specimen AISC-8 after Completion of Fabrication – Backside of Link.....	66
Figure 2.36: Specimen AISC-6 – Overall Layout	67
Figure 2.37: Specimen AISC-7 – Overall Layout	67
Figure 2.38: Specimens AISC-6 & 7 – Connection Details	68
Figure 2.39: Specimens AISC-6 & 7 – Secondary Stiffener Detail	68
Figure 2.40: Overall View of Specimen AISC-6 after Completion of Fabrication.....	69
Figure 2.41: Specimen AISC-6 – Link-to-Column Connection Region – Frontside of Link.....	69
Figure 2.42: Specimen AISC-6 after Completion of Fabrication – Backside of Link.....	70
Figure 2.43: Overall View of Specimen AISC-7 after Completion of Fabrication.....	70
Figure 2.44: Specimen AISC-7 – Link-to-Column Connection Region – Frontside of Link.....	71
Figure 2.45: Specimen AISC-7 after Completion of Fabrication – Backside of Link.....	71
Figure 2.46: Transducers to monitor link deformation (Okazaki; 2004).....	73
Figure 2.47: 2005 AISC Loading Protocol.....	75

Figure 2.48: Measured reactions and movement of reaction rods (Okazaki; 2004)	76
Figure 2.49: Data for the Link Deformation and Rotation (Okazaki; 2004)	78
Figure 3.1: Link Shear vs. Total Rotation for Specimen AISC-1.....	100
Figure 3.2: Link Shear vs. Inelastic Rotation for Specimen AISC-1.....	100
Figure 3.3: Failure of Specimen AISC-1	101
Figure 3.4: Link Flange Fracture in Specimen AISC-1	101
Figure 3.5: Extension of link flange fracture to the link web – AISC-1.....	102
Figure 3.6: Link Shear vs. Total Rotation for Specimen AISC-2.....	102
Figure 3.7: Link Shear vs. Inelastic Rotation for Specimen AISC-2.....	103
Figure 3.8: Link Flange Fracture in Specimen AISC-2.....	103
Figure 3.9: Link Shear vs. Total Rotation for Specimen AISC-3.....	104
Figure 3.10: Link Shear vs. Inelastic Rotation for Specimen AISC-3.....	104
Figure 3.11: Failure of Specimen AISC-3 during loading cycle at $\gamma = + 0.11$ rad	105
Figure 3.12: AISC-3 – Fracture of the Bottom Link Flange during loading cycle at $\gamma = - 0.09$ rad	105
Figure 3.13: AISC-3 – Fracture of the Top Link Flange during loading cycle at $\gamma = + 0.11$ rad	106
Figure 3.14: Link Shear vs. Total Rotation for Specimen AISC-4.....	106
Figure 3.15: Link Shear vs. Inelastic Rotation for Specimen AISC-4.....	107
Figure 3.16: Specimen AISC-4 after Loading Cycle at $\gamma = \pm 0.11$ rad (Last full loading cycle prior failure).....	107
Figure 3.17: Specimen AISC-4 – Web Cracks adjacent to stiffener welds after loading cycle at $\gamma = \pm 0.11$ rad.....	108

Figure 3.18: Fracture of Link Web adjacent to stiffener's weld during loading cycle of $\gamma = + 0.13$ rad	108
Figure 3.19: Failure of Specimen AISC-4 during loading cycle of $\gamma = + 0.13$ rad	109
Figure 3.20: Link Shear vs. Total Rotation (rotation based on $e_{total} = 38.6''$) – AISC-5	109
Figure 3.21: Link Shear vs. Inelastic Rotation (rotation based on $e_{total} = 38.6''$) – AISC-5	110
Figure 3.22: Link Shear vs. Total Rotation (rotation based on $e_{active} = 33.1''$) – AISC-5	110
Figure 3.23: Link Shear vs. Inelastic Rotation (rotation based on $e_{active} = 33.1''$) – AISC-5	111
Figure 3.24: Specimen AISC-5 prior to Testing and Whitewash	111
Figure 3.25: Specimen AISC-5 after First Loading Cycle at $\gamma = + 0.11 / -0.13$ rad (Last full loading cycle prior failure).....	112
Figure 3.26: Yielding restricted primarily away from the link-to-column connection (Last full loading cycle prior to failure).....	112
Figure 3.27: Failure of Specimen during 2 nd Loading Cycle at $\gamma = + 0.11 / - 0.13$ rad (Failure by fracture of the link web at the termination of the stiff. weld)	113
Figure 3.28: Specimen AISC-5 – Fracture of the Link Web	113
Figure 3.29: Link Shear vs. Total Rotation (rotation based on $e_{total} = 38.6''$) – AISC-6	114
Figure 3.30: Link Shear vs. Inelastic Rotation (rotation based on $e_{total} = 38.6''$) – AISC-6	114

Figure 3.31: Link Shear vs. Total Rotation (rotation based on $e_{active} = 33.4''$) – AISC-6	115
Figure 3.32: Link Shear vs. Inelastic Rotation (rotation based on $e_{active} = 33.4''$)– AISC-6	115
Figure 3.33: Specimen AISC-6 prior to Testing and Whitewash	116
Figure 3.34: Specimen AISC-6 – Link-to-Column Connection	116
Figure 3.35: Specimen AISC-6 after First Loading Cycle of $\gamma = + 0.12 / - 0.13$ rad (Last full loading cycle prior to failure).....	117
Figure 3.36: Specimen AISC-6 – Yielding confined in the Unreinforced portion (Last full loading cycle prior to failure).....	117
Figure 3.37: Failure of Specimen AISC-6 during 2 nd loading cycle of $\gamma = + 0.12 / - 0.13$ rad (Failure by fracture of the link web adjacent to vertical stiffener).....	118
Figure 3.38: Link Shear vs. Total Rotation (rotation based on $e_{total} = 38.6''$) – AISC-7	118
Figure 3.39: Link Shear vs. Inelastic Rotation (rotation based on $e_{total} = 38.6''$) – AISC-7	119
Figure 3.40: Link Shear vs. Total Rotation (rotation based on $e_{active} = 33.4''$) – AISC-7	119
Figure 3.41: Link Shear vs. Inelastic Rotation (rotation based on $e_{active} = 33.4''$)– AISC-7	120
Figure 3.42: Specimen AISC-7 prior to Testing.....	120
Figure 3.43: Specimen AISC-7 after loading cycle of $\gamma = \pm 0.11$ rad (Last full loading cycle prior to failure).....	121

Figure 3.44: Link Bottom Flange at the Link-to-Column Connection after cycle of $\gamma = \pm 0.11$ rad (Last full loading cycle prior to failure).....	121
Figure 3.45: Cracks at the termination of the fillet welds of the two vertical stiffeners furthest from the connection (Last full loading cycle prior to failure).....	122
Figure 3.46: Failure of Specimen AISC-7 during Loading Cycle of $\gamma = + 0.12 / -0.13$ rad (Failure by Fracture of Link Web adjacent to middle vertical stiffener).....	122
Figure 3.47: Yielding restricted primarily in the unreinforced portion of the Link after Failure of Specimen AISC-7 during Loading Cycle of $\gamma = + 0.12/-0.13$ rad	123
Figure 3.48: No apparent distress in the Link-to-Column Connection after Failure of Specimen AISC-7 during Loading Cycle of $\gamma = + 0.12 / - 0.13$ rad	123
Figure 3.49: Link Shear vs. Total Rotation (rotation based on $e_{total} = 38.6''$) – AISC-8	124
Figure 3.50: Link Shear vs. Inelastic Rotation (rotation based on $e_{total} = 38.6''$) – AISC-8	124
Figure 3.51: Link Shear vs. Total Rotation (rotation based on $e_{active} = 33.1''$) – AISC-8	125
Figure 3.52: Link Shear vs. Inelastic Rotation (rotation based on $e_{active} = 33.1''$)– AISC-8	125
Figure 3.53: Specimen prior to Whitewash and Testing.....	126
Figure 3.54: Specimen AISC-8 after Loading Cycle of $\gamma = \pm 0.07$ rad (Last full loading cycle prior to failure).....	126

Figure 3.55: AISC-8 Link Bottom Flange at the Link-to-Column Connection after Loading Cycle of $\gamma = \pm 0.07$ rad (Last full loading cycle prior to failure).....	127
Figure 3.56: Failure of Specimen AISC-8 during Loading Cycle of $\gamma = \pm 0.09$ rad (Failure by Fracture of Link Bottom Flange)	127
Figure 3.57: Link-to-Column Connection after Failure of Specimen AISC-8 during Loading Cycle of $\gamma = \pm 0.09$ rad	128
Figure 3.58: Link-to-Column Connection after Failure of Specimen AISC-8 during Loading Cycle of $\gamma = \pm 0.09$ rad (Front View)	128
Figure 3.59: Link-to-Column Connection after Failure of Specimen AISC-8 during Loading Cycle of $\gamma = \pm 0.09$ rad (Back View).....	129
Figure 3.60: Location of Yielding at the Link Flanges after Failure of Specimen AISC-8 during Loading Cycle of $\gamma = \pm 0.09$ rad	129
Figure 4.1: Link end moment relationship of Specimen AISC-1	140
Figure 4.2: Link end moment relationship of Specimen AISC-2	140
Figure 4.3: Link end moment relationship of Specimen AISC-3	141
Figure 4.4: Link end moment relationship of Specimen AISC-4	141
Figure 4.5: Link end moment relationship of Specimen AISC-5	142
Figure 4.6: Link end moment relationship of Specimen AISC-6	142
Figure 4.7: Link end moment relationship of Specimen AISC-7	143
Figure 4.8: Link end moment relationship of Specimen AISC-8	143
Figure 4.9: Active Link end moment relationship of Specimen AISC-5	144
Figure 4.10: Active Link end moment relationship of Specimen AISC-6	144
Figure 4.11: Active Link end moment relationship of Specimen AISC-7	145
Figure 4.12: Active Link end moment relationship of Specimen AISC-8	145

CHAPTER 1

Introduction

1.1 GENERAL

This thesis describes the results of an experimental research program, conducted at the Phil M. Ferguson Structural Engineering Laboratory of the University of Texas at Austin. The research was aimed at developing practical and economical link-to-column connection details for seismic-resistant steel Eccentrically Braced Frames (EBFs) which satisfy the performance requirements of the *2005 AISC Seismic Provisions*.

After the 1994 Northridge and 1995 Kobe Earthquakes, significant damage was observed at welded beam-to-column moment connections in steel moment resisting frames, raising concerns about the performance of welded steel frames in major earthquakes. Prior to the 1994 Northridge Earthquake, link-to-column connections in EBFs were similar to those used in Special Moment Frames (SMF). Thus, link-to-column connections of EBFs are likely to share many of the problems observed in moment frame connections.

Following these two earthquakes, a great deal of research was conducted to study the causes of the connection failures. This research resulted in a significantly improved understanding of moment connection behavior and in recommendations for improved design, detailing and welding practices. This research also resulted in major changes in the building code provisions (AISC 1997, 2002, 2005) for seismic resistant steel moment connections. However, less attention was given to the connection details of EBFs. According to the *2005 AISC Seismic Provisions*, revised connections for moment frames may not necessarily perform adequately when used as an EBF connection since the load

and deformation demands at a link-to-column connection in an EBF are substantially greater than those at a beam-to-column connection in an SMF. Thus, ongoing research is being done in this field, trying to identify suitable link-to-column connections for EBFs.

1.2 BACKGROUND ON EBFs

Eccentrically Braced Frames (EBFs) are a lateral force resisting system that combines high elastic stiffness with significant energy dissipation capability to accommodate large seismic forces. A typical EBF consists of a beam, one or two braces, and columns. Its configuration is similar to traditional braced frames, with the exception that at least one end of each brace must be eccentrically connected to the frame. The eccentric connection introduces bending and shear forces in the beam adjacent to the brace. The short segment of the frame where these forces are concentrated is called a *link*.

EBFs are an alternative to the more conventional Moment-Resisting Frames (MRFs) and the Centrically Braced Frames (CBFs), trying to combine the individual advantages of each. In Figure 1.1 several types of EBFs are presented with the link lengths identified by letter e.

In EBFs, the axial force carried from the diagonal brace is transferred to the column or to another brace through shear and bending of the link. A well designed EBF permits development of large cyclic inelastic deformations. The inelastic action is restricted primarily to the links, which are designed and detailed to be the most ductile elements of the frame (Engelhardt, Popov; 1989b). The ductile behavior of the link permits achieving ductile performance of the structure as a whole.

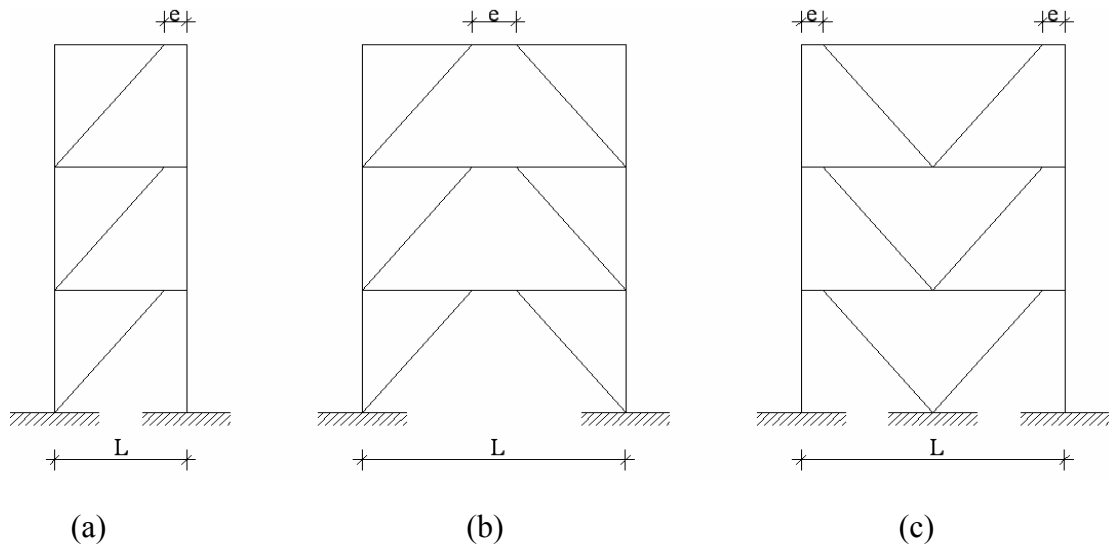


Figure 1.1: Typical bracing arrangements for EBFs

Links in EBFs are designed for code level forces, and then detailed in such a way so that non-ductile failure modes such as local buckling, lateral-torsional buckling, or fracture, will be delayed until adequate inelastic rotations are developed. On the other hand, the diagonal braces, the beam segments outside the links, and the columns are not designed for code level seismic forces, but rather for the maximum forces generated by the fully yielded and strain hardened links (Popov, Engelhardt; 1988). This approach assures that inelasticity occurs primarily within the ductile links elements.

The forces in an EBF link are characterized by a high shear that is constant along its entire length, reverse curvature bending, and a small axial force. On the other hand, the beam segment outside the link as well as the brace, are subjected to high axial forces and bending. The force distribution can be seen in the figure below.

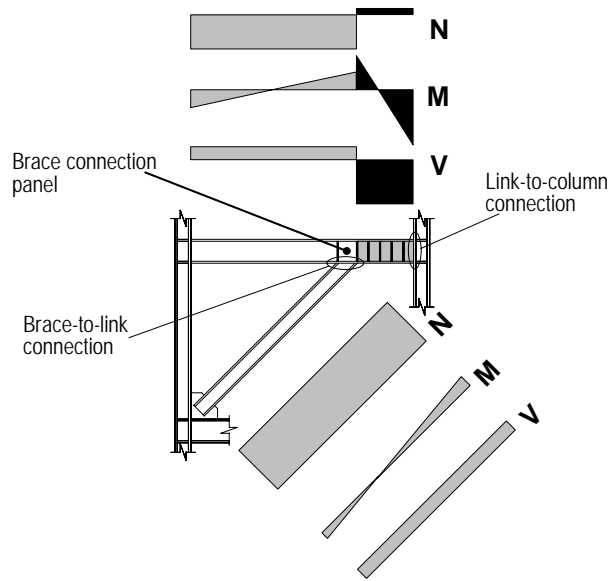


Figure 1.2: Typical force distribution in EBFs (Okazaki 2004)

As can be observed from the above figure, the link-to-column connection is subjected to a combination of significant shear and flexure. Figure 1.3 illustrates further the force distribution of a link. The moments at the beam end and at the column end are expressed as M_B and M_C , respectively, and the constant shear along the link as V . The axial force in the link is omitted since it is usually small.

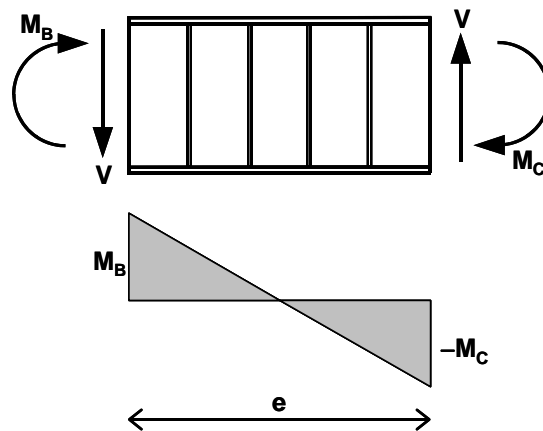


Figure 1.3: Free body diagram of the link (Okazaki 2004)

In the special case where the link end moments are of equal magnitude, $M_B = M_C = M$, applying equilibrium we get that: $V * e = 2 * M$. For this case, if one considers simple plastic theory, that is to say no strain hardening and no M-V interaction, it is simple to derive that a link of length $e = 2 * M_p / V_p$ is the theoretical dividing line between a link that yields in shear and one that yields in flexure. In this equation, M_p and V_p are the fully plastic moment and the fully plastic shear capacity of the section respectively. These two section properties are defined by the following equations:

$$V_p = 0.6F_y(d - 2t_f)t_w \quad (1.1)$$

$$M_p = F_y Z_p \quad (1.2)$$

Where, F_y is the yield strength of the steel, Z_p is the plastic modulus, d the beam depth, t_w is the web thickness and t_f is the flange thickness.

However, experimental results indicate that while the assumption of no M-V interaction is reasonable, an assumption of perfect plasticity is not. That is to say, links can exhibit a high degree of strain hardening. Recent tests on rolled wide-flange links constructed of A992 steel (Arce; 2002) showed strength increases due to strain hardening ranging from 1.2 to 1.45, with an average value of about 1.30. Past tests on rolled wide-flange links constructed of A36 steel have sometimes shown strength increases due to strain hardening in excess of 1.5 (Hjelmstad and Popov; 1983, Engelhardt and Popov; 1989a). Using these past experiments, Kasai and Popov (1986) proposed that, in order to assure shear yielding of the link, the link length must comply with the following limitation:

$$e \leq 1.6 \frac{M_p}{V_p} \quad (1.3)$$

Further, the Seismic Provisions indicate that flexural yielding will dominate the inelastic response if the link length is:

$$e \geq 2.6 \frac{M_p}{V_p} \quad (1.4)$$

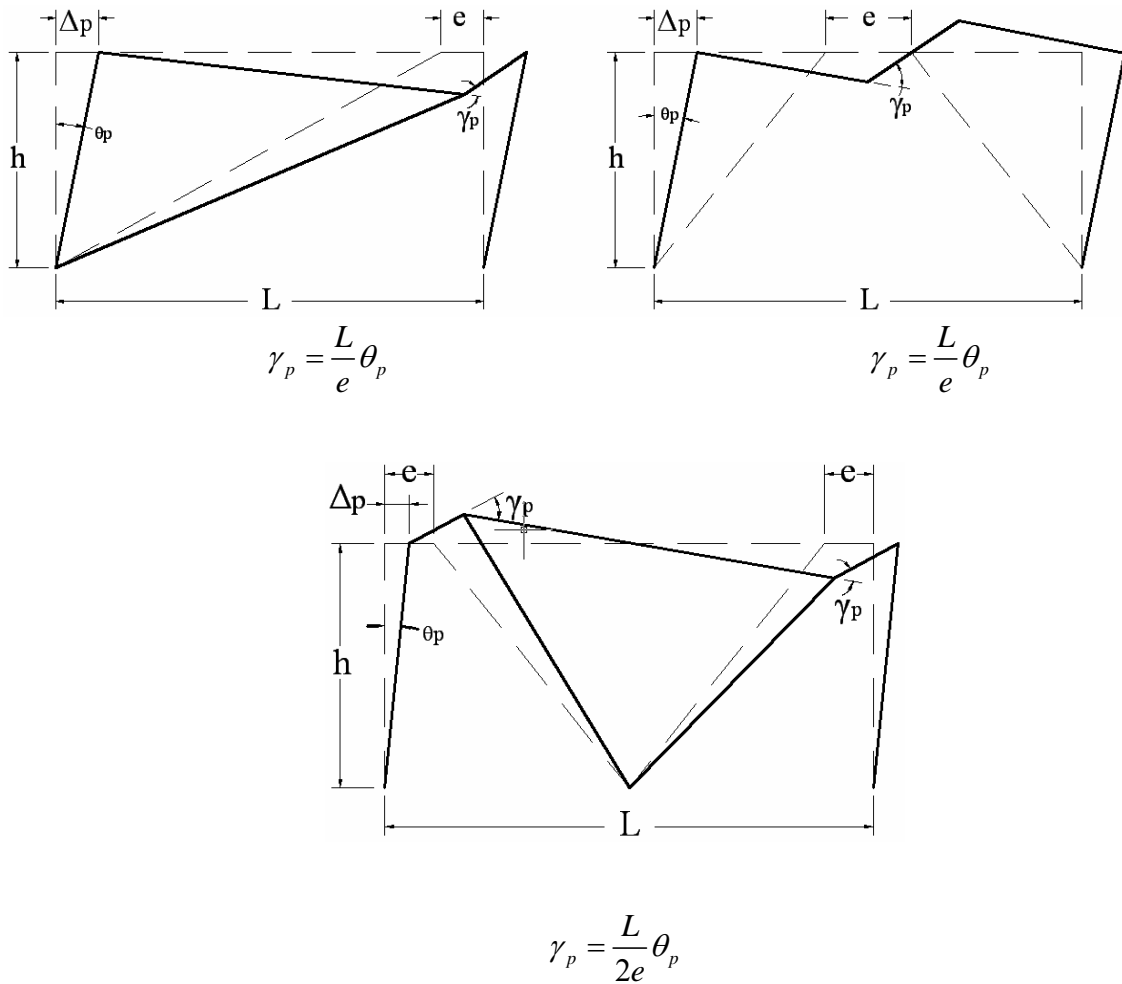
Finally, a combination of shear and flexural yielding will characterize the inelastic response of links with intermediate lengths. That is to say:

$$1.6 \frac{M_p}{V_p} < e < 2.6 \frac{M_p}{V_p} \quad (1.5)$$

The energy dissipation capacity and ultimate failure mechanisms for the first two classes of the links differ substantially. Short links (or shear links) provide for the best overall EBF stiffness, strength and ductility (Engelhardt, Popov; 1989b). The use of long flexural yielding links in EBFs generally result in lower stiffness, strength and ductility, and are therefore less desirable than short shear yielding links from a structural performance point of view. Long links are sometimes used, however, to satisfy architectural requirements for large frame opening to accommodate doors, windows or other architectural features.

For design purposes, inelastic link rotations of links in EBFs need to be estimated in order to quantify the ductility demands on the links. This can be most easily done by constructing Energy Dissipation Mechanisms, or in other words, plastic collapse mechanisms, assuming rigid-plastic behavior of the members. In the *Seismic Provisions*, the link rotation angle is the primary variable used to describe inelastic link deformation. The link plastic rotation angle is the inelastic portion of the rotation angle between the link and the portion of the beam outside the link. According to the *Seismic Provisions*,

the link rotation angle can be estimated by assuming that the EBF bay will deform in a rigid-plastic mechanism as illustrated for different EBF configurations in Figure 1.4. In this figure, the link rotation angle is quantified by the symbol, γ_p . The link rotation angle can be related to the plastic story drift angle, θ_p , using the relationships shown in the Figure 1.4. As it can be seen, this relationship depends on the configuration of the EBF and must be determined from the appropriate mechanism using geometry. Furthermore, the plastic story drift angle can be computed as the plastic story drift, Δ_p , divided by the story height, h .



L = bay width

θ_p = plastic story drift angle (= Δ_p / h)

h = story height

γ_p = link rotation angle

Δ_p = plastic story drift

Figure 1.4: Link rotation angle (*Seismic Provisions*)

The AISC *Seismic Provisions* require links to develop different levels of inelastic rotation depending on their length. The inelastic deformation capacity of links is, generally, greatest for shear yielding links, and smallest for flexural yielding links. Based

on experimental evidence, the link rotation angle is limited to $\gamma_p = 0.08$ radian for shear yielding links ($e \leq 1.6M_p/V_p$) and $\gamma_p = 0.02$ radian for flexural yielding links ($e \geq 2.6M_p/V_p$). For links in the combined shear and flexural yielding range ($1.6M_p/V_p < e < 2.6M_p/V_p$), the limit on link rotation angle is determined according to the link length by linear interpolation between 0.08 and 0.02 radian. The Figure 1.5 depicts, graphically, the link inelastic rotation requirements of the *Seismic Provisions*.

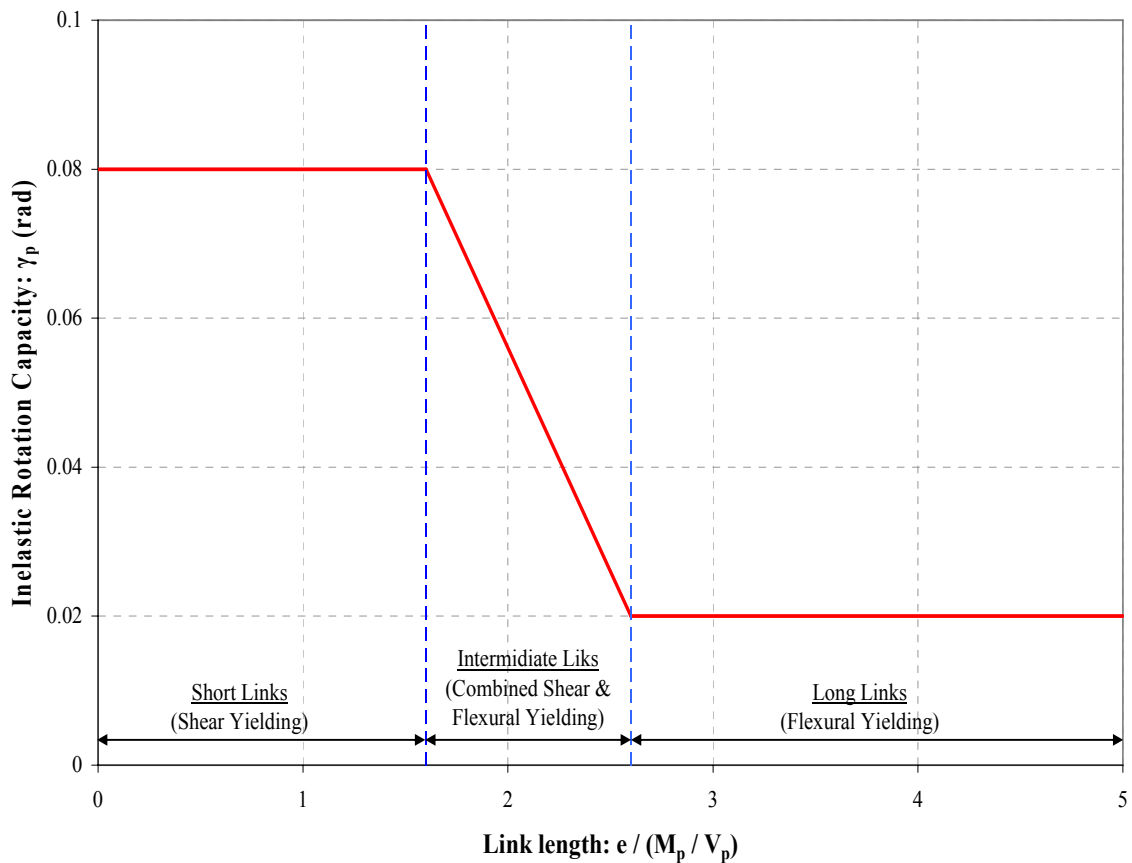


Figure 1.5: Link Inelastic Rotation Requirements

For a satisfactory link-to-column connection, the inelastic link rotation developed prior to connection failure must be greater than the required inelastic link rotation as

stated above. The inelastic link rotation capacity can be defined as the maximum inelastic link rotation amplitude sustained for at least one full cycle of loading prior to link shear force dropping below the nominal shear strength of the link.

1.3 BACKGROUND ON LINK-TO-COLUMN CONNECTIONS

1.3.1 General

In those types of EBFs where at least one end of the link is connected to the column (Fig. 1.1.a and 1.1.c), the link-to-column connection is a vital element affecting the ductile performance of the link, and therefore, the safety and ductile performance of the seismic-resistant EBF.

As mentioned above, the widespread damage in steel moment frames after the two major earthquakes of Northridge (1994) and Kobe (1995) raised a lot of concerns about the link-to-column connections of EBFs constructed prior to 1994 since they were typically designed, detailed and constructed substantially similar to beam-to-column connections in SMFs. In other words, it is strongly believed that many of the same design aspects and construction practices which led to the poor performance of moment frame connections may be present in EBF connections.

However, most of the post-Northridge research concentrated on modification of beam-to-column connections of Moment Frames. As noted earlier, post-Northridge details developed for the connections in moment frames may not necessarily perform adequately when used as a link-to-column connection in an EBF. Thus, the need for experiments of EBF link-to-column connections has risen. The AISC *Seismic Provisions* require that satisfactory performance of link-to-column connections be verified by testing

under a prescribed loading protocol in accordance with Appendix S, or by the use of prequalified link-to-column connections in accordance with Appendix P.

Experiments done to evaluate the pre-Northridge moment connections showed that the use of the low fracture toughness weld metal, as well as the practice of leaving backing bars and weld tabs in place after the completion of the beam flange groove welds, were significant factors contributing to the premature failure of the pre-Northridge moment frame connections (Engelhardt and Sabol; 1997).

1.3.2 Differences of link-to-column connections in EBFs and beam-to-column connections in MRFs

The force and deformation environment at EBF link-to-column connections is significantly different and in some cases more severe than at moment frame connections. Specifically, a shear link-to-column connection must sustain very large shear forces, on the order of $1.5V_p$, and relatively less bending moments, on the order of M_p , which creates a force environment different from that of moment connections in which the column is required to resist very large bending moments and relatively small shear forces. Meanwhile, shear yielding links must sustain very large cyclic inelastic link rotations on the order of 0.08 rad, which are not typically encountered in moment connections. Finally, the large moment gradient along the relatively short length of a shear link is typically much higher than in MRF beams.

1.4 PREVIOUS RESEARCH ON LINK-TO-COLUMN CONNECTIONS

1.4.1 Pre-Northridge research on link-to-column connections

Prior to the 1994 Northridge earthquake, only limited research was done on link-to-column connections for EBFs, leading to several recommendations for the design

practice. The use of welded flange – welded web, instead of the welded flange – bolted web connection was recommended after tests done by Malley and Popov (1984). Evaluating the performance of the welded flange – bolted web detail for links, they observed that the large cyclic shear force developed in EBF links could cause repetitive bolt slippage, which in turn induced sudden failure of the connection by fracture near the link flange groove weld.

The use of EBFs with long (flexural) links ($e > 1.6 M_p/V_p$) attached to columns was recommended to be avoided, based on tests done by Engelhardt and Popov (1989a; 1992). These tests showed that failure of such EBF configurations is controlled by failure of the link flanges near the groove welds at the link-to-column connection. These failures typically occurred prior to the development of any significant inelastic deformation in the link.

The use of link flange – to column web connection was recommended to be avoided based on tests done by Malley and Popov (1983; 1984) The questionable reliability observed in beam-to-column web connections for MRFs (Tsai and Popov; 1988) led to the recommendation by Engelhardt and Popov that the use of link-to-column web connections should be restricted.

1.4.2 Post-Northridge research on link-to-column connections

Research conducted on moment frame connections following the Northridge Earthquake led to a number of improvements in the design and construction practice (FEMA 2000). These included:

- the use of electrodes with designated notch toughness requirement,
- the use of improved weld access hole configurations (recommended by FEMA 2000)

- the use of top beam flange backing bars fillet welded to the column flange and the removal of the bottom backing bar followed by the placement of a supplemental reinforcement fillet weld,
- the removal of weld tabs at both top and bottom flanges

Tsai et al. (2000) conducted some experiments on shear link-to-box column connections in order to investigate the seismic performance of this EBF type connection. Some of the connections tested were constructed using the improvements mentioned above. Unfortunately, none of the specimens managed to develop the inelastic link rotation required in the *2002 AISC Seismic Provisions*. The specimens typically failed by fracture of the link flange near the groove weld. These results raised more concerns about the safety of the link-to-column connections in EBFs since despite the fact that the modifications mentioned above were used, only small improvement in the link rotation was gained.

Richards and Uang (2003) recognized that the loading protocol of the 2002 Seismic Provisions was too severe for shear links requiring too many inelastic loading cycles prior to reaching the required rotation for shear links. After a study conducted by Richards and Uang (2004), a revised protocol was suggested and finally adopted in the 2005 Seismic Provisions. This revised protocol represents the demands of an earthquake ground motion in a more realistic manner.

Next, Okazaki et al (2003; 2004) conducted an extensive series of experimental and analytical studies on link-to-column connections for seismic resistant EBFs. Twelve large-scale link-to-column specimens were constructed from ASTM A992 steel shapes, and tested using the qualifying cyclic test procedure specified in Appendix S of the 2002

AISC Seismic Provisions. The primary test parameters for this investigation were the connection type and the link length.

Three different link lengths, designated as S, I, M, were used in order to represent the three different link categories specified in the *Seismic Provisions* - shear, intermediate, and flexural links, respectively. For each of these three link lengths, a set of four different connection types, designated as PN, MW, FF, NA was used. The PN connection was used in order to simulate the detailing and construction practice in the pre-Northridge era. The MW connection detail was used in order to examine the benefits from the modifications in welding, adopted for the moment frame connections. The FF connection was used to simulate the free flange connection developed by Choi et al. (2000). Finally, the NA connection detail was a recently developed connection in Japan (Suita et al. 1999) based on the concept of eliminating the weld access hole. For a more detailed description of the connection detail configurations, see Okazaki et al. (2006a).

Unfortunately, only one of the twelve specimens sustained the link rotation required in the AISC Seismic Provisions. Moreover, almost all specimens failed by fracture at the link-to-column connection.

Specifically, the three PN specimens achieved no more than half of their required inelastic link rotations, and failed due to fracture of the link flange near the groove weld. As a result, this poor performance suggested that link-to-column connections in EBFs constructed using pre-Northridge practices may not perform as intended.

One of MW specimens, which incorporated welding improvements, achieved only a 20% improvement in inelastic link rotation comparing with the equivalent Pre-Northridge specimen PNS. Furthermore, the other two MW specimens achieved no improvement in inelastic link rotation. Again, all the specimens failed due to fracture of the link flanges near the groove welds. The very useful observation made from these

three specimens was that although the modifications in welding are beneficial, this alone is not sufficient to improve the connection performance to the required level.

The FF specimens sustained significantly greater link rotations compared to the corresponding PN and MW specimens. Moreover, these specimens were successful in preventing or delaying the occurrence of the link flange fracture. Finally, the NA specimens achieved significantly greater link rotations compared to the corresponding PN and MW specimens. The dominant failure mode of this type of connection was fracture of the link flange initiating at the outer edge of the flange, and not at the center portion of the flange as was observed for most other specimens which had a weld access hole. A more detailed description of the specimens and the test results can be found in Okazaki et al. (2006a).

Finally, Okazaki et al. (2005) observed that the loading protocol can have a significant effect on the performance of links in EBFs. Thus, they concluded that the use of the more realistic revised loading protocol, instead of the protocol used for the testing of the specimens mentioned above, may have resulted in a better performance of shear link specimens.

1.5 RESEARCH MOTIVATION

In the Post-Northridge era, the limited research done on Eccentrically Braced Frames has not lead to a satisfactory link-to-column connection. On the other hand, almost all tests done showed poor performance of EBF connections, either by using the Pre-Northridge practice, or by using welding modifications and improved moment frame connections.

As a result of the absence of a satisfactory link-to column connection detail, the 2005 AISC *Seismic Provisions* suggest avoiding EBF configurations with links attached to columns until further research shows a satisfactory link-to-column connection.

1.6 RESEARCH OBJECTIVES

The main objective of this research project is to develop practical and economical link-to-column connection details for Eccentrically Braced Frames (EBFs) that satisfy the performance requirements of the 2005 AISC *Seismic Provisions*.

CHAPTER 2

Experimental Setup and Test Specimens

2.1 INTRODUCTION

This chapter provides a description of the test setup and the test specimens used in the experimental investigation. Furthermore, the instrumentation used is presented and the test procedures are depicted.

First, there is a brief description of the test setup designed and built at the University of Texas at Austin. Second, the eight specimens tested in this project are described. This description includes the connection concept development, the section sizes and material properties, and the connection and welding details. Third, the instrumentation used to gather the data from each specimen is presented. Finally, the test procedure, based on the qualifying cyclic test procedure for link-to-column connections provided in the Appendix S of the 2005 AISC *Seismic Provisions*, is described. This section provides information about the loading protocol and the data collection procedure.

2.2 TEST SETUP

The test setup was designed and built by Okazaki (2004) and Arce (2002) for investigations on the experimental performance of EBFs under seismic loads. It is composed of the loading system and the lateral bracing system.

2.1.1 Loading System

The loading system, shown in Figure 2.1, was designed to reproduce the forces and deformations that will occur in the link of an EBF under lateral load, for EBF configurations with links attached to columns. Such EBF configurations are shown in Figures 1.1 (a) and (c), and have one end of the link connected to the column and the other end connected to a beam and a diagonal brace.

The shaded portion in Figure 2.1 shows the link-to-column connection specimen. This is the only part of the assembly that changes for each experiment. It consists of the link and the column. The link length that can be accommodated by this test setup varies from 25 to 75 inches, so that shear, intermediate, and flexural links can be tested. In this project, two different sections, W18x40 and W10x68, were used as links with a total link length equal to 38.6 inches for all specimens. The vertical column was oriented in such a way to resist in-plane moment by bending about the strong axis. A W12x120 section was used as the column for every experiment.

Outside the link-to-column connection there is a horizontal beam connected to the left end of the link. This beam, a W18x76 section, was designed to remain elastic, and was reinforcing with flange cover plates, a web doubler plate and web stiffeners in the region adjacent to the link. The rest of the test setup consists of four reaction rods each attached to one end of the vertical column or horizontal beam, and a 450-kip hydraulic loading ram, which is located under the column. This ram imposes a vertical cyclic load and displacement to the column.

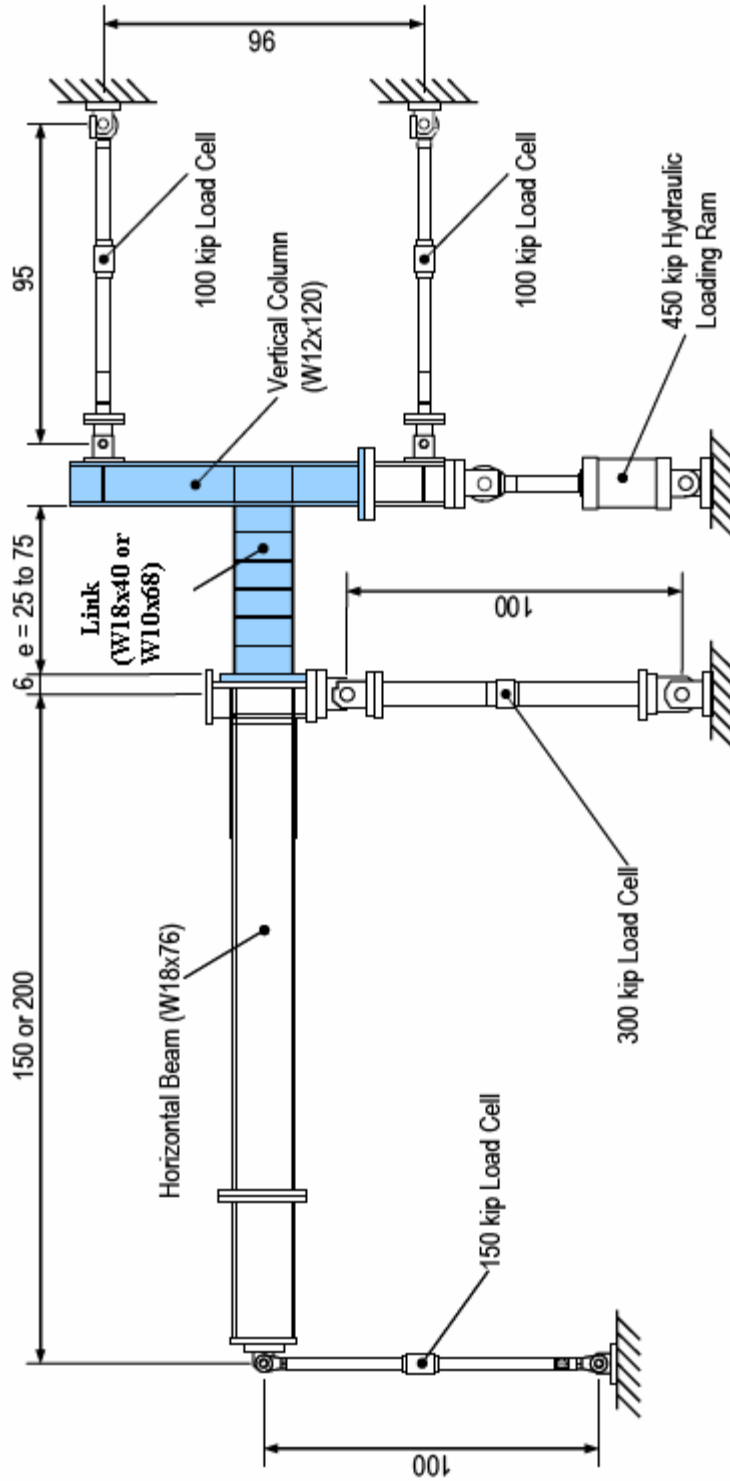


Figure 2.1: Loading System details (dimensions in inches)

In Figure 2.2, the typical force distribution of an ordinary single diagonal EBF arrangement is compared with that of the loading system. As it can be observed, the test setup replicates the actual link forces introduced on an EBF in an accurate manner. Specifically, a link specimen, placed in the test setup, is subjected to constant shear throughout its length and to reverse curvature bending. Typically, in an actual EBF with links attached to the columns, the moment at the column end is greater than at the beam end of the link for elastic response. The test setup was designed to replicate this condition. In addition, the test setup introduces minimal axial force into the link. This is normally also the case in an actual EBF.

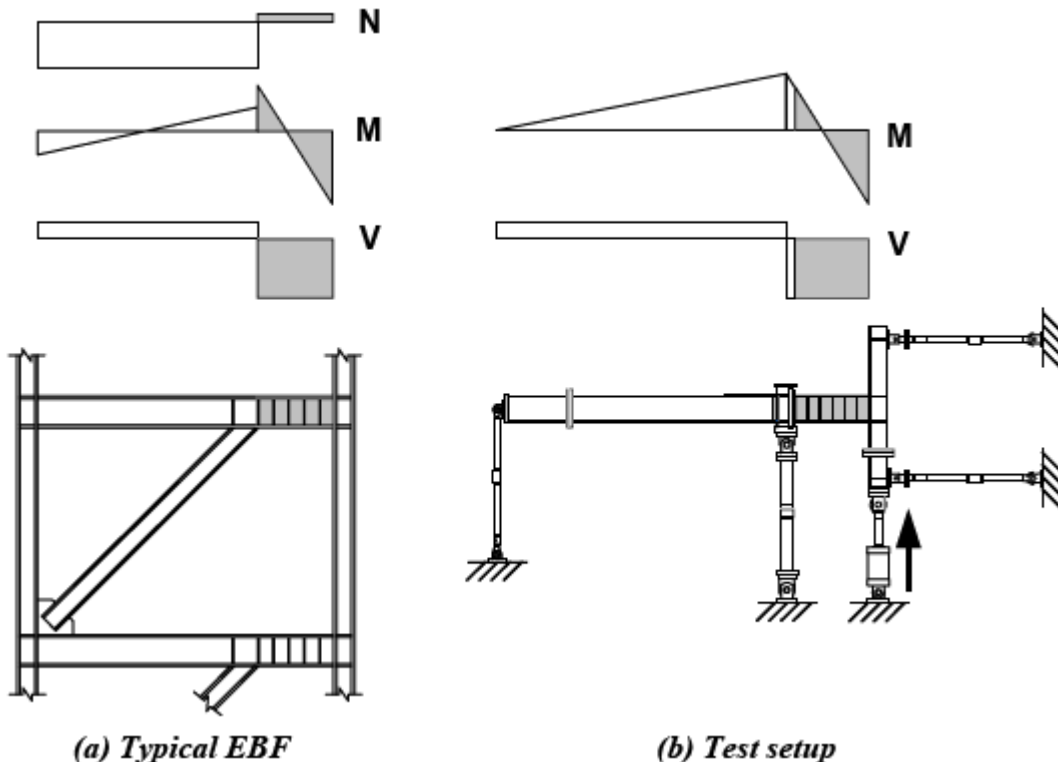


Figure 2.2: Link force distributions (Okazaki 2004)

In addition to replicating the forces expected in the link of an actual EBF, the test setup was also designed to replicate the rigid-plastic energy dissipation mechanism of an EBF, as shown in Figure 1.4. In an actual EBF, the beam outside of the link remains perpendicular to the column, when the frame is deformed as a rigid-plastic mechanism. This condition is also replicated in the test setup.

In the test setup, the left end of the link is welded to a 2" thick plate, which is then bolted to the beam segment. This configuration and welding details were designed to minimize the possibility of a connection failure at the left end of the link, so as to permit study of the link-to-column connection detail at the right end of the link. A description of the connections details at the left end of the link are provided by Okazaki (2004). As shown in Figure 2.2, link rotation can be achieved by quasi-statically displacing the column segment of the test setup, until a target link rotation is achieved, as required by the loading protocol of the *AISC Seismic Provisions*.

2.1.2 Lateral Bracing System

Figure 2.3 depicts the lateral bracing system used to prevent the out-of-plane displacement of the test setup. This lateral support was provided at four points in the frame at locations as shown in the figure. Each of the bracing points was designed in such a way to allow free motion in the plane of the test setup, while limiting the out-of-plane motion. The contact surfaces between the lateral braces and the test frame were coated with Teflon in order to ensure that friction associated with the in-plane displacement will be minimal.

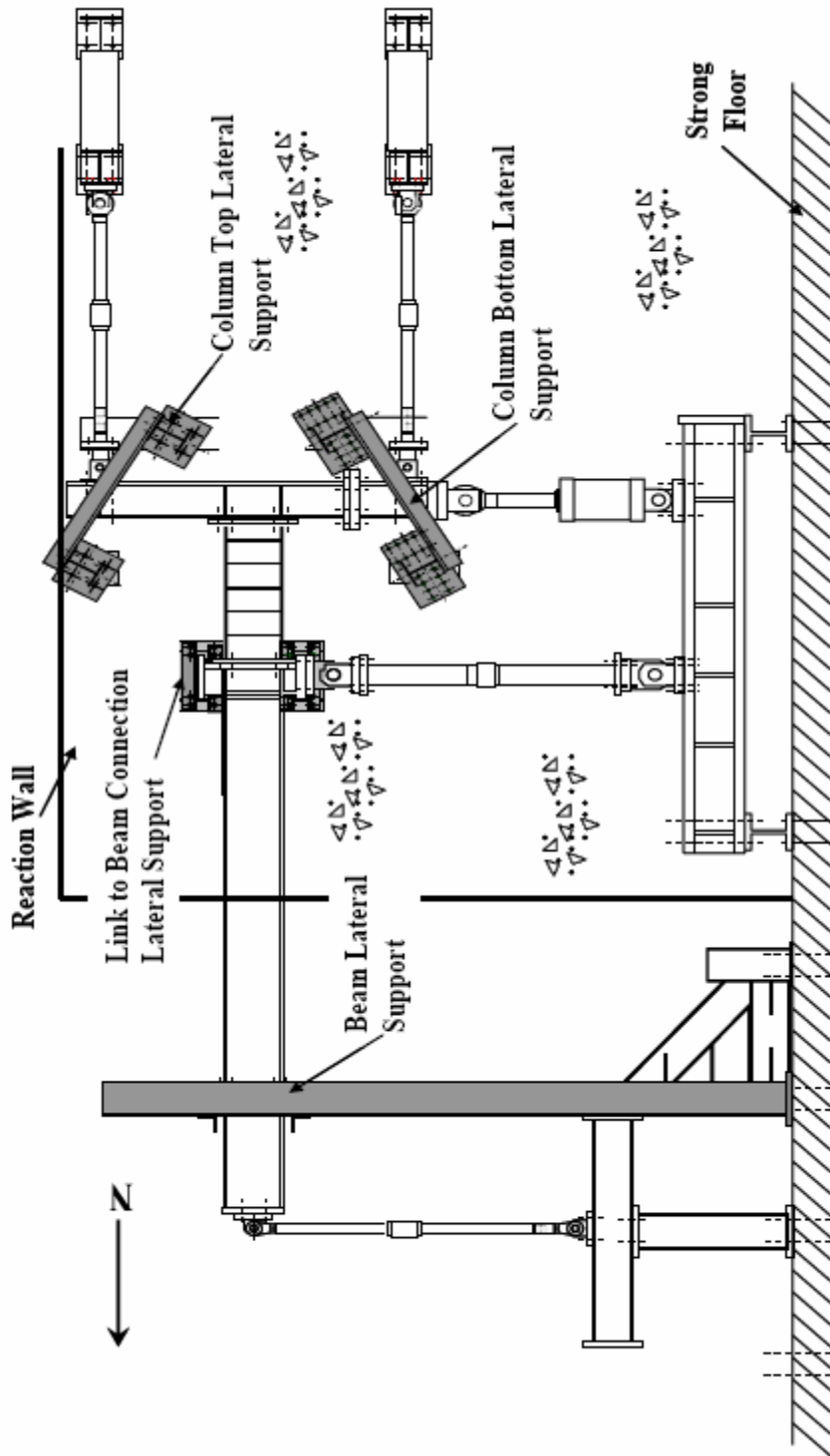


Figure 2.3: Lateral Bracing System (Galvez 2004)

2.3 TEST SPECIMENS

2.3.1 General

A series of eight specimens were tested in this research program to investigate the cyclic loading performance of link-to-column connections. This research project was an extension of a previous project on link-to-column connections conducted by Okazaki (2004) using the same test setup. As described in Chapter 1, Okazaki tested four different link-to-column connection details. One of these details represented pre-Northridge practices for link-to-column connections. The other three details represented attempts at achieving improved performance of link-to-column connections. As discussed in Chapter 1, none of the connection details tested in this previous program showed consistently satisfactory performance. That is, none of the details was able to consistently satisfy the link plastic rotations requirements of the AISC *Seismic Provisions*.

To follow-up on the work of Okazaki (2004), this current test program was conducted to collect experimental data on two new link-to-connection details that were thought to show potential for good cyclic loading performance. The test program was divided into two phases corresponding to the two connection details studied in this program. The two connection details and corresponding test phases are described below.

➤ **Phase I** consisted of four tests on a shop-welded link-to-column connection detail (Column-tree construction). These tests were done by Okazaki, Schell and Engelhardt from November, 2004 until March, 2005. The writer was responsible to summarize all the calculated results.

The fundamental concept of the shop-welded link-to-column connection is illustrated in Figure 2.4. In this connection detail, both the link-to-column connection and a brace stub-to-link connection are shop welded. The brace and beam segment outside the

link are then connected in the field using bolted or welded splices. Furthermore, the link-to-column connection consists simply of double-sided fillet welds on the link flanges and web. Consequently, no weld access holes are needed as in the case with complete joint penetration groove welds. However, because the fillet welds between the link and the face of the column permit little tolerance for fit-up, this connection detail is most likely suitable primarily for shop welding.

Despite the fact that link-to-column connections are normally field welded in US practice, the “column-tree” approach offers some advantages. First of all, both the link-to-column connection and the brace-to-link connection can be constructed in the shop in a single assembly. Moreover, the beam segment outside the link can be made of a different wide flange section than the link. This can be advantageous in satisfying the EBF design requirement that the beam segment outside of the link remain essentially elastic under the forces generated by a fully yielded and strain hardened link. This requirement is often difficult to satisfy when the link and the beam are the same section. On the other hand, the possible difficulty of shipping the column-link assembly to the job site, as well as, the additional cost of the splices in the beam and the brace are the disadvantages of this connection detail.

➤ **Phase II** consisted of four tests on a field-welded link-to-column connection detail. Specifically, in this proposed detail, the link flanges and link web are connected to the column flange using CJP groove welds. The connection is then reinforced with two supplemental stiffeners in the first panel of the link adjacent to the column. One supplemental stiffener is provided on each side of the link, and is placed parallel to the link web. Each supplemental stiffener is welded to the column flange and to the first vertical web stiffener using either CJP groove welds for two of the specimens, and one-sided fillet welds for the other two specimens. The supplemental stiffeners are not

connected to the link flanges. The concept of the reinforced Link-to-Column connection detail is portrayed in Figure 2.5. The Phase II tests were conducted in a joint study with Hong and Uang (2005, 2006) at the University of California at San Diego (UCSD). In the UCSD portion of the study, finite element studies were conducted on this connection detail, to coordinate with the experiments described herein.

In this connection detail, the link flanges and link web are connected to the face of the column using CJP (complete joint penetration) groove welds. The weld access holes for the link flange groove welds are prepared according to the recommendations of FEMA-350, “Recommended Seismic Design Criteria for New Steel Moment-Frame Buildings” (FEMA 2000). The link web is bolted to a shear tab, which is previously welded to the column flange. Thus, the shear tab serves as an erection device and as backing for the CJP groove weld between the link web and the column flange.

In fabricating the Phase II specimens, welding processes, electrodes and welding positions were used for the different stages of the specimen construction to simulate the conditions of actual construction. For the shop welds, the gas-shielded FCAW (flux cored arc welding) welding process was used, while for the field welds the self-shielded FCAW process was selected. These processes are commonly used by structural steel fabricators and erectors for shop and field welding. To further simulate the real connection detail, the field welds were made by putting the specimen in the same position as it would be at the field. As a result, two downhand CJP groove welds, for the link flanges, as well as five vertical CJP groove welds, for the link web and the supplemental stiffeners, were needed. This large number of vertical CJP field welds is one of the disadvantages of this connection detail due to the slower deposition rate for these welds.

The objective of this connection detail is to shift the link plastic hinge away from the face of the column to reduce the large inelastic strain demands at the link flange

groove welds. Thus, the reinforcement of the link-to-column connection with supplemental stiffeners increases the flexural and the shear capacity of the link at the face of the column, forcing the yielding to occur away from the connection. Link yielding is therefore limited primarily to the unreinforced portion of the link, outside the link-to-column connection. The reinforced portion of the link is designed to remain essentially elastic. The design details of this connection were based on finite element studies by Hong and Uang (2005, 2006).

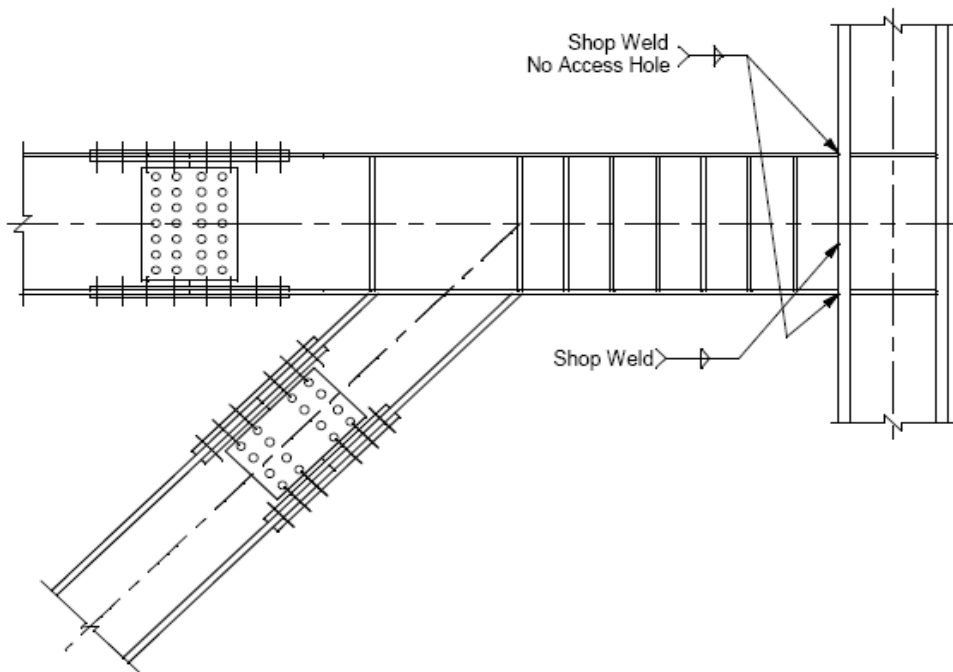


Figure 2.4: Concept of “Column-Tree” Link-to-Column Connection Detail (Phase I)

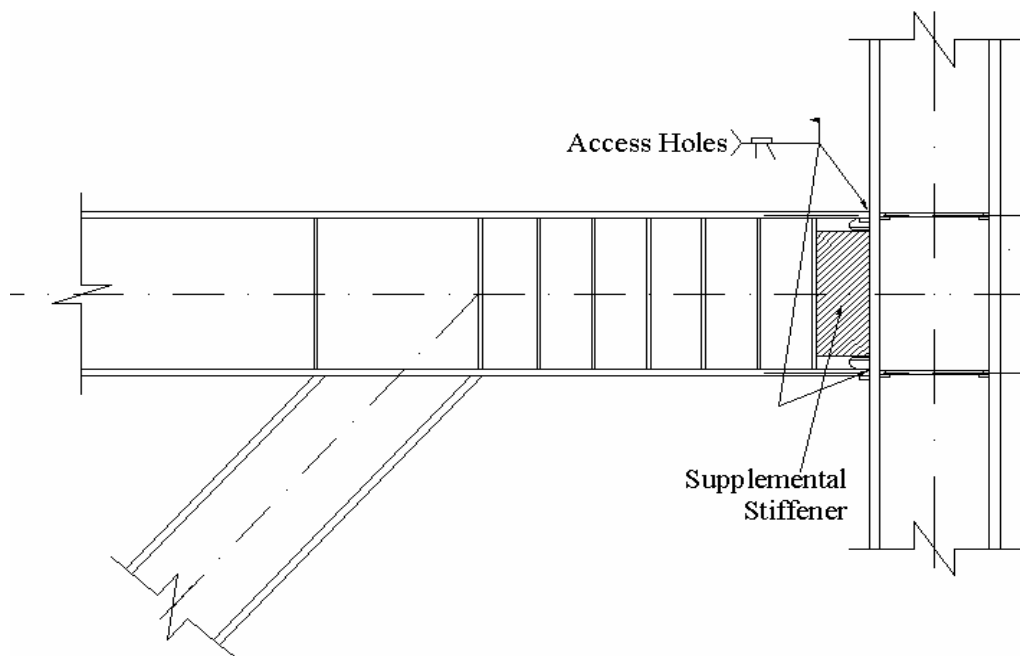


Figure 2.5: Concept of the “Reinforced” Link-to-Column Connection Detail (Phase II)

2.3.2 Connection Concept Development

2.3.2.1 Phase I

The connection concept for the first four test specimens was motivated by successful tests of a similar detail in an investigation by Arce and Okazaki (Arce et al 2003, Okazaki et al 2005). In these previous investigations, links were subject to cyclic loading to study flange buckling and flange slenderness limits. Consequently, it was necessary to be able to test links without premature failure of the link end connections. For these tests, links were fillet welded to heavy end plates, which in turn, were bolted to the test frame (Okazaki et al 2005). The sizes of fillet welds was chosen to be 1.5 times the thickness of the connected link flange or web, and were made using the shielded metal arc welding (SMAW) welding process. Further, small weld tabs were placed at the

outer edges of the link flanges for run-off the link flange to end plate fillet welds. This connection detail was developed by trial and error in the laboratory. It was not originally intended to represent a realistic link end connection, but was simply developed to permit laboratory testing of links without the occurrence of link end connection failure. This detail was used successfully in over fifty link tests. Based on this successful experience, the concept of the shop welded link-to-column connection was developed, and evaluated in the four pilot tests described herein.

2.3.2.2 Phase II

As described above, the connection concept for the Phase II specimens was to shift the formation of the plastic hinge away from the link-to-column connection. The connection design was studied using finite element analysis at the University of California at San Diego (Hong and Uang 2005, 2006). These studies evaluated various options for choosing the thickness of the supplemental stiffeners, and for connecting the supplemental stiffeners to the link and column. The design of the test specimens was based on recommendations developed in the finite element studies.

2.3.3 Section Dimensions & Material Properties

The test specimens used in this program were constructed using either a W18x40 or W10x68 link and a W12x120 column. All sections were ASTM A992 steel. The W18x40 and W12x120 sections left over from the previous program on link-to-column connections by Okazaki (2004), while the W10x68 sections were left over from a previous project done by Arce (2002).

Table 2.1 compares the nominal and the measured dimensions of the W18x40 and W10x68 link sections and the W12x120 column section. Furthermore, Table 2.2 and Table 2.3 list the cross-section properties of the two link sections, based on the nominal and measured dimensions shown in Table 2.1. The nominal values of V_p and M_p are computed per the 2005 AISC Seismic Provisions as:

$$V_p = 0.6F_y(d - 2t_f)t_w$$

$$M_p = Z_x F_y$$

Where, F_y is taken as the minimum specified yield strength of A992 steel (50 ksi) and nominal section dimensions are used.

The cross-section properties of Table 2.3 are based on the measured dimensions and yield stresses. Specifically, the actual values of V_p and M_p are calculated using the following equations:

$$V_p = 0.6t_w(d - 2t_f)F_{yw}$$

$$M_p = Z_{flange}F_{yf} + Z_{web}F_{yw} + Z_{fillets}F_{yw}$$

Where,

Z_{flange} = plastic section modulus of the flanges calculated using the measured dimensions

F_{yf} = average yield stress of the flange coupons

Z_{web} = plastic section modulus of the web calculated using the measured dimensions

F_{yw} = yield stress of the web coupon

$Z_{fillets}$ = nominal plastic section modulus of the fillets

A different F_y was used for the flanges and the web. Furthermore, an average of the dynamic and static yield stress was computed to estimate the yield strength during the

test. However, the yield stresses used are only an approximation since the loading rate used for the tensile coupons differs from the loading rate used in the link-to-column connection tests.

Table 2.1: Dimensions of link and column sections

Section	Dimension	Measured (in)	Nominal (in)
W18x40	d	17.82	17.9
	b _f	6.094	6.00
	t _f	0.50	0.525
	t _w	0.310	0.315
W10x68	d	10.4	10.4
	b _f	10.26	10.00
	t _f	0.773	0.77
	t _w	0.449	0.47
W12x120	d	13.25	13.12
	b _f	12.51	12.32
	t _f	1.080	1.105
	t _w	0.708	0.710

Table 2.2: Nominal Cross-Section Properties

Section	Z_x (in³)	V_p (kips)	M_p (in-kips)	$\frac{M_p}{V_p}$ (in)
W18x40	78.4	159	3920	24.7
W10x68	85.3	124.93	4265	34.1

Table 2.3: Calculated Cross-section Properties based on Measured Yield Stresses and Dimensions

Section	V_p (kips)	M_p (in-kips)	$\frac{M_p}{V_p}$ (in)
W18x40	184	4137	22.5
W10x68	144	4264	29.6

2.3.3.1 Tensile Coupon Tests

As described above, the link sections used for this project were selected to be the same as those used by Okazaki and Arce in their projects. As a result, the tensile coupon tests were conducted by them as a part of these previous projects.

➤ **W10X68** (Arce 2002)

For the W10x68 section, four coupons from different locations were made; one coupon in each flange, one coupon at the mid-depth of the web, and one coupon in the web near the k-area. Figure 2.6 illustrates the location of the coupons. Each coupon was machined down to a thickness of 0.25 inches and had a 2-inch gage length. Further details of the coupon testing procedure are reported in Arce (2002).

Table 2.4 lists various parameters measured in the tensile coupon tests. The dynamic and static yield strength is reported for each coupon. The dynamic yield strength was calculated using the 0.2% strain offset rule. On the other hand, the static yield strength was obtained by stopping the test three times while the coupon was in the yield plateau range. The static yield strength was taken as the average of these three values.

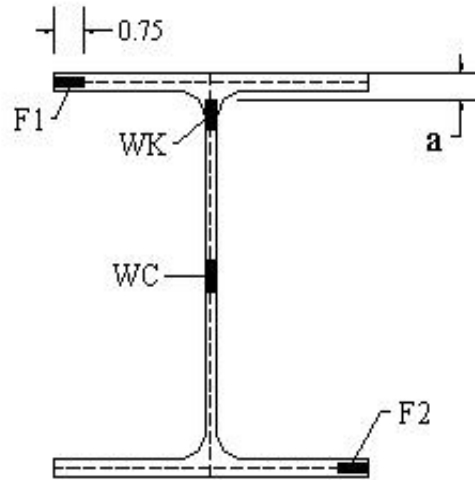


Figure 2.6: Location of tensile coupon tests for W10x68 ($a = 1\text{-}3/8$ inches) (Arce 2002)

Table 2.4: Tensile coupon data for W10x68 (Arce 2002)

Section	Location of coupon	$F_{y,dynamic}$ (Ksi) ^(d)	$F_{y,static}$ (Ksi) ^(c)	F_u (Ksi) ^(a)	$\left(\frac{F_u}{F_y}\right)_{dyn}$	$\frac{F_{y,dynamic}}{F_{y,nominal}}$ ^(e)	% Elong. ^(b)
W10x68	F1	48.7	46.3	67.1	1.38	0.97	32
	F2	48.7	46.1	71.9	1.47	0.97	33
	WC	61.0	58.6	77.0	1.26	1.22	34
	WK	76.8	73.7	88.9	1.16	1.54	18

Notes:

- (a) Dynamic ultimate tensile strength at loading rate of 0.125in/min.
- (b) % Elongation based on a 2-inch coupon.
- (c) Static yielding after a one-minute pause.
- (d) Dynamic yielding strength at a loading rate of 0.02in/min.
- (e) $F_{y,nominal}=50\text{Ksi}$

Table 2.5 lists the yield stresses that were used to calculate the cross-sectional properties of the W10x68 section as shown in Table 2.3. As one can observe, there is significant variation in the yield stress between the flange and the web.

The k-area coupons show significantly elevated yield and tensile strength values, along with significantly reduced elongation. Moreover, the k-area does not meet the maximum yield strength requirement for ASTM A992 steel which is 65 ksi and the minimum elongation of 21% for a 2-inch gage length. However, because the extent of k-area is rather small, the k-area yield stress values were not used when computing the values of V_p and M_p reported in Table 2.3.

Table 2.5: Average yield stresses used for W10x68

Location of Section	Average Yield Stress (ksi)
Flange	47.5
Web	59.8
K-area	75.3

➤ **W18x40** (Okazaki 2004)

As shown in Figure 2.7, tension coupons for the W18x40 were sampled from six different locations of the cross-section: two coupons from the edges of each flange; one coupon from the mid-depth of the web; and one coupon from the k-area region of the web. The coupons had a gauge length of 2 inches, a width of ½ inch, and thickness ranging between ¼ inch and 3/8 inch. Further details of the coupon testing procedure are reported in Okazaki (2004).

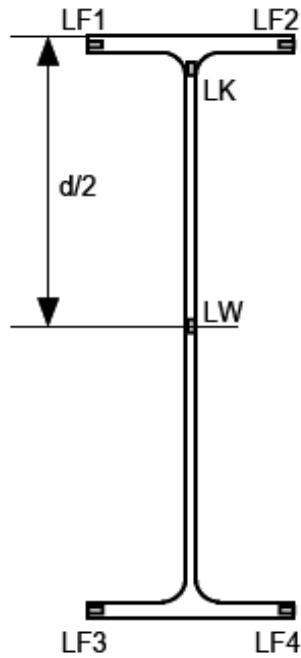


Figure 2.7: Location of tensile coupon tests for W18x40 (Okazaki 2004)

Table 2.6 summarizes the coupon test results. The static yield stress values were taken by stopping the crossheads and waiting for 3 minutes. The static yield stresses reported in the following table were evaluated by taking the averaged value of three readings for each coupon.

From Table 2.6, one can observe that the coupon taken from the k-area, LK, exhibited significantly higher yield strength and significantly reduced elongation compared to the other five coupons. Furthermore, there is no value for the static yield stress of this coupon since there was no yield plateau observed for the LK coupon.

Finally, Table 2.7 lists the average yield stresses used to calculate the cross-sectional properties of the W18x40 section. Again, the yield strength of the k-area was not used in the calculations.

Table 2.6: Tensile coupon data for W18x40 (Okazaki 2004)

Section	Location of coupon	$F_{y \text{ dynamic}}$ (Ksi) ^(d)	$F_{y \text{ static}}$ (Ksi) ^(c)	F_u (Ksi) ^(a)	$\left(\frac{F_y}{F_u}\right)_{\text{dyn}}$	% Elongation ^(b)
W18x40	LF1	54.9	51.9	72.6	0.76	34.4%
	LF2	52.2	49.8	71.8	0.73	32.8%
	LF3	56.2	53.1	74.4	0.76	33.6%
	LF4	52.2	49.3	70.8	0.74	33.6%
	LK	78.8	N.A.	89.6	0.88	15.0%
	LW	60.8	57.0	76.4	0.80	31.4%

(a) Dynamic ultimate tensile strength at loading rate of 0.125in/min.

(b) % Elongation based on a 2-inch coupon.

(c) Static yielding after a three-minute pause.

(d) Dynamic yielding strength at a loading rate of 0.02in/min.

Table 2.7: Average yield stresses used for W18x40

Location of Section	Average Yield Stress F_y (ksi)
Flange	52.5
Web	58.9
K-area	78.8

2.3.4 Test Specimen Parameters and Details

A total of eight specimens were tested in this research program. The specimens are designated as AISC-1 to AISC-8. The description of the eight test specimens will be divided into two sections corresponding to the two different phases of the experimental program. The Phase I specimens were AISC-1 to AISC-4, and the Phase II specimens were AISC-5 to AISC-8

2.3.4.1 Phase I (Specimens AISC-1 to AISC-4)

The specimens of this phase were constructed using W18x40 or W10x68 sections as links and W12x120 sections as columns, all of them from A992 steel. Furthermore, all the links had a length of $e = 38.6$ inches, so that all the specimens will be in or near the shear yielding range. The differences of the four specimens were focused on different weld details and welding processes. Tables 2.8 and 2.9 list various parameters of each specimen.

Specimens AISC-1 through AISC-3 had the same link section, W18x40, and thus the same link target plastic rotation γ_p equal to 0.073 rad, as defined by the 2005 AISC *Seismic Provisions*. Specimen AISC-4 had a W10x68 link section and a link target plastic rotation of 0.08 rad.

As a reminder, the link target plastic rotation depends on the ratio of $e / (M_p / V_p)$ and can be determined from Figure 1.5. Furthermore, the target values of γ_p noted above are based on the ratio $e / (M_p / V_p)$, where M_p and V_p are computed using measured yield stresses and section dimensions (Table 2.3).

The 2005 AISC *Seismic Provisions* propose that the link length must be smaller than $1.6 M_p / V_p$ in order to have a shear yielding link. From Table 2.8, one can observe that the first three specimens are very close to this requirement, and thus it can be

assumed that the links will yield primarily in shear. Furthermore, AISC-4 satisfies the above requirement very easily since the existing link length is well below $1.6 M_p / V_p$.

Table 2.9 describes the basic connection detail and welding process used for each specimen. Specifically, AISC-1 and AISC-2 used double-sided fillet welds sized to be approximately 1.5 times the connected flange or web thickness. These two specimens differed in just the welding process and the electrode used. Specimen AISC-1 was welded using the SMAW (Shielded Metal Arc Welding) process with E7018 electrodes. Although SMAW with E7018 electrodes can provide very high levels of notch-toughness (Johnson; 2000), it is not favored in fabrication practice due to very low deposition rates, and consequent high cost (Okazaki et al; 2006b). Specimen AISC-2 was welded using the FCAW-GS (Gas-Shielded Flux Cored Arc Welding) process with E70T-9 electrodes. This process and electrode is preferred by the fabricators due to higher deposition rates. Both types of electrodes satisfy the notch-toughness requirements for demand critical welds in the 2005 AISC *Seismic Provisions* (Okazaki et al; 2006b). These two specimens were intended to evaluate the suitability of FCAW-GS welding for this application since this welding process is more commonly used for shop welding by US fabricators.

Specimen AISC-3 was also welded using FCAW-GS, in the same way as AISC-2. However, the double-sided fillet welds on AISC-3 had a leg size approximately equal to the thickness of the connected flange or web. This specimen was designed to evaluate the feasibility of using smaller sized fillet welds. Drawings and pictures of the connection and welding details of Specimens AISC-1 through 3 are shown in Figures 2.8 to 2.16.

Specimen AISC-4 had a different link flange weld detail. For links with thick flanges, the use of double-sided fillet welds with a leg size equal to 1.5 times the flange thickness can result in exceedingly large and costly fillet welds. Thus, for such cases an alternative connection detail was evaluated. In this connection, the link web was welded

to the column using double-sided fillet welds for 1.5 times the web thickness, similar to Specimens AISC-1 and 2. However, the link flanges were welded to the column flange using a partial joint penetration groove weld. The bevels were made from the outer surface of each flange at a 45-degree angle. The bevel was nearly the full depth of the flange, leaving a small amount of land on the flange, with a height of about ¼-inch. Consequently, the weld was close to being complete joint penetration, except there was no open root, and no backing bars were required. Finally, on the inside face of each link flange, a fillet weld, with a leg size approximately equal to the flange thickness, was placed. A description of the connection and welding details of Specimen AISC-4 is provided in Figures 2.17 through 2.22.

For all the specimens, weld run-off tabs, with a thickness approximately the same as the flange thickness, were used at the outer edges of the link flanges. All the fillet welds were extended over these tabs which remained in-place after the completion of welding. This additional feature was adopted after observing some beneficial effects of the weld tabs in previous tests conducted by Arce and Okazaki (Arce et al.; 2003, Okazaki; 2004). These weld tabs provided an area to terminate the fillet welds away from the flange edges.

Finally, for the test specimens AISC-1 to 3, six vertical stiffeners were used only on the front side of the link web. The dimensions of the stiffeners were 16.85" x 2-3/4" x 3/8", and they were equally distributed along the link length, $e = 38.6"$. Only 2 vertical stiffeners located on the front side of the link web were used for AISC-4. The dimensions of the stiffeners were 9-1/2" x 4-7/8" x 3/8", and they were equally distributed along the link length. Stiffener spacing, size and welding details were chosen to be in conformance with the requirements of the 2005 AISC *Seismic Provisions*.

Table 2.8: Link Sections used for test specimens (Phase I)

Specimen	Link Section	Link length, e (in)	$\frac{e}{M_p/V_p}$	Target γ_p (rad)
AISC-1	W18x40	38.6	1.72	0.073
AISC-2	W18x40	38.6	1.72	0.073
AISC-3	W18x40	38.6	1.72	0.073
AISC-4	W10x68	38.6	1.30	0.08

Table 2.9: Specimen connection and welding details (Phase I)

Specimen	Welding Process and electrode	Connection detail
AISC-1	SMAW E7018	Double sided fillet welds; 3/4 inches fillets on flanges; 1/2-inch fillets on web
AISC-2	FCAW-GS E70T-9	Double sided fillet welds; 3/4 inches fillets on flanges; 1/2-inch fillets on web
AISC-3	FCAW-GS E70T-9	Double sided fillet welds; 1/2 inch fillets on flanges; 5/16-inch fillets on web
AISC-4	FCAW-GS E70T-9	Flanges: partial penetration on outside surface of flange and fillet weld on inside face Web: double sided 11/16-inch fillet welds

Note: All specimens: weld tabs were used for flange welds and left in-place

The four test specimens of Phase I were designed to evaluate the viability of the shop welded detail. Summarizing, the specific objectives of these tests were as follows (Okazaki et al 2006b):

- Determine the performance of a fillet weld detail, when the link is welded directly to a column flange rather than to a thick end plate.
- Determine the performance of the welding with the use of gas-shielded flux cored arc welding process (FCAW-GS) rather than with the use of SMAW since FCAW-GS is preferred by fabricators for shop-welding.
- Determine the performance of the fillet weld, if the size of the weld is smaller than the suggested from the previous tests value of 1.5-times the connected plate (link web or flange) thickness.
- Determine if the welding detail of the link flanges can be taken as a partial penetration groove weld made from the outer side of the flange, combined with a fillet weld placed on the inside face of the link flange, instead of the double sided fillet weld that was used for the previous specimens. This detail may prove very useful for link with thick flanges, as the W10x68 used, since it may permit considerable savings in welding.

Figures 2.8 to 2.22 that follow depict the overall geometry of the specimens, the link-to-column connection details, and the welding details for the Phase I specimens.

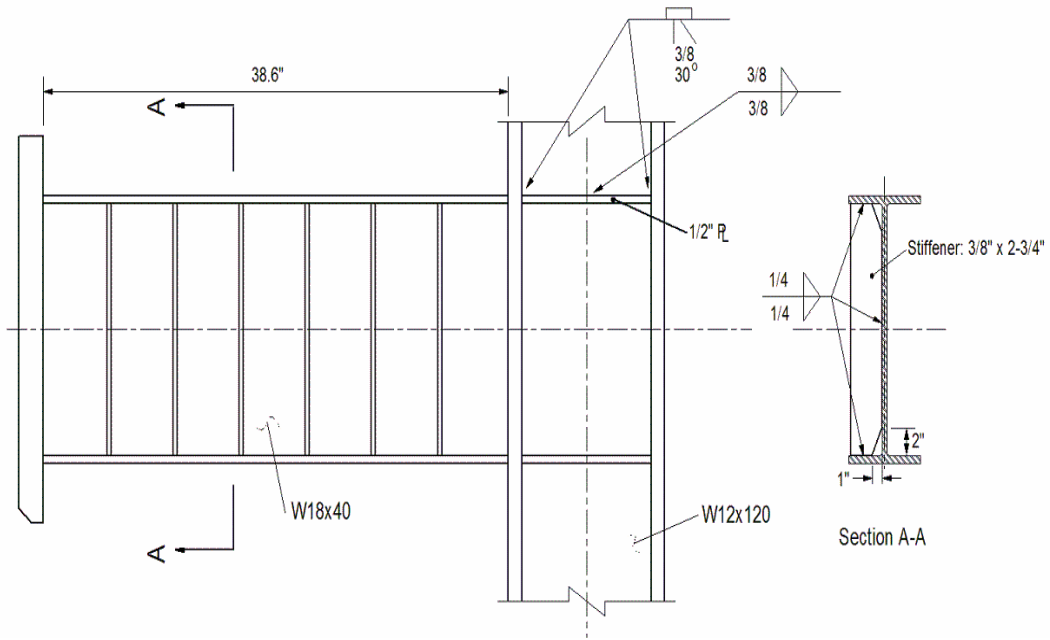


Figure 2.8: Specimens AISC 1 to 3 – Overall Layout

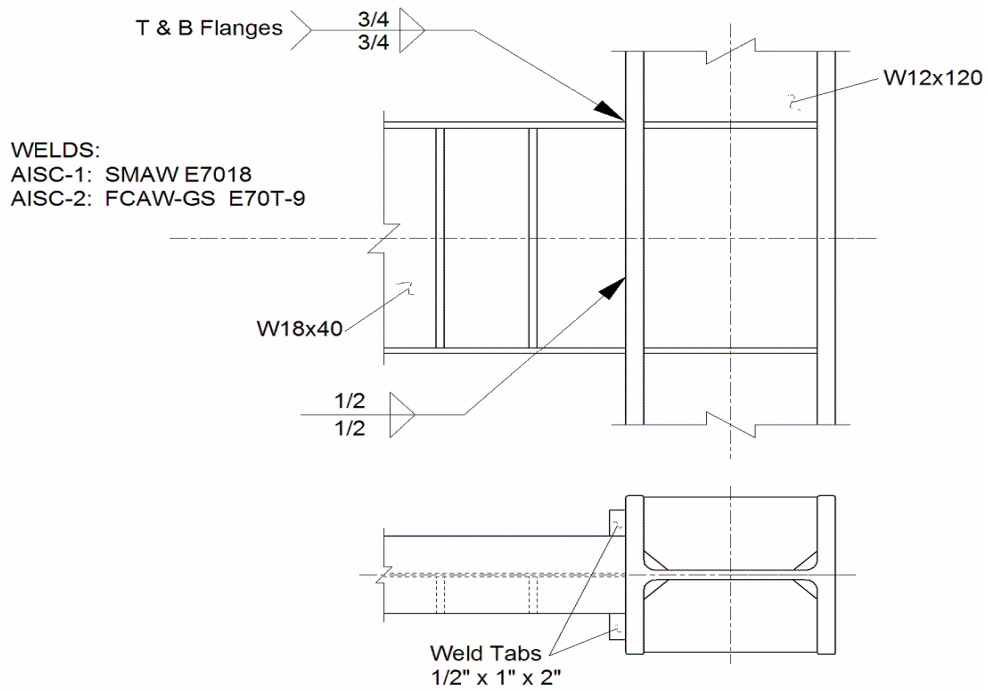


Figure 2.9: Specimens AISC 1 and 2 – Connection Detail

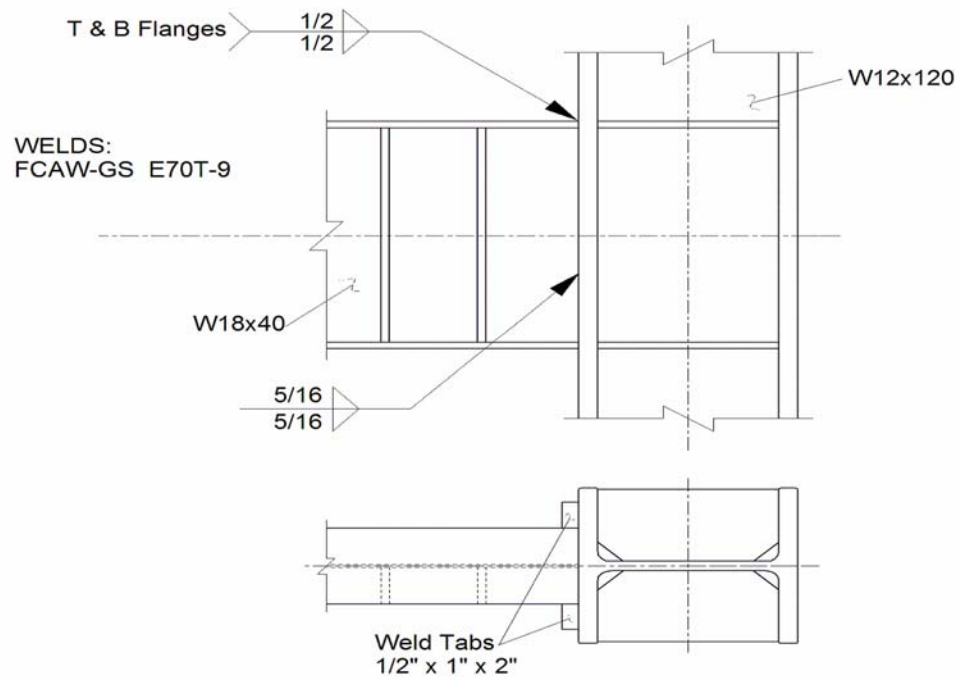


Figure 2.10: Specimen AISC 3 – Connection Detail



Figure 2.11: Overall details of specimens AISC 1 to 3



Figure 2.12: Link-to-Column connection detail for Specimens AISC 1 to 3

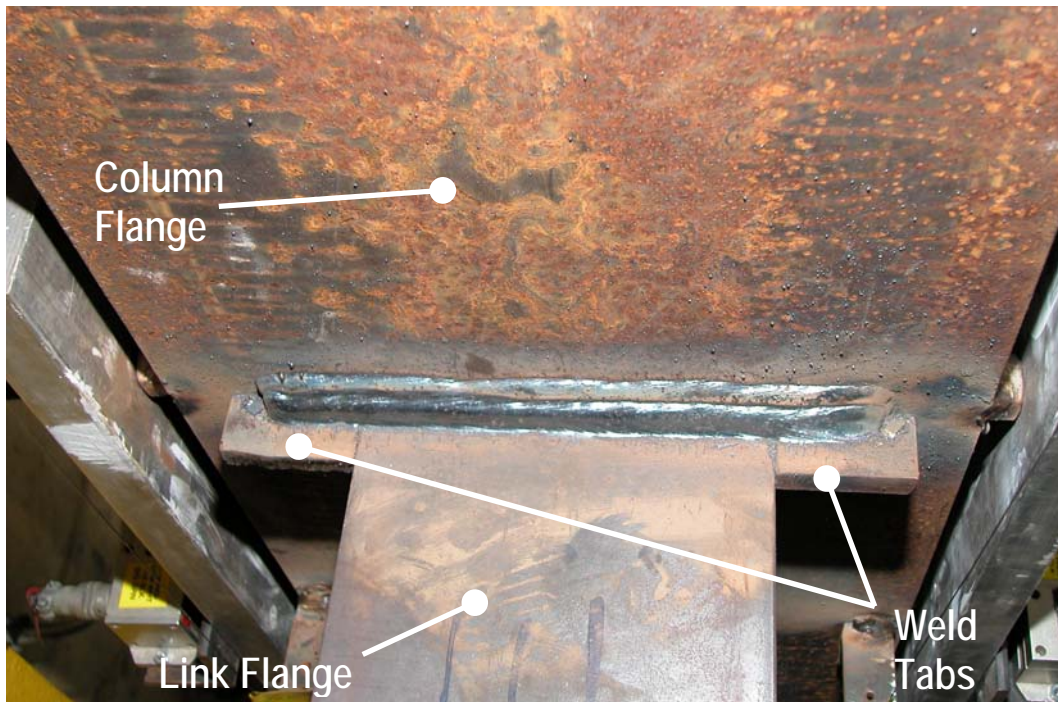


Figure 2.13: Link top flange welding detail for Specimens AISC 1 to 3

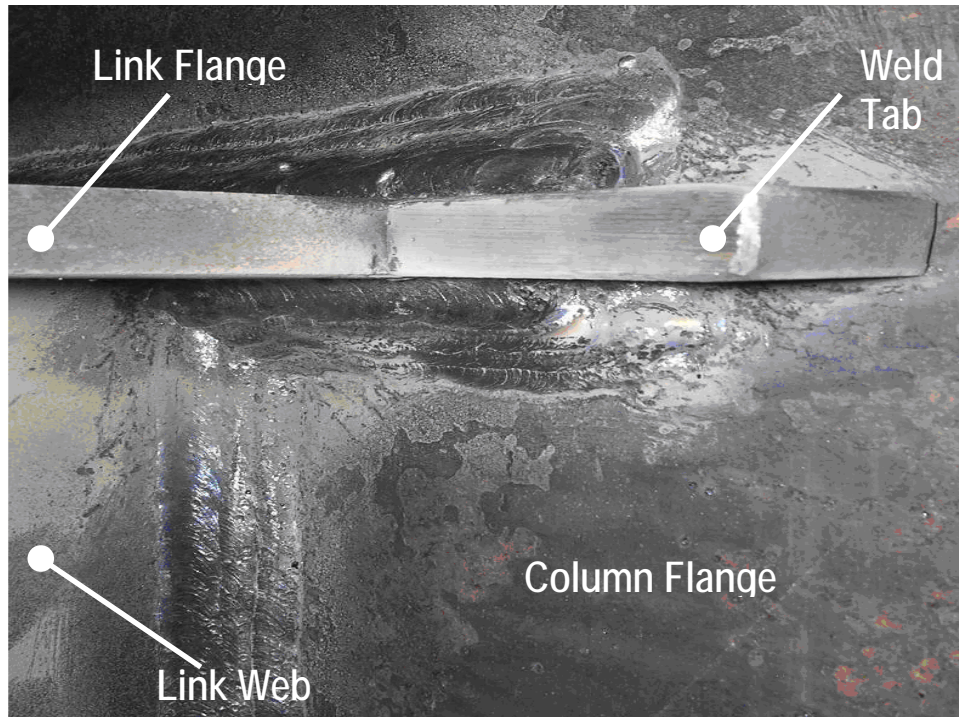


Figure 2.14: Fillet welds of the link flange and web to the column flange in AISC-1

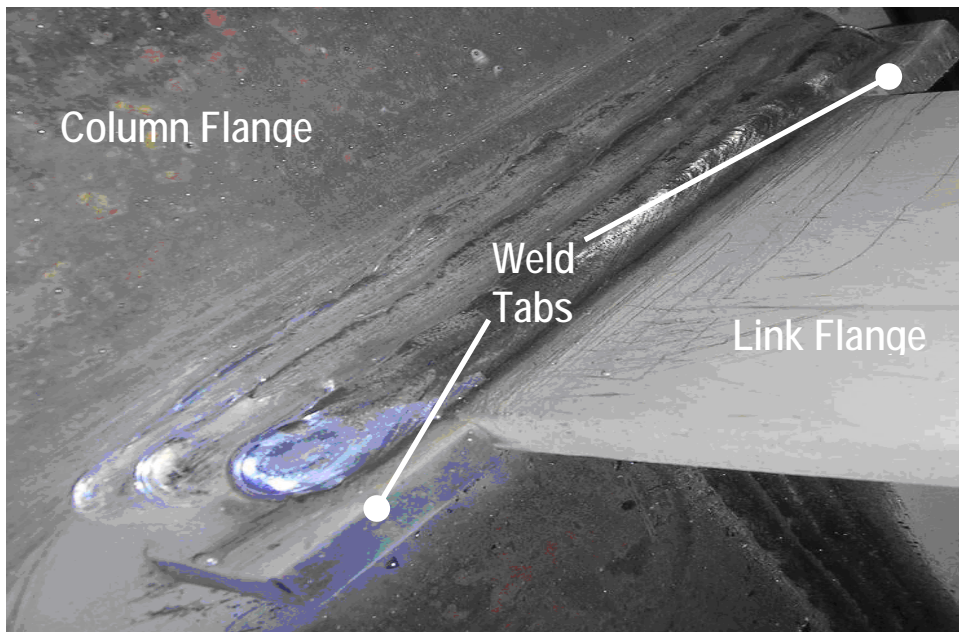


Figure 2.15: Fillet weld between link flange and column flange in Specimen AISC-2

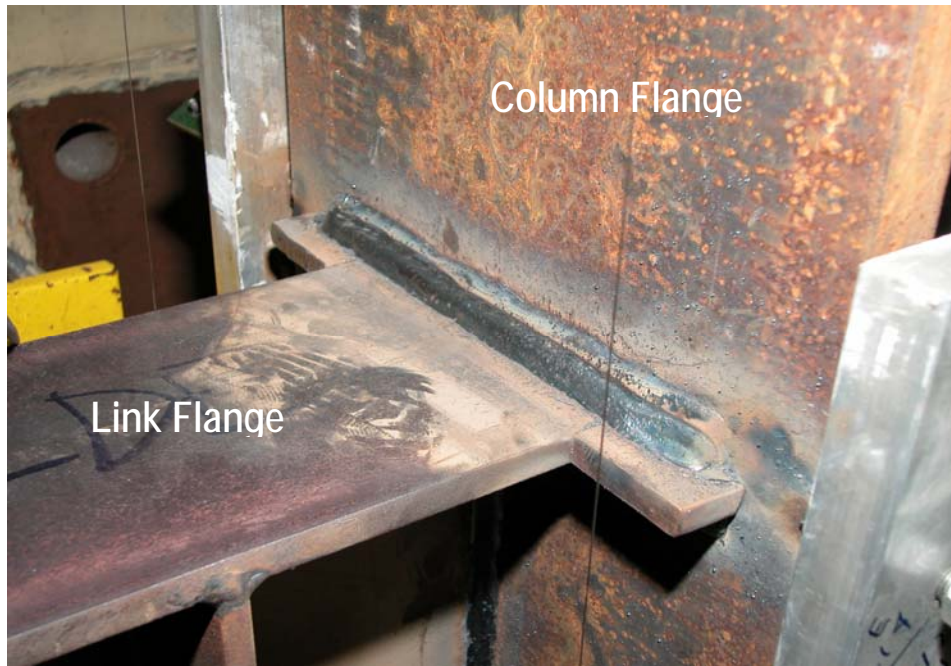


Figure 2.16: Fillet weld between link top flange and column flange in specimen AISC-2

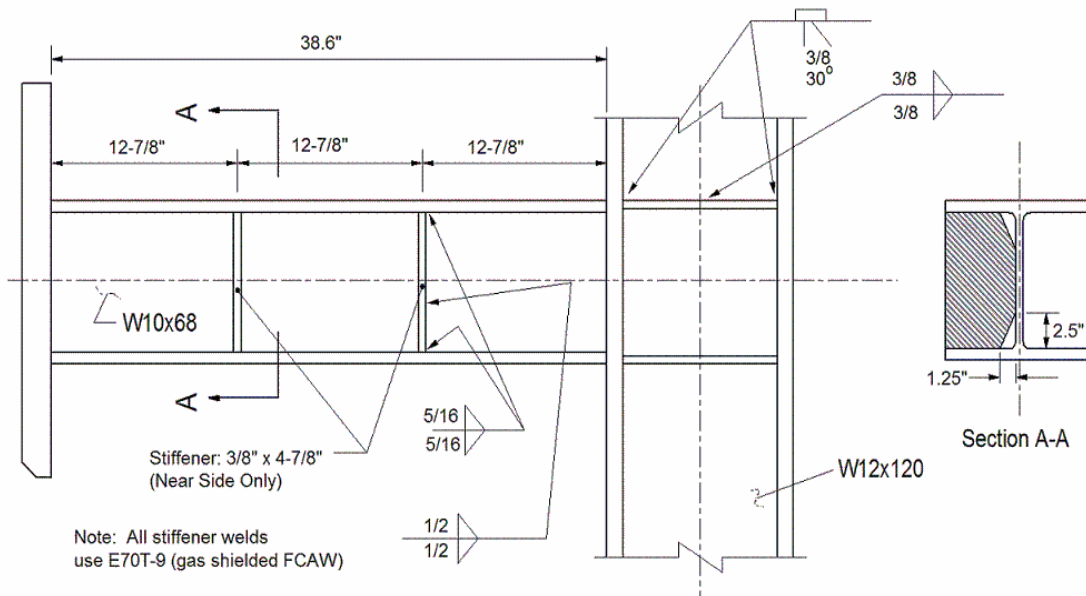


Figure 2.17: Specimen AISC-4 – Overall Layout

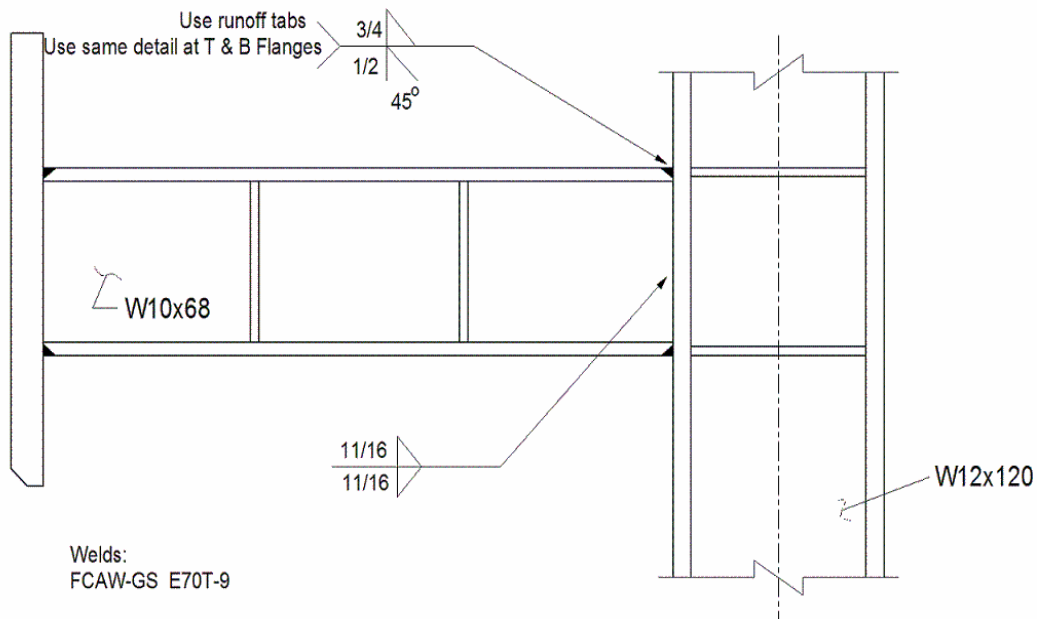


Figure 2.18: Specimen AISC-4 – Connection Detail

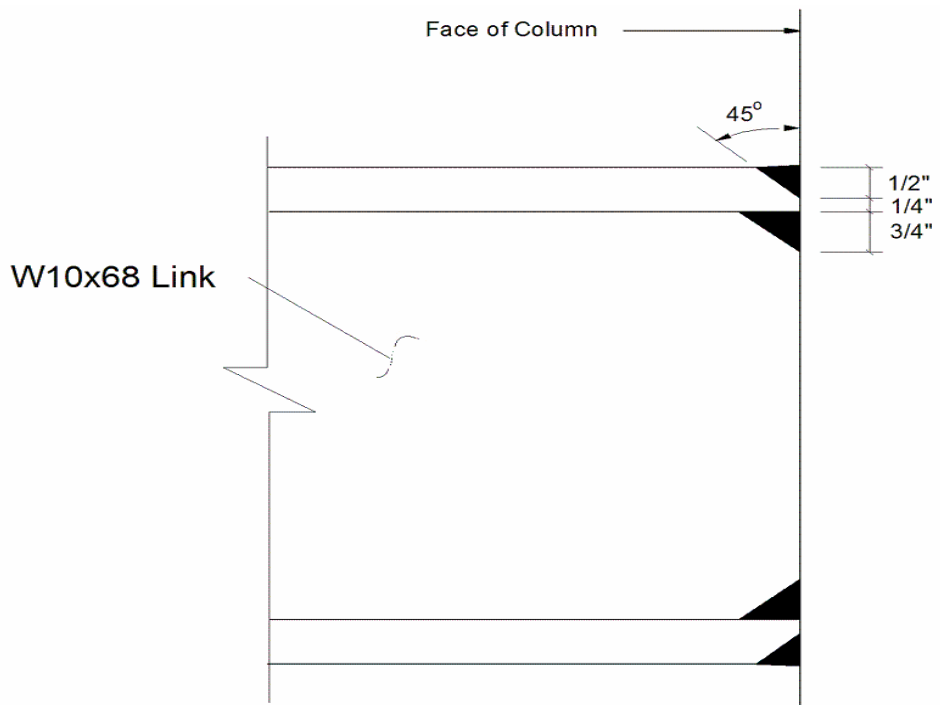


Figure 2.19: Specimen AISC-4 – Link End Preparations and Welds



Figure 2.20: Overall Layout - Specimen AISC-4

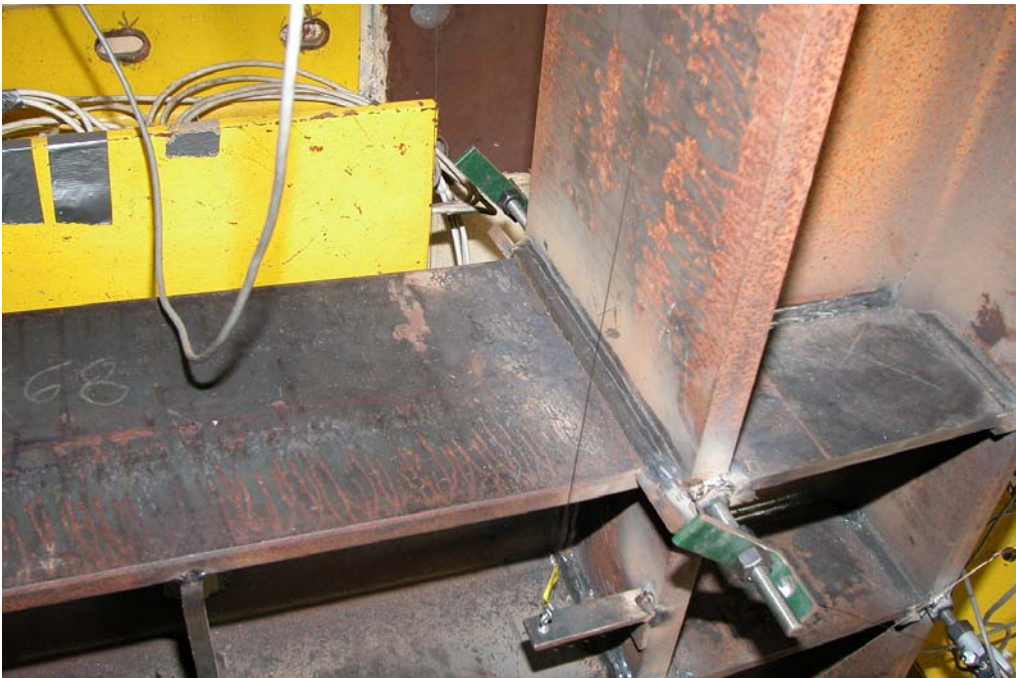


Figure 2.21: Partial penetration groove weld of the link top flange – Specimen AISC-4

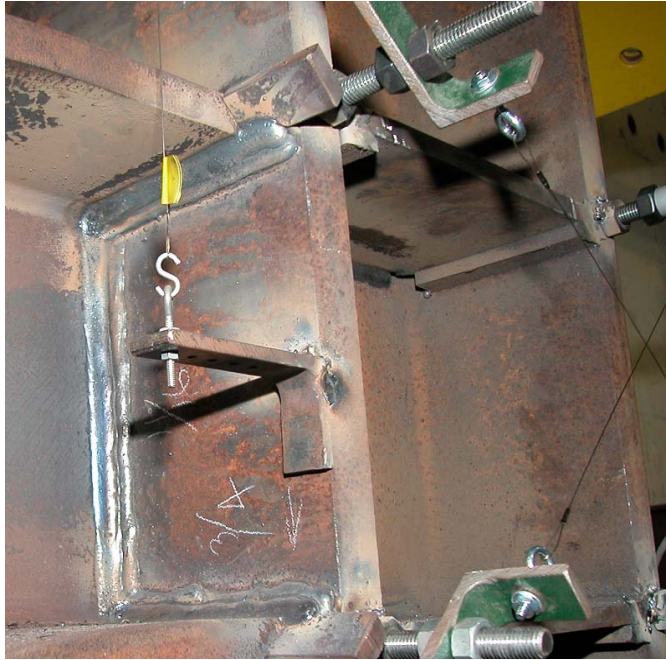


Figure 2.22: Fillet welds of the link web and the inside face of the flanges – Specimen AISC-4

2.3.4.2 Phase II (Specimens AISC-5 to AISC-8)

For the Phase II test specimens, W18x40 links were used for Specimens AISC-5 and AISC-8; and W10x68 links were used for Specimens AISC-6 and AISC-7. All specimens used W12x120 sections as columns. The total link length remained 38.6 inches for all specimens. The link-to-column connection detail for all specimens was reinforced with two supplemental stiffeners, which in turn were designed to shift the yielding away from the connection. Thus, only the unreinforced or “active” part of the link was intended to yield, while the reinforced portion was designed to remain essentially elastic. The unreinforced link length can be calculated by subtracting the length of the stiffened panel from the total link length. Table 2.10 summarizes the

sections used for each specimen, their properties and the target plastic rotation for each. The non-dimensional link length $e / (M_p / V_p)$ as well as the target rotation are reported using both the total link length (38.6-inches) and the active link length.

Specimens AISC-5 through 8 differed in the thickness of the supplemental stiffener and in the welding details use for the supplemental stiffeners. Specifically, for specimens AISC-5 and 6 thicker supplemental stiffeners were used and were welded using CJP groove welds, while for specimens AISC-7 and 8 thinner supplemental stiffeners were used and were welded using one-sided fillet welds.

A Welding/Fabrication Sequence and a Welding Procedure were prepared for each specimen. Two different welding processes were used in order to simulate welding that can be done at the shop and in the field, together with different electrodes for welds made in a flat position and for welds made in vertical and overhead positions. For shop-welds, such as the fillet welds of the vertical stiffeners to the link, the gas-shielded FCAW process with the E70T-9 electrode were used. For the field welds, the self-shielded FCAW process, with the E71T-8 and E70T-6 electrodes was used. The E71T-8 electrode was used for the vertical groove weld of the link web to the column flange, and the vertical welds of the secondary stiffeners to the column flange and the first vertical stiffener. The E70T-6 electrode was preferred for flat position groove welds, such as the CJP groove welds of the link flanges to the column flange.

The Welding and Fabrication procedure was the same for every Specimen of this Phase, except for the welding detail of the supplemental stiffeners. A typical fabrication procedure is presented in the Appendix A.

The Link-to-Column connection of all Specimens was constructed as follows:

1. A Shear Tab was first welded to the column flange using double-sided fillet welds with sizes 3/16" on the front side and 5/16" on the back side.

2. The link was bolted to the shear tab, using fully tensioned bolts installed using the turn-of-nut method.

3. The link flanges were welded to the column flange using CJP groove welds with 3/8" root and a 30° bevel. Backing bars, which extended approximately 2-inches beyond the end of the link flange, were used along with weld tabs.

4. The backing bar of the bottom link flange was removed and the weld was inspected. A 5/16" fillet weld was placed underneath the root of the CJP groove weld. The backing bar of the link top flange remained in-place and was welded with a 5/16" fillet weld to the column flange.

5. All the weld tabs from the top and bottom flanges were removed using carbon arc gouge, and the link flange edges were ground smooth.

6. The link web was welded to the column flange using a CJP groove weld with 1/4" root and a 45° bevel. The shear tab played the role of the backing bar.

7. The supplemental stiffeners were welded to the column flange and to the first vertical stiffener using either CJP groove welds, or one-side fillet welds with a leg size equal to the supplemental stiffener thickness.

All these welds were made using the self-shielded FCAW process with either the E71T-8 or the E70T-6 electrodes.

Specimens AISC-5 and 6 had two supplemental stiffeners with thicknesses 3/8" and 7/8" respectively, welded to the column flange and the first vertical stiffener using CJP groove welds with a 1/4" root and a 45° bevel. Four 3/8" thick backup bars were also used with a length that was approximately 1" larger than that the length of the secondary stiffeners. Specimens AISC-7 and 8 had two secondary stiffeners with thicknesses 3/8" and 3/16" respectively, welded to the column flange and the first vertical stiffener using one-side fillet welds with a size equal to the stiffener's thickness. The design procedure

of the supplemental stiffeners will be presented later on in this chapter. Table 2.11 summarizes the link-to-column connection detail for each specimen.

Table 2.10: Link Sections used for test specimens (Phase II)

Specimen	Link Section	Total Link Length, e(in)	Unreinforced Link Length, e_{active} (in)	Target γ_p (rad), based on e	Target γ_p (rad), based on e_{active}
AISC-5	W18x40	38.6 (= $1.72M_p/V_p$)	33.1 (= $1.47M_p/V_p$)	0.073	0.08
AISC-6	W10x68	38.6 (= $1.30M_p/V_p$)	33.4 (= $1.13M_p/V_p$)	0.08	0.08
AISC-7	W10x68	38.6 (= $1.30M_p/V_p$)	33.4 (= $1.13M_p/V_p$)	0.08	0.08
AISC-8	W18x40	38.6 (= $1.72M_p/V_p$)	33.1 (= $1.47M_p/V_p$)	0.073	0.08

Table 2.11: Specimen connection and welding details (Phase II)

Specimen	Supplemental Stiffener Detail
AISC-5	Thickness 3/8-inch CJP groove weld with 1/4-inch root and 45° bevel
AISC-6	Thickness 7/8-inch CJP groove weld with 1/4-inch root and 45° bevel
AISC-7	Thickness 3/8-inch One-sided fillet welds; 3/8-inch fillet welds
AISC-8	Thickness 3/16-inch One-sided fillet welds; 3/16-inch fillet welds

In regard to the vertical web stiffeners used in the links, for Specimens AISC-5 and 8, seven stiffeners were used; six on the front side and one on the back side. The stiffener on the back side was used in order to place the backside supplemental stiffener. The dimensions of the stiffeners were 3/8" x 2-7/8" x 16-7/8", and they were equally distributed along the link length. Similarly, specimens AISC-6 and 7 had four stiffeners; three on the front side and one on the back side. The dimensions of the stiffeners were 3/8" x 4-7/8" x 8-7/8", and they were equally distributed along the link length.

The supplemental stiffeners were designed based on the finite element analysis conducted at UCSD, combined with simplified calculations and the requirements of the

2005 AISC Seismic Provisions. Based on research done by UCSD, the supplemental stiffener's design includes the following (see Figure 2.23):

1. Location (s) at which the supplemental stiffener has to be placed - $s = b_f / 4$
2. Thickness (t_s) – larger than or equal to the link web thickness ($t_s \geq t_w$)
3. Depth (d_s) – $d_s \geq (d - 2t_f - 2")$
4. Length (a_s) – lesser of a (intermediate stiffener spacing as specified in the 2005 AISC Seismic Provisions), or $d / 2$
5. Welding – groove or fillet welds on vertical sides only, and no connection to the link flange
6. Gap (g) between the supplemental stiffener and the inside face of the link flange – less than or equal to 1 inch
7. Strength check using simplified strength model (described below).

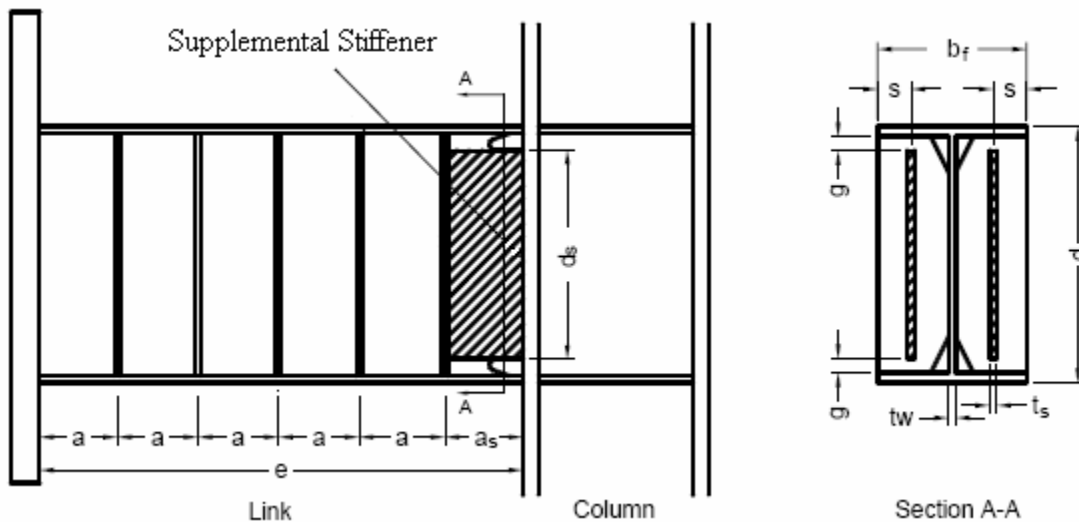


Figure 2.23: Supplemental Stiffener's Configuration (Hong, Uang; 2006)

While steps 1 and 3-6 can be very easily calculated using the above equations, the calculation of the supplemental stiffener's thickness (Step 2) needs to be estimated based on strength calculations. The procedure for the calculation of the supplemental stiffener thickness for specimens AISC-5 and 6 is described below.

Figure 2.24 shows the assumed shear force and moment diagrams for specimen AISC-5, for the case where the link has achieved its fully yielded and strain hardened strength. The “active” link length is 33.1 inches and the reinforced region 5.5 inches. The cross-sectional properties can be taken from Table 2.3: $M_p = 4137$ in-k, $V_p = 184k$, $M_p/V_p = 22.5$ inches.

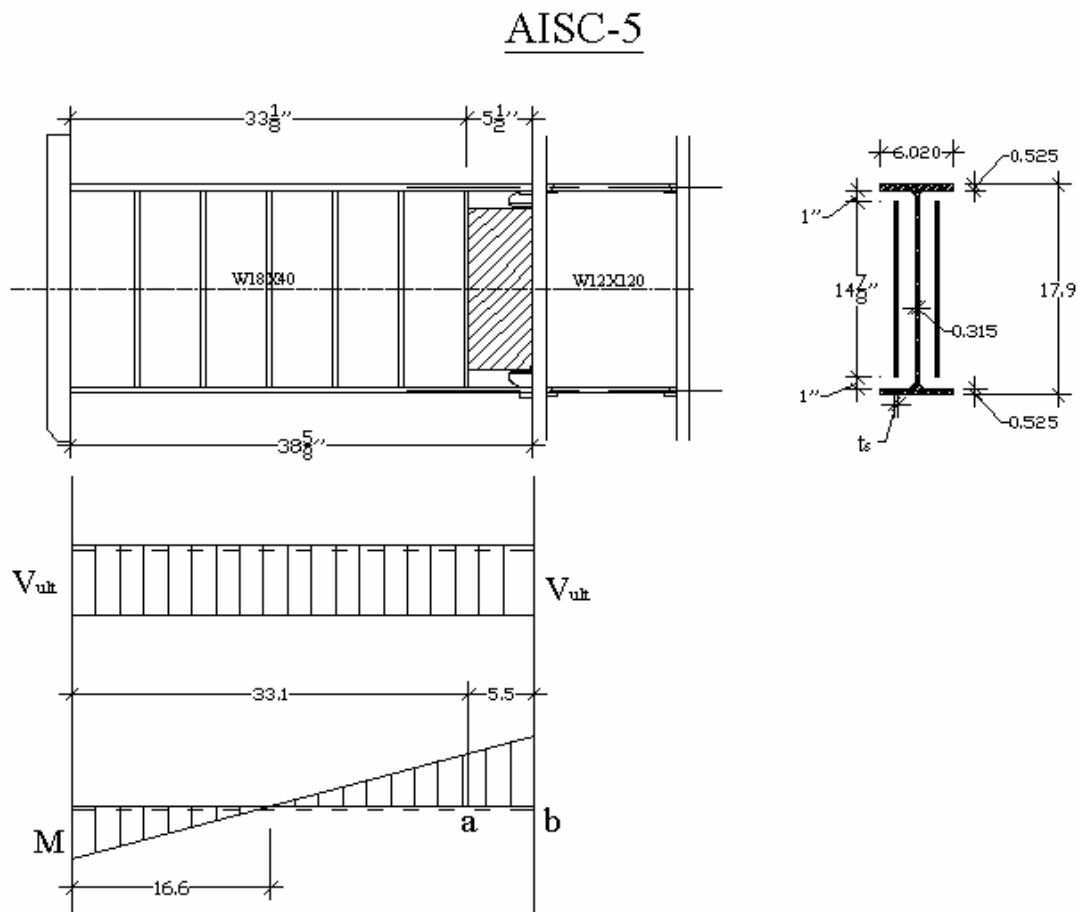


Figure 2.24: Shear Force and Moment Diagrams for Specimen AISC-5

The first step of this design procedure is to estimate the maximum shear force and moment at the face of the column (point b). Specifically, assuming that the maximum shear force along the length of the link will be $V_{ult} = 260kips (=1.41V_p)$, based on measured V_{ult} for Specimen AISC-4, and that the point of inflection is situated at the mid length of the active link length (as shown in Figure 2.24), one can calculate the moment at the points a and b of the link as follows:

$$M_a = (260kips)(16.6") = 4315in - k (=1.08M_p)$$

$$M_b = (260kips)(16.6" + 5.5") = 5750in - k$$

Thus, the estimated maximum forces in the link at the face of the column are:

$$V_{ult} = 260kips$$

$$M_{ult} = 5750in - kips$$

Next, the cross-sectional properties of the reinforced section must be calculated and then compared with the forces computed above. From the geometry of the reinforced section, as shown in Figure 2.24, one can calculate:

$$A = A_{W18x40} + A_{\text{reinf}} = 11.8in^2 + 2(14.85")t_s = 11.8in^2 + 29.7t_s$$

$$A_{\text{shear}} = (17.9" - 2 * 0.525")(0.315") + 2(14.85")t_s = 5.31in^2 + 29.7t_s$$

$$Z_{\text{stiffeners}} = \frac{2[(14.85)^2 t_s]}{4} = 110.3t_s$$

$$M_{p,\text{stiff}} = Z_{\text{stiff}} (50ksi) = 5513t_s$$

$$M_{p,\text{total}} = M_{p,W18x40} + M_{p,\text{stiff}} = 4137 + 5513t_s$$

Finally, the design criteria checked are:

1. $M_{p,total} \geq M_{ult} \Leftrightarrow 4137 + 5513t_s \geq 5750 \Leftrightarrow t_s \geq 0.29"$
2. $V_{p,total} \geq V_{ult} \Leftrightarrow 184k + (29.7t_s)(0.6 * 50ksi) \geq 260k \Leftrightarrow t_s \geq 0.085"$
3. $t_s \geq t_w \Leftrightarrow t_s \geq 0.315"$

The controlling criterion, in this case, for the design of the supplemental stiffeners is that the thickness must be at least equal to the thickness of the link web. Thus, the thickness of the supplemental stiffener for the AISC-5 specimen was selected to be $t_s = 3/8$ -in.

Similarly, the same procedure was used for the design of the supplemental stiffener of specimen AISC-6. Figure 2.25 shows the shear and moment diagrams of specimen AISC-6, as well as the cross-sectional dimensions used for the calculations.

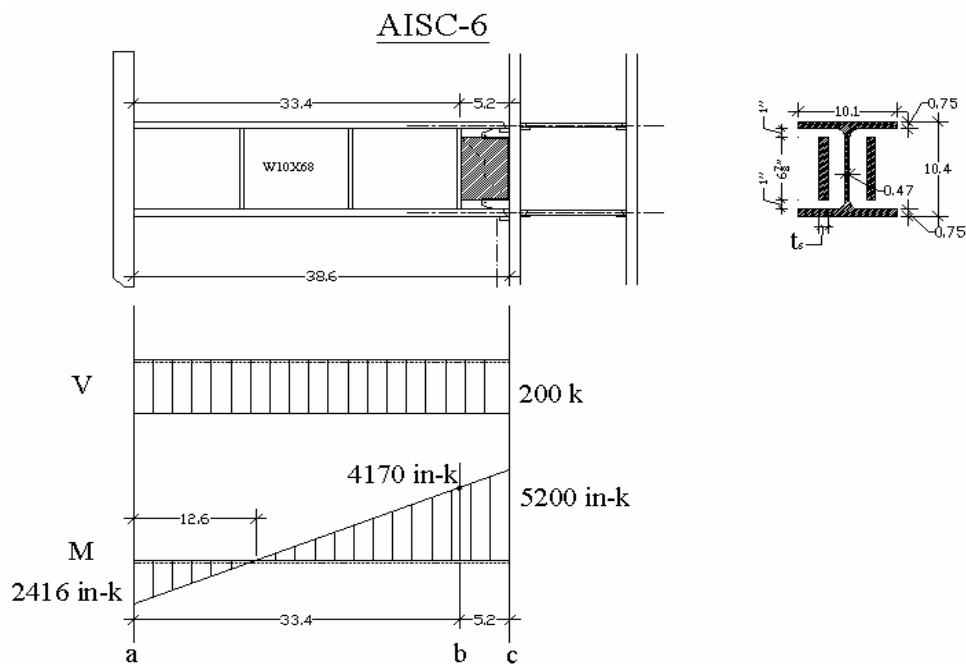


Figure 2.25: Shear Force and Moment Diagrams for Specimen AISC-6

The “active” link length is 33.4 inches and the reinforced region 5.2 inches. The cross-sectional properties can be taken from Table 2.3: $M_p = 4264 \text{ in-k}$, $V_p = 144k$, $M_p/V_p = 29.6 \text{ inches}$

The first step, again, is to estimate the link ultimate shear and moment. Specifically, it is assumed that the ultimate shear force at the link is $V_{ult} = 200k$, based on the test results of specimen AISC-4. Furthermore, it is assumed that the link end moments will not equalize since specimen AISC-6 is a short link ($e < 1.6(M_p/V_p)$) attached to a column. Finally, it is assumed that the moment adjacent to the reinforced section will reach the value of $M_p = 4264 \text{ in-k}$.

From the moment diagram of Figure 2.25, one can calculate the link end moments as follows:

$$\frac{M_a + M_b}{33.4} = V \Leftrightarrow \frac{M_a + 4264}{33.4} = 200k \Leftrightarrow M_a = 2416 \text{ in-k}$$

$$M_c = 200k(20.8 + 5.2) = 5200 \text{ in-k}$$

Thus, the maximum forces expected at the face of the column are:

$$V_{ult} = 200k$$

$$M_{ult} = 5200 \text{ in-k}$$

Next, the cross-sectional properties of the reinforced section must be calculated and then compared with the forces computed above. From the geometry of the reinforced section, as shown in Figure 2.25, one can calculate:

$$Z_{stiff} = \frac{2t_s(6.9")^2}{4} = 23.8t_s$$

$$M_{pr} = M_{p,W10x68} + M_{p,stiff} = 4264 + 23.8(t_s)(50ksi) = 4264 + 1190t_s$$

$$V_{pr} = V_{p,W10x68} + V_{p,stiff} = 144 + 2(t_s)(6.9")(0.6 * 50ksi) = 144 + 414t_s$$

Finally, the design criteria checked are:

$$M_{pr} \geq M_{ult} \Leftrightarrow 4264 + 1190t_s \geq 5200 \Leftrightarrow t_s \geq 0.787 \text{ in}$$

$$V_{pr} \geq V_{ult} \Leftrightarrow 144 + 414t_s \geq 200 \Leftrightarrow t_s \geq 0.14 \text{ in}$$

$$t_s \geq t_w \Leftrightarrow t_s \geq 0.47 \text{ in}$$

The controlling criterion, in this case, for the design of the supplemental stiffeners is the flexural capacity of the reinforced section of the link at the face of the column. Thus, the thickness of the supplemental stiffener for the AISC-5 specimen was selected to be $t_s = 7/8$ -in.

The design of the supplemental stiffeners for Specimens AISC-7 and 8 was based mainly on the finite element analysis conducted at UCSD. The objective of this analysis was to refine the supplemental stiffener concept by reducing the thickness of the supplemental stiffeners and by using fillet welds instead of groove welds. According to the unpublished paper “ABAQUS Analysis of Specimen AISC-7” (Uang and Hong 2007), the potential for fracture at the link flange groove welds, as determined by various fracture indices was very similar for supplemental stiffener thicknesses varying between 0 and 1.5 t_w , where t_w is the link web thickness. Furthermore, the shear deformation at the reinforced panel is limited to about 35% of that at the interior panels with supplemental stiffeners whose thickness is larger than 0.5 t_w . It is interesting to note that this analysis

also showed that the shear force at each supplemental stiffener is 18~23% of the link shear. Thus, only $\frac{1}{2}$ of the total load is transferred to the link web, while each supplemental stiffener carries $\frac{1}{4}$ of the total load.

Based on evaluation of the finite element analysis, the thickness of each supplemental stiffener was calculated as the larger of:

1. $V_{\text{reinf}} \geq V_{\text{ult}} \Leftrightarrow \phi_v(0.6F_y)h_s t_s \geq \frac{1}{4} \times 1.25 \times R_y \times V_p \Leftrightarrow t_s \geq \frac{(1/4) \times 1.25 \times R_y \times V_p}{\phi_v(0.6F_y)h_s}$
2. $t_s \geq 0.5t_w$

Where, $R_y = 1.1$ for A992 Steel, $V_p =$ measured Shear Capacity, $\phi_v = 0.90$ (LRFD),

$F_y = 50$ ksi, and $h_s =$ height of the supplemental stiffener

After the estimation of the thickness of each supplemental stiffener, the size of the fillet welds needs to be determined. The design strength of the fillet weld is given in the following equation:

$$\phi R_n = 0.75(0.6F_{EXX})A_e = 0.75(0.6)(70)h_s(0.707a)$$

This design strength is compared to the design shear at each supplemental stiffener which is assumed to be $\frac{1}{4}$ of the total shear. Thus, the required size of the fillet weld is given in the following equation:

$$a \geq \frac{(1/4) \times 1.25 \times V_p}{\phi(0.6F_{EXX})h_s \times 0.707} \text{ (inches)}$$

Using the results of the finite element analysis, as well as the aforementioned equations, estimation was made for the thickness of each supplemental stiffener and the size of the fillet welds for Specimens AISC-7 and 8.

Specifically, for Specimen AISC-7 the required thickness of the supplemental stiffener is the larger of:

1. $t_s \geq 0.266 \text{ in}$
2. $t_s \geq 0.235 \text{ in}$

Thus, it was selected to use two supplemental stiffeners with thickness $t_s = 3/8 \text{ in}$. The required size of the fillet weld is:

$$a \geq \frac{(1/4)1.25(144)}{0.707 \times 0.75(0.6)(70)6.9} \Leftrightarrow a \geq 0.293 \text{ in}$$

It was decided to use fillet welds with size the same as the supplemental stiffener's thickness. That is to say, $a = 3/8 \text{ in}$.

Similarly, for Specimen AISC-8 the required thickness of the supplemental stiffener is the larger of:

1. $t_s \geq 0.158 \text{ in}$
2. $t_s \geq 0.158 \text{ in}$

Thus, it was selected to use two supplemental stiffeners with thickness $t_s = 3/16 \text{ in}$. The required size of the fillet weld is:

$$a \geq \frac{(1/4)1.25(184)}{0.707 \times 0.75(0.6)(70)14.85} \Leftrightarrow a \geq 0.174 \text{ in}$$

It was decided to use fillet welds with size the same as the supplemental stiffener's thickness. That is to say, $a = 3/16 \text{ in}$.

In the following Figures 2.26 through 2.45, drawings and pictures that describe the overall geometry of the specimens, the link-to-column connection detail, and the supplementary stiffener's detail are presented. The drawings and pictures were grouped according to the link section used. Thus, specimens AISC-5 & 8 are shown first, and specimens AISC-6 & 7 follow.

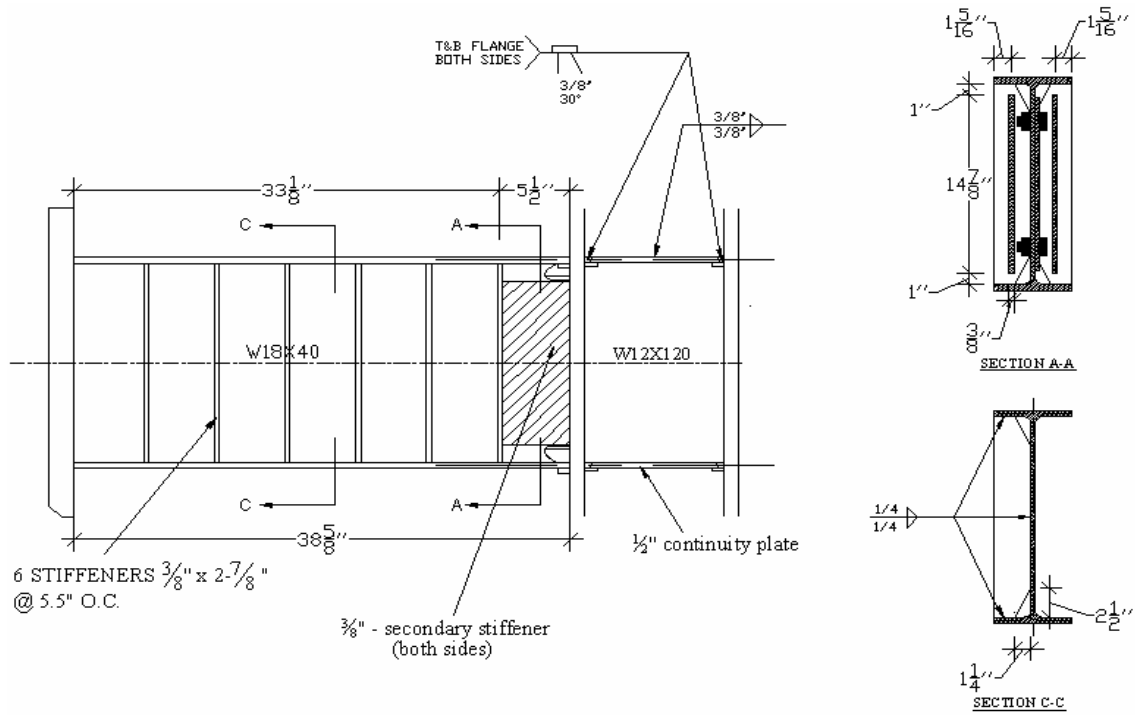


Figure 2.26: Specimen AISC-5 – Overall Layout

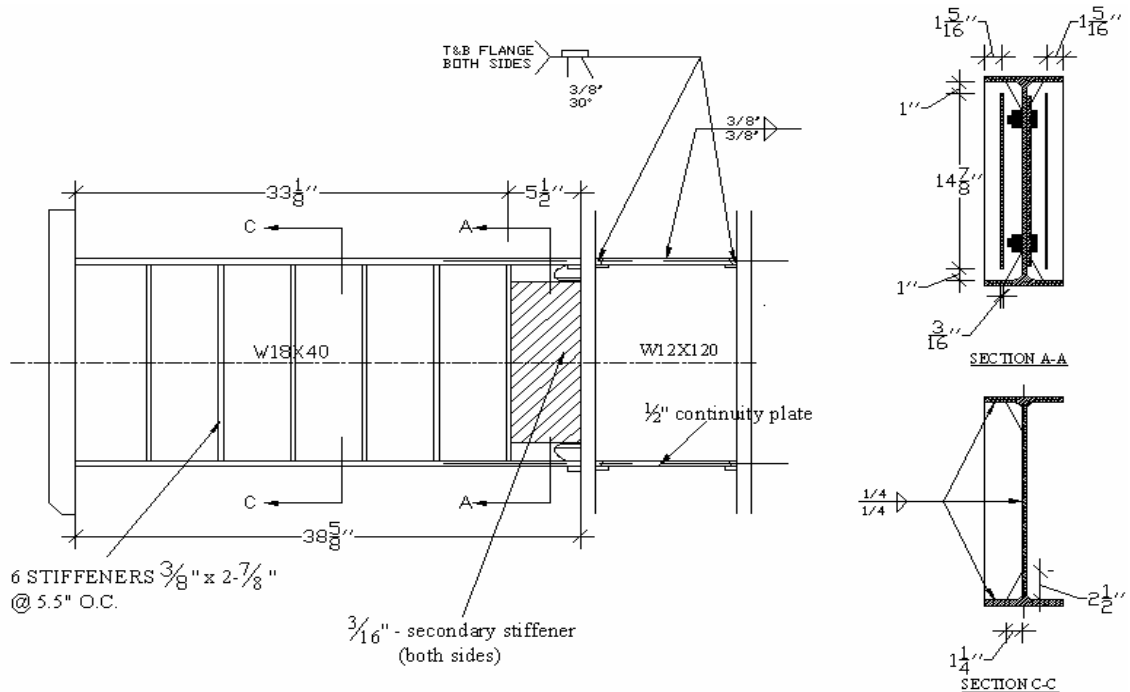


Figure 2.27: Specimen AISC-8 – Overall Layout

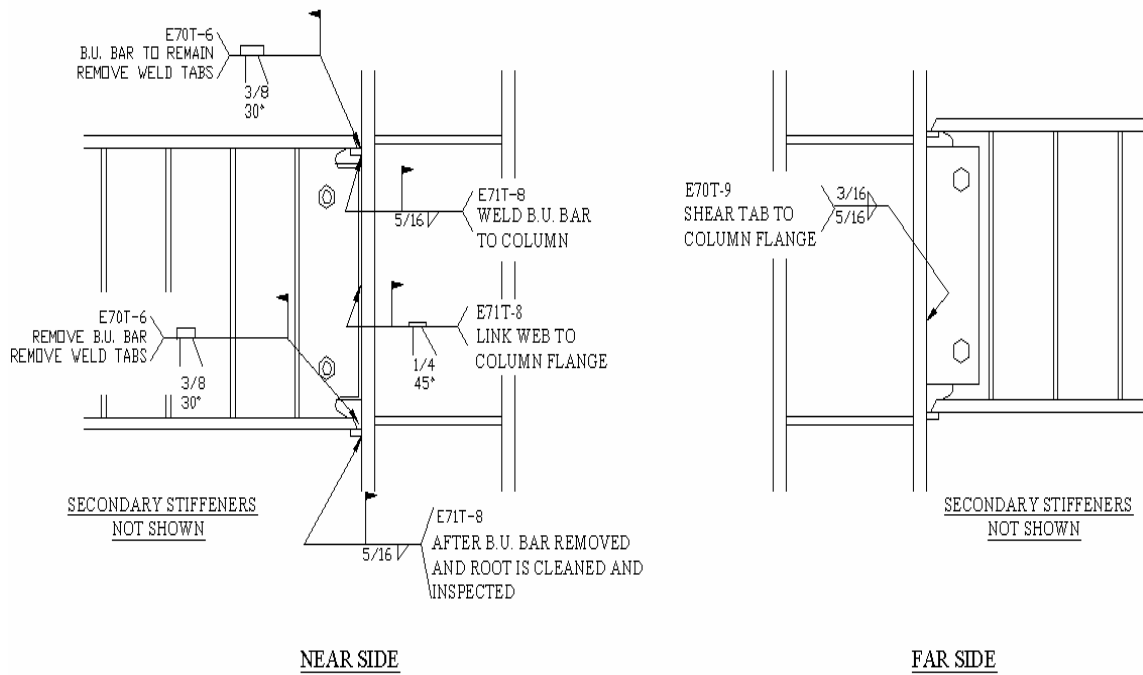


Figure 2.28: Specimens AISC-5 & 8 – Connection Details

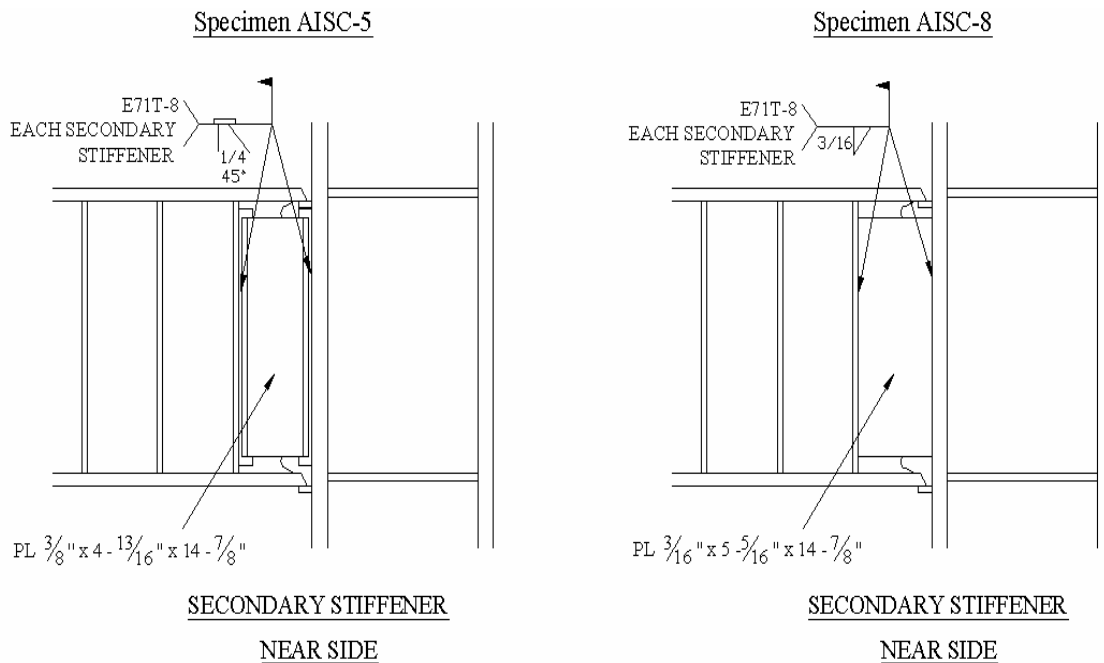


Figure 2.29: Specimens AISC-5 & 8 – Secondary Stiffener Detail



Figure 2.30: Overall View of Specimen AISC-5 after Completion of Fabrication



Figure 2.31: Specimen AISC-5 – Link-to-Column Connection Region – Frontside of Link



Figure 2.32: Specimen AISC-5 after Completion of Fabrication – Backside of Link



Figure 2.33: Overall View of Specimen AISC-8 after Completion of Fabrication



Figure 2.34: Specimen AISC-8 – Link-to-Column Connection Region – Frontside of Link



Figure 2.35: Specimen AISC-8 after Completion of Fabrication – Backside of Link

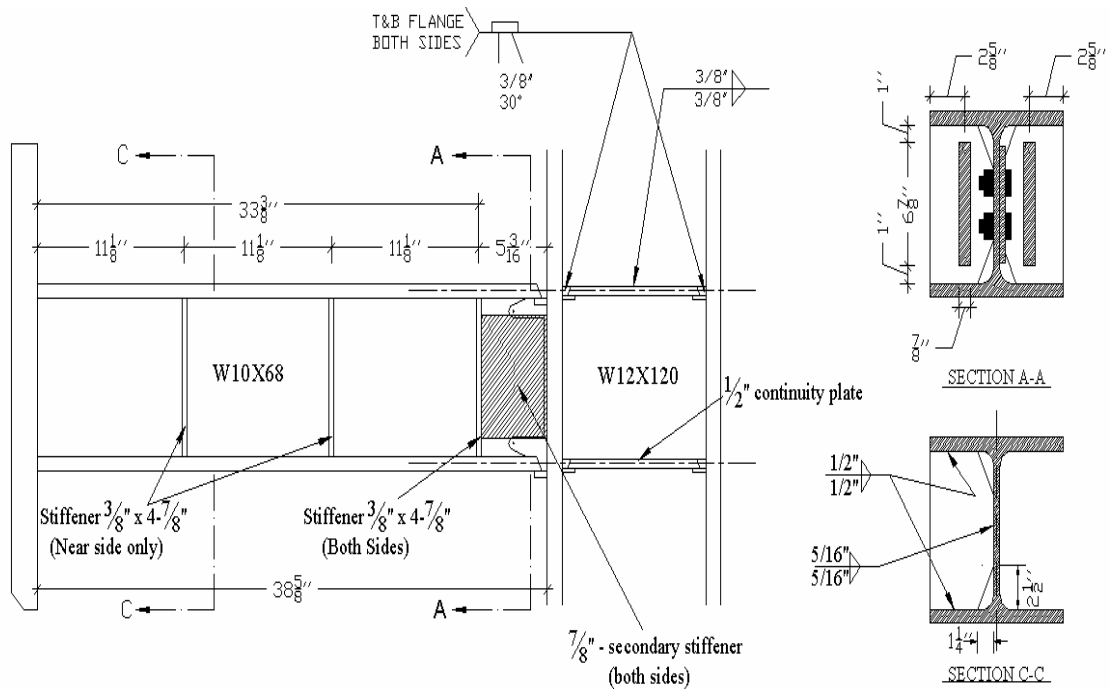


Figure 2.36: Specimen AISC-6 – Overall Layout

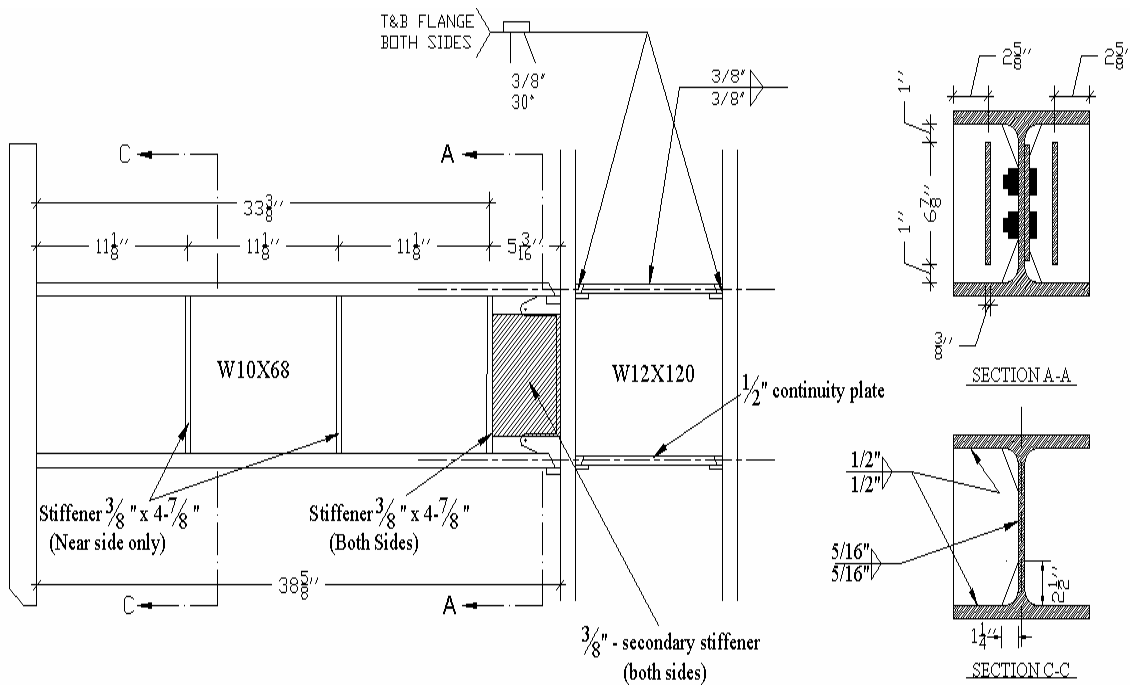


Figure 2.37: Specimen AISC-7 – Overall Layout

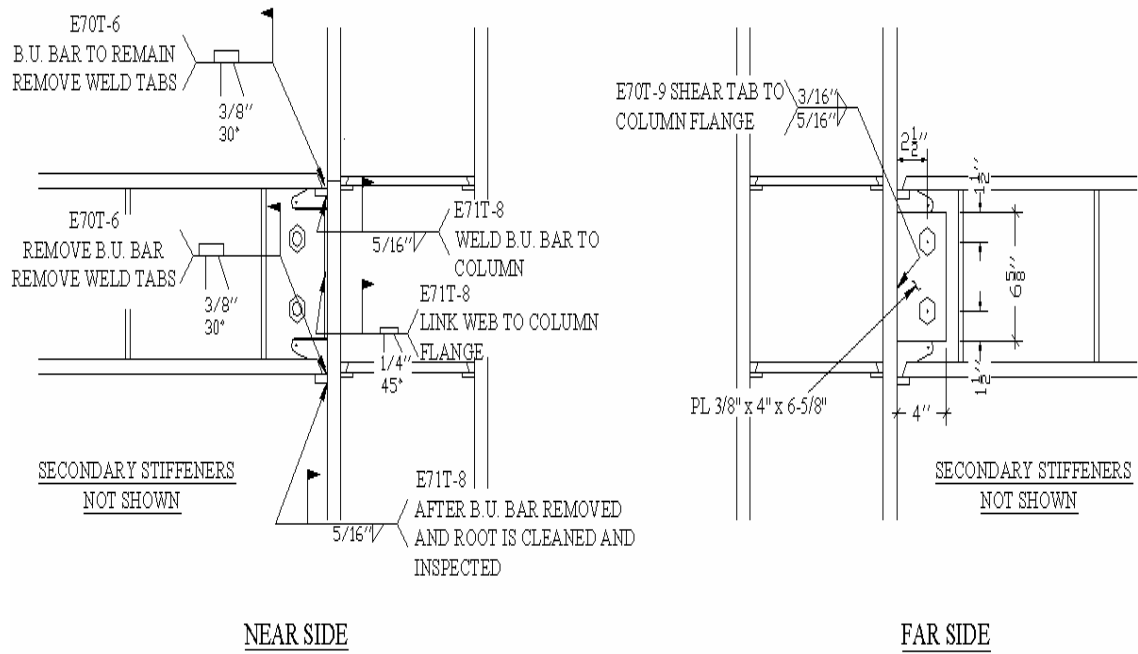


Figure 2.38: Specimens AISC-6 & 7 – Connection Details

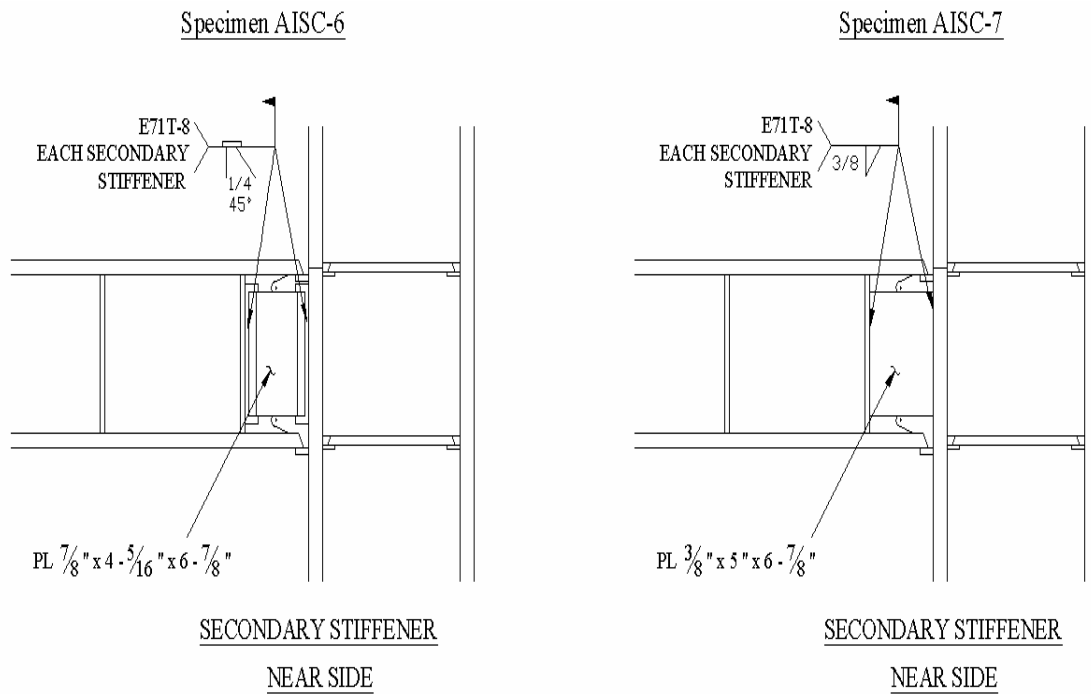


Figure 2.39: Specimens AISC-6 & 7 – Secondary Stiffener Detail



Figure 2.40: Overall View of Specimen AISC-6 after Completion of Fabrication



Figure 2.41: Specimen AISC-6 – Link-to-Column Connection Region – Frontside of Link



Figure 2.42: Specimen AISC-6 after Completion of Fabrication – Backside of Link



Figure 2.43: Overall View of Specimen AISC-7 after Completion of Fabrication

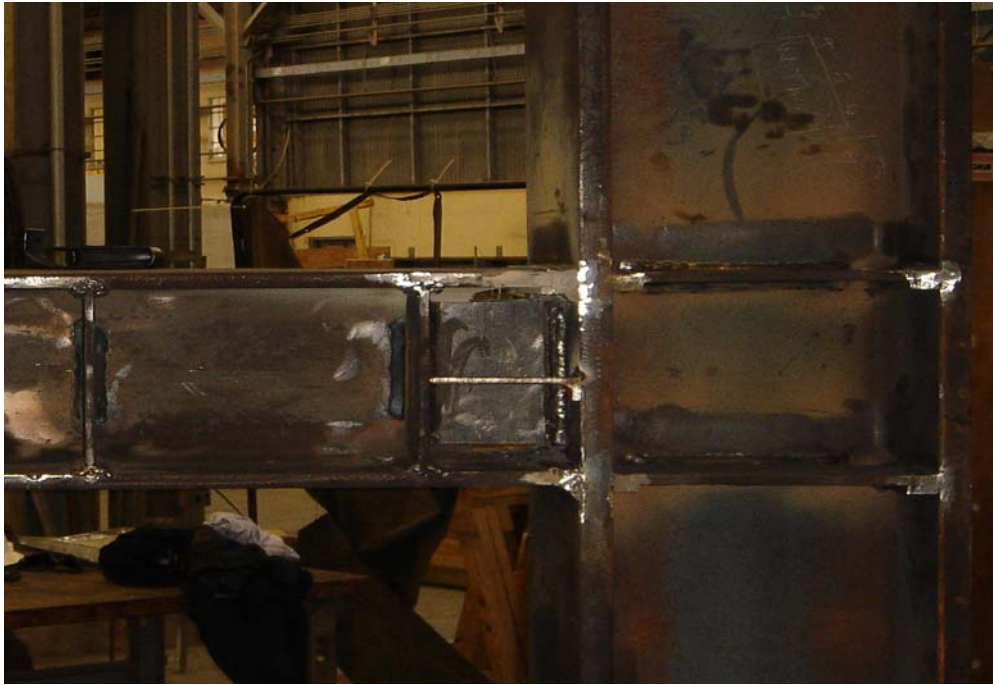


Figure 2.44: Specimen AISC-7 – Link-to-Column Connection Region – Frontside of Link



Figure 2.45: Specimen AISC-7 after Completion of Fabrication – Backside of Link

2.4 INSTRUMENTATION

The instrumentation of the test setup was originally designed by Okazaki and Arce, in such a way to permit the calculation of the forces and deformations of the link. To be more precise, the link forces, such as the shear force in the link and the link end moments, can be derived from the reactions measured at the four load cells of the test setup, as shown in Figure 2.1. Furthermore, the link deformations are quantified using the displacement transducers, as shown in Figure 2.46. The rotation transducers were not used for this project.

The displacement transducers of the greatest interest are those measuring the vertical displacements of the two link ends. By dividing the relative vertical displacement of the link with the link length, one can define the most important parameter of the investigation, the link rotation. Thus, at the link ends, two transducers, one on each side, were used in order to assure accurate results. The relative displacement was calculated by subtracting the displacement of the left end from that of the right end. The displacements were taken as the mean values of the two transducers.

For the specimens of Phase II, one additional displacement transducer was placed at the link top flange at the first vertical stiffener, in order to monitor the displacement history of the unreinforced part of the link also. By monitoring the displacement history of the unstiffened part of the link, one can calculate the plastic rotation of the active link.

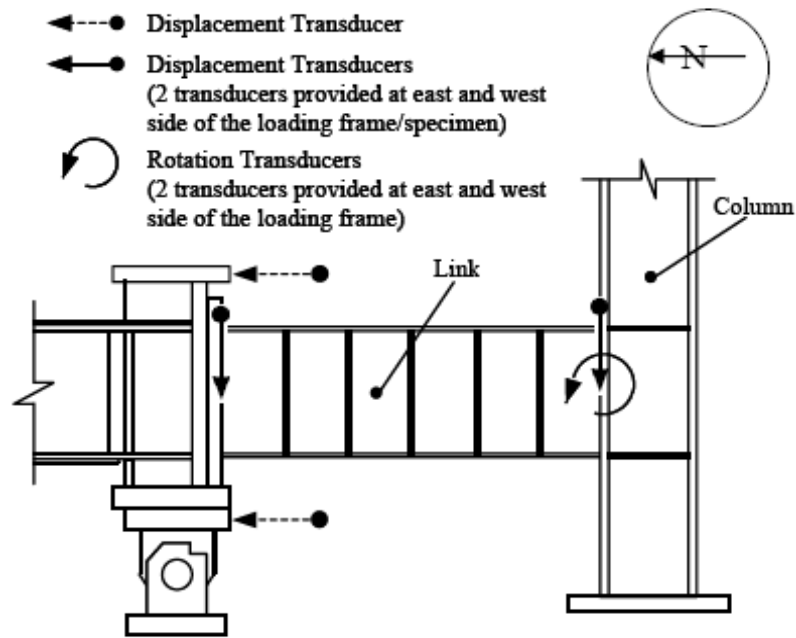


Figure 2.46: Transducers to monitor link deformation (Okazaki; 2004)

2.5 TEST PROCEDURE

2.5.1 Loading Protocol

The tests were conducted by applying increasing levels of cyclic link rotation angle, γ . The link rotation is calculated by dividing the relative vertical displacement of the link over the link length. Further information will be presented in Section 2.5.2.

The cyclic loading sequence was in accordance with the predetermined loading protocol stated in the Appendix S of the 2005 AISC *Seismic Provisions*. This loading protocol was suggested by Richards and Uang (2003) after an extensive study on testing short shear links subjected to strong ground motions, which showed that the previously adopted AISC protocol was unrealistically too severe for testing these short shear links. The loading protocol is summarized in the Table 2.12 and portrayed in Figure 2.47.

As one can observe, this loading protocol requires a large number of small elastic cycles. Furthermore, it requires that the total link rotation angle will be increased in increments of 0.02 rad after the specimen reaches a rotation of 0.05 rad. Significant yielding of the link normally occurs at a total link rotation angle of about 0.01 rad.

Table 2.12: AISC Seismic Loading Protocol

Total Link Rotation Angle, γ (rad)	Number of Cycles
± 0.00375	6
± 0.005	6
± 0.0075	6
± 0.01	6
± 0.015	4
± 0.02	4
± 0.03	2
± 0.04	1
± 0.05	1
± 0.07	1
± 0.09	1
± 0.11	1
± 0.13	1
Continue at increments of $\gamma = \pm 0.02$ rad with one cycle at each amplitude	

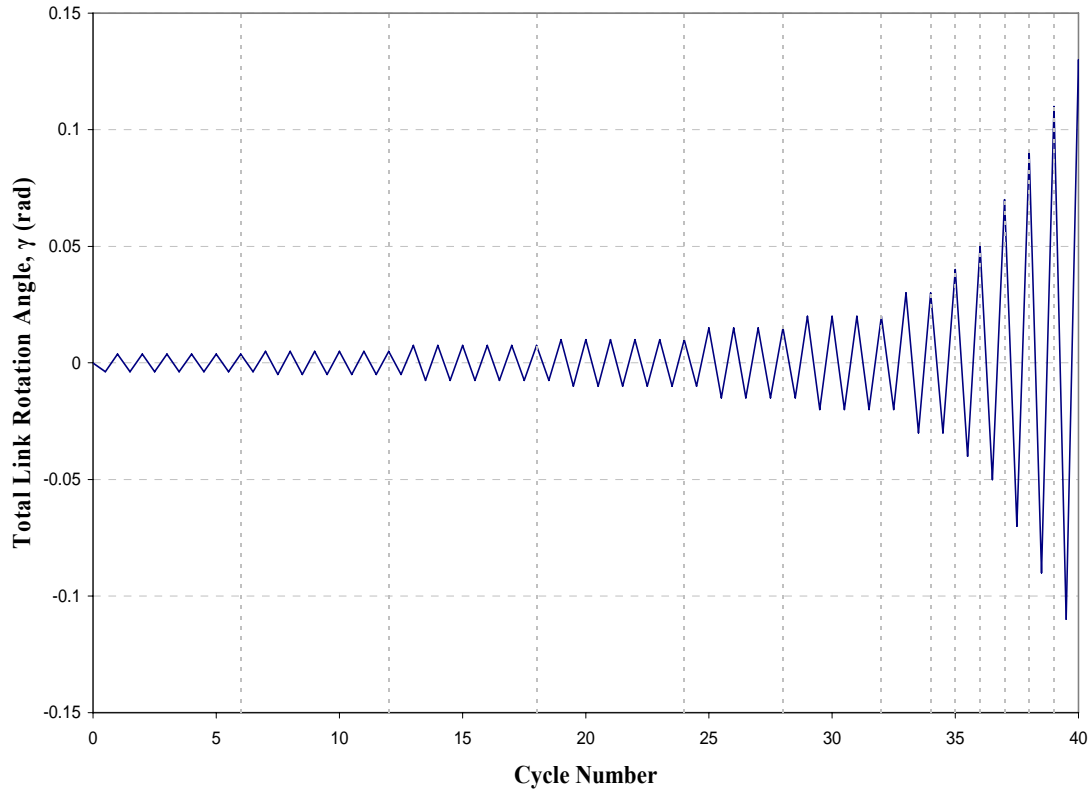


Figure 2.47: 2005 AISC Loading Protocol

2.5.2 Data Reduction Procedure

The most important parameters to be calculated are: the link shear force, V , the column face bending moment, M_c , and the link rotation angle, γ . These quantities can be computed by applying simple static equilibrium and using the data from the four reaction rods, $R_1 - R_4$, and the loading ram, P . Figure 2.48 shows the numbering of the reaction rods.

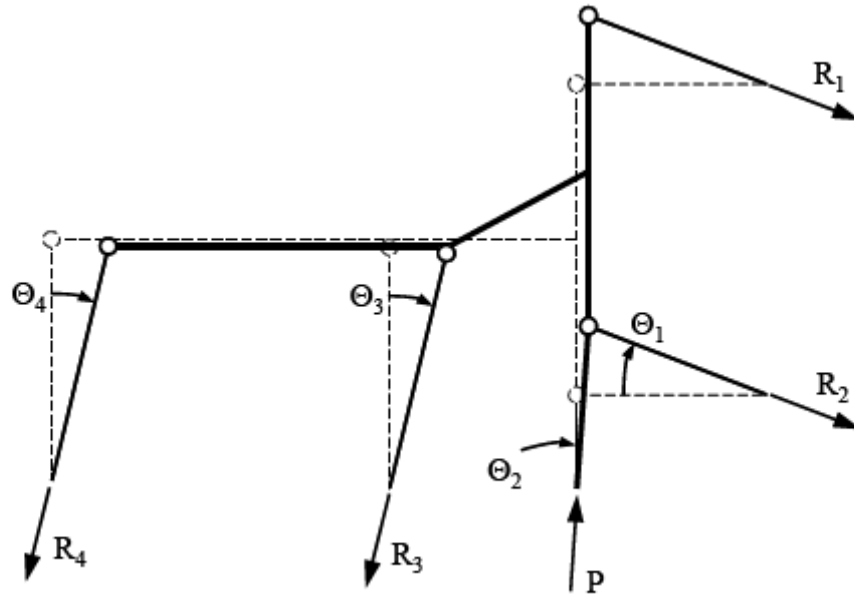


Figure 2.48: Measured reactions and movement of reaction rods (Okazaki; 2004)

The angles Θ_1 to Θ_4 , formed due to the deformation of the test setup, are defined as shown in Figure 2.48. The angles Θ_3 and Θ_4 can be calculated as follows:

$$\Theta_3 = \frac{\Delta_3}{100}$$

$$\Theta_4 = \frac{\Delta_4}{100}$$

Where, Δ_3 and Δ_4 is the distance of the clevis-hinge point movement and the quantity 100 is the length, in inches, of the reaction rods 3 and 4. The angles Θ_2 to Θ_4 are very small and assumed to be zero.

The link forces V , M_b , M_c can be computed as follows:

$$\begin{aligned} V &= R_3 \cos(\Theta_3) + R_4 \cos(\Theta_4) \\ M_b &= -206 R_4 \cos(\Theta_3) - 6 R_3 \cos(\Theta_4) \\ M_c &= V \cdot L - M_b \end{aligned} \quad (2.1)$$

Where, 206 inches and 6 inches are the lengths of the beam from the reaction rods 4 and 3 to the link, respectively.

Finally, the definition of the link rotation angle, γ , and link end rotations, θ_b and θ_c , are illustrated in Figure 2.49. The link rotation, γ , is a combination of the rotation at the two ends of the link, and the elastic-plastic deformation of the link itself. Moreover, the rotation at the beam end side of the link comes from the flexural deformation of the horizontal beam, while the rotation at the column end side comes from the column panel zone deformation, in addition to the flexural deformation of the column.

The AISC *Seismic Provisions* do not use the total (elastic + plastic) rotation angle, γ , to evaluate the performance of the link. Instead, the *Seismic Provisions* utilize only the plastic component of the link rotation angle, γ_p . To obtain the plastic link rotation, the elastic component of the link rotation is subtracted from the total link rotation angle, as follows:

$$\gamma_p = \gamma - \gamma_e \Leftrightarrow \gamma_p = \gamma - \frac{V}{K_e} \quad (2.2)$$

NOTE:
 Δ_1 and Δ_2 are evaluated by taking
the average of the values measured
from the east and west sides of the link.

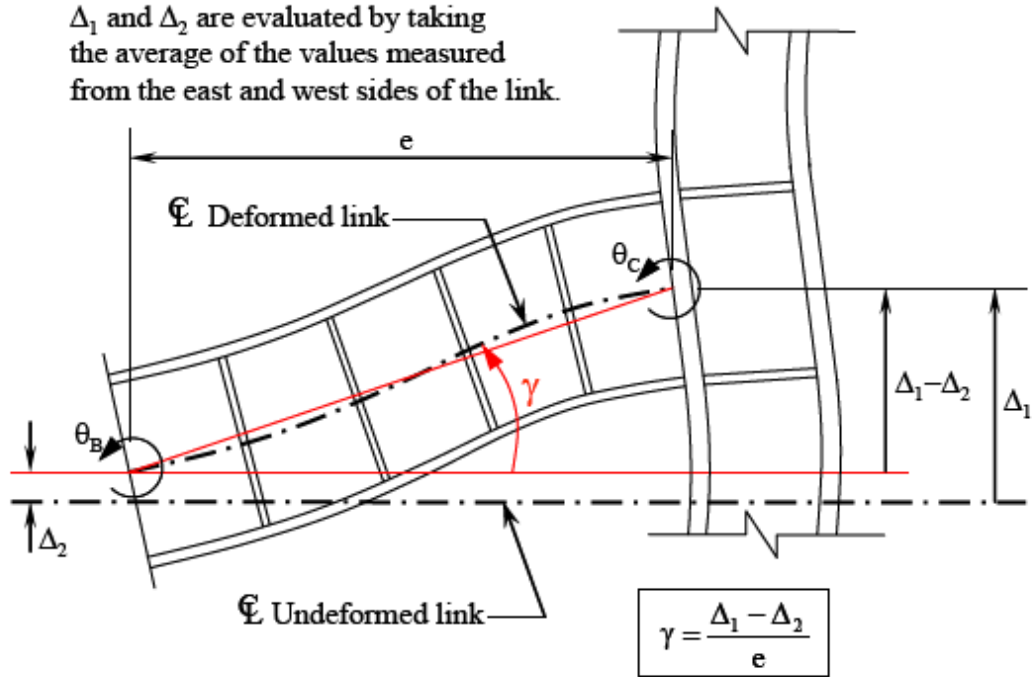


Figure 2.49: Data for the Link Deformation and Rotation (Okazaki; 2004)

CHAPTER 3

Test Results

3.1 GENERAL

This chapter provides a description of the experimental performance of the eight specimens tested in this research project. First the essential parameters which characterize the load versus deformation response of the links are reviewed. Next, the performance of each specimen is described along with key events such as yielding, development of various forms of instability, and fracture. Possible instabilities that can occur are local buckling (flange or web) and lateral-torsional buckling. The initiation of yielding as well as the area yielding was observed in each specimen is mentioned. Description of yielding is based on observations of the flaking of whitewash. Later in this chapter, a general discussion about the specimens' performance and the two different link-to-column connection details is provided. Finally, the basic load-deformation response plots are presented together with photographs characterizing the response and the failure mode of the specimens.

3.2 LINK RESPONSE PARAMETERS

The key response parameters used to evaluate the performance of the specimens are the link shear force, V , the total link rotation angle, γ , and the plastic link rotation angle, γ_p . The link shear force can be calculated using equation (2.1), while the quantities γ and γ_p are calculated based on Figure 2.49 and equation (2.2), respectively. For the Phase II specimens, γ and γ_p were computed based both on the total link length, e , and on the unreinforced link length, e_{active} .

As noted in equation (2.2) the link plastic rotation, γ_p , is calculated by subtracting the elastic, or recoverable, component of the link rotation from the total link rotation angle, γ . The elastic component of the link rotation, γ_e , is computed as the link shear divided by the elastic stiffness, K_e . The elastic stiffness K_e in turn, is taken as the slope of the shear force versus total link rotation diagram determined from the first few elastic cycles. Since all parts of the test setup outside the links remained elastic during testing, γ_p reflects only the inelastic deformations developed within the link

The plastic link rotation developed by each specimen, “Test γ_p ”, is compared to the required plastic link rotation based on the link length, “Target γ_p ”, as stated in Tables 2.8 and 2.10. The actual plastic rotation achieved by each specimen was determined as the plastic rotation sustained for at least one full cycle of loading, prior to the degradation of the shear resistance of the specimen below the nominal shear strength of the link, V_p . This method of defining the plastic rotation of a test specimen is specified in the 2005 *AISC Seismic Provisions*.

3.3 DESCRIPTION OF TEST SPECIMEN PERFORMANCE

This section describes the experimental performance of each specimen. The four specimens of Phase I, AISC-1 through 4, are presented first, followed by the four specimens of Phase II, AISC-5 through 8.

3.3.1 Specimen AISC-1

Specimen AISC-1 was the first specimen tested to evaluate the shop-welded link-to-column connection detail, or “Column-Tree” approach. The link-to-column connection was composed of simple all-around fillet welds with a leg size equal to 1.5-times the

thickness of the connected flange or web. The fillet welds were made using the SMAW process with E7018 electrodes of 5/32" diameter. Although this process and electrode used is not favored in practice due to low deposition rates; it has been shown to provide high levels of notch-toughness (Johnson 2000). Thus, this specimen was used to compare the performance of the gas-shielded FCAW process with E70T-9 electrodes used in the remaining three specimens.

Specimen AISC-1 had a link of length $e = 38.6" = 1.72M_p / V_p$. Based on this link length, the required, or target, plastic rotation per the 2005 AISC *Seismic Provisions* is ± 0.073 rad.

Up through completion of the loading cycle at $\gamma = \pm 0.11$ rad, no significant distress at the link-to-column connection or within the link was observed and there was no deterioration in strength. Three independent cracks along the toe of the fillet weld between the link flange and the column flange; two at the two edges of the link flanges, and a third crack at the mid-width of the link flange were observed, starting from the loading cycle at $\gamma = \pm 0.09$ rad ($\gamma_p = \pm 0.075$ rad). These cracks were visible at both the top and bottom link flanges. After the cycle at $\gamma = \pm 0.11$ rad, the stroke of the loading ram was, nearly, exhausted in one direction of loading. Loading was then continued by applying additional cycles at $\gamma = + 0.12 / - 0.13$ rad until failure of the specimen. Failure occurred at the beginning of the second cycle at $\gamma = + 0.12$ rad, by fracture of the link top flange near the fillet weld to the column flange. This fracture extended to the link web, as shown in Figure 3.5. After completion of the first loading cycle at $\gamma = - 0.13$ rad, as the top flange was subjected to tension, the fracture at the mid-width of the link flange developed rapidly, causing the strength degradation of the specimen, as shown in Figure 3.4.

Figure 3.3 shows specimen AISC-1 after failure. The flaking of the whitewash reveals the extensive yielding that took place in the link web panels. Figure 3.3 demonstrates the local buckling occurred in the link flanges near both ends of the link. Finally, it has to be mentioned that small cracks were also observed in the link web at the termination of the stiffeners' welds. However, the specimen failed at the link-to-column connection before the link web fracture developed significantly.

The hysteretic response of Specimen AISC-1 is shown in Figures 3.1 and 3.2. Based on a total link length of $e = 38.6$ inches, the plastic rotation achieved by this specimen was, approximately, $\gamma_p = + 0.109 / - 0.118$ rad. This specimen showed outstanding overall performance. The target plastic rotation angle of 0.073 rad was achieved, and in fact exceeded by 50-percent. Consequently, the link-to-column connection of Specimen AISC-1 satisfied the performance requirements of the 2005 *AISC Seismic Provisions*.

3.3.2 Specimen AISC-2

Specimen AISC-2 had the same link-to-column connection detail and the same size of fillet welds as specimen AISC-1. The two specimens differed only in the welding process and electrode used. Specifically, specimen AISC-2 was fabricated by using the FCAW-GS process with E70T-9 electrodes of 3/32-inch diameter. This electrode has specified notch-toughness values that satisfy the requirements of Demand Critical Welds of the 2005 *Seismic Provisions*.

Specimen AISC-2 had a link of length $e = 38.6" = 1.72M_p / V_p$. Based on this link length, the required plastic rotation per the 2005 AISC Seismic Provisions is ± 0.073 rad.

Up through completion of loading cycle at $\gamma = \pm 0.11$ rad, no significant distress at the link-to-column connection or within the link was observed and there was no deterioration in strength. During the loading cycle at $\gamma = \pm 0.09$ rad ($\gamma_p = \pm 0.075$ rad), four independent cracks, including three cracks along the toe of the fillet weld, as in Specimen AISC-1, and a crack in the throat of the fillet weld were noticed. The throat crack propagated along the interface of the weld passes. The cracks were observed at both the link top and bottom flanges. Figure 3.8 depicts the four independent cracks of the link top flange. After the cycle at $\gamma = \pm 0.11$ rad, the loading was continued by applying an additional cycle at $\gamma = \pm 0.13$ rad. Failure occurred at the beginning of this cycle before the specimen reached $\gamma = + 0.12$ rad, by a propagation of the crack initiating at the edge of the link top flange, as shown in Figure 3.8.

Although the failure of the specimen was due to a fracture of the link top flange, fractures were also developing, very similarly, in the link bottom flange. It is likely that the link top flange fractured first, primarily, due to the order of cyclic loading which subjects the link top flange to tension, at a given rotation level first, before the link bottom flange is subjected to tension by reversing the loading.

Fractures were also observed in the link web at the termination of the stiffener welds. However, the specimen failed at the link-to-column connection before the link web fracture developed significantly.

The hysteretic response of Specimen AISC-2 is shown in Figures 3.6 and 3.7. Based on a total link length of $e = 38.6$ inches, the plastic rotation achieved by this specimen was approximately $\gamma_p = \pm 0.093$ rad. This specimen showed outstanding overall performance. The target plastic rotation angle of 0.073 rad was achieved and in fact exceeded by approximately 25-percent. Consequently, the link-to-column connection of

Specimen AISC-2 satisfied the performance requirements of the 2005 AISC *Seismic Provisions*.

3.3.3 Specimen AISC-3

Specimen AISC-3 was also welded using the FCAW-GS process with the E70T-9 electrodes of 3/32-inch diameter, similar to Specimen AISC-2. The two specimens differed only in the leg size of the fillet welds used in the link-to-column connection. Specimen AISC-3 had a leg size approximately equal to the thickness of the connected flange or web. The intent of this experiment was to evaluate the viability of smaller sized fillet welds.

Specimen AISC-3 had a link of length $e = 38.6" = 1.72M_p / V_p$. Based on this link length, the required plastic rotation per the 2005 AISC *Seismic Provisions* is ± 0.073 rad.

Up through completion of loading cycle at $\gamma = \pm 0.07$ rad, no significant distress at the link-to-column connection or within the link was observed and there was no deterioration in strength. Loading was then continued by applying an additional cycle at $\gamma = \pm 0.09$ rad. Before $\gamma = - 0.09$ rad was reached, a fracture at the link bottom flange, adjacent to the link-to-column fillet weld occurred, as shown in Figure 3.12. However, the specimen did not lose all of its strength. Another loading cycle was then applied at $\gamma = \pm 0.11$ rad. Failure occurred at the beginning of the cycle at $\gamma = + 0.11$ rad, by a fracture at the link top flange, adjacent to the link-to-column fillet weld, as shown in Figure 3.13.

The hysteretic response of Specimen AISC-3 is shown in Figures 3.9 and 3.10. Based on a total link length of $e = 38.6$ inches, the plastic rotation achieved by this specimen was approximately, $\gamma_p = \pm 0.057$ rad. Thus, the target plastic rotation of 0.073 rad was not achieved. Consequently, Specimen AISC-3 did not satisfy the performance

requirements of the 2005 AISC *Seismic Provisions*. This Specimen indicated that fillet welds with a leg size equal to the thickness of the connected flange are not adequate for the link to column connection.

3.3.4 Specimen AISC-4

Specimen AISC-4 differed completely from the previously three specimens tested in Phase I. A W10x68 section was used in order to evaluate the viability of a shop-welded link-to-column connection detail specially designed for links with thick flanges. Specifically, the link web was welded to the column flange with a double-sided fillet weld with a leg size 1.5-times the link web thickness. The link flanges were connected to the column flange using a partial joint penetration groove weld. The bevels were made in the outer surface of each flange, while the inside faces of the flanges were fillet welded with a leg equal to the thickness of the link flange.

Specimen AISC-4 had a link of length $e = 38.6" = 1.30M_p / V_p$. Based on this link length, the required plastic rotation per the 2005 AISC *Seismic Provisions* is ± 0.08 rad.

Up through completion of the loading cycle at $\gamma = \pm 0.11$ rad, no significant distress at the link-to-column connection or within the link was observed and there was no deterioration in strength. After the completion of the loading cycle at $\gamma = \pm 0.05$ rad, small cracks were noticed at the termination of the stiffener welds of both stiffeners. During loading cycles at $\gamma = \pm 0.07$ rad and ± 0.09 rad, the web cracks at the termination of the stiffener welds grew in size, without causing any strength loss. At the loading cycle of $\gamma = \pm 0.11$ rad, the final full cycle before failure, the crack in the link web propagated along the fillet weld of the stiffener closest to the connection, as shown in Figure 3.17. However, no distress was observed at the connection, and no loss in strength occurred

during this cycle. Loading was then continued by applying an additional cycle at $\gamma = \pm 0.13$ rad. Failure occurred during the cycle to $\gamma = + 0.13$ rad, by fracture of the link web, with the fracture initiating at the termination of a fillet weld of the vertical stiffener closest to the link-to-column connection, as seen in Figure 3.18 and 3.19. At the end of the test there was no sign of fracture initiation or any other form of distress at the link-to-column connection.

Cracks in the link web at the termination of the fillet welds of the stiffener furthest from the connection were also observed. However, the specimen failed before these cracks propagated. After the loading cycle at $\gamma = \pm 0.11$ rad, a small amount of flange local buckling was noticed at the two link ends. At the end of the test, a large amount of flange and web local buckling was observed near the link-to-column connection, due to the severe failure of the link web.

The hysteretic response of Specimen AISC-4 is shown in Figures 3.14 and 3.15. Based on a total link length of $e = 38.6$ inches, the plastic rotation achieved by this specimen was, approximately, $\gamma_p = \pm 0.095$ rad. This specimen showed outstanding overall performance. The target plastic rotation angle of 0.08 rad was achieved and in fact exceeded by approximately 19-percent. Consequently, the partial penetration weld detail of Specimen AISC-4 satisfied the performance requirements of the 2005 AISC *Seismic Provisions*.

3.3.5 Specimen AISC-5

Specimen AISC-5 was the first specimen tested to evaluate the “reinforced” link-to-column connection detail. The specimen was constructed using a W18x40 link section. The connection was reinforced with two 3/8-inch thick supplemental stiffeners placed in the first panel of the link adjacent to the column. One supplemental stiffener was

provided on each side of the link and was placed parallel to the link web. Each supplemental stiffener was welded to the column flange and to the first vertical web stiffener using CJP groove welds. The supplemental stiffeners were designed based on the procedure discussed in Section 2.3.4.2.

Specimen AISC-5 had a link of length $e = 38.6" = 1.72M_p / V_p$. Based on this link length, the required, or target, plastic rotation per the 2005 AISC *Seismic Provisions* is ± 0.073 rad. However, based on the active link length of the specimen which was $e_{active} = 33.1" = 1.47M_p / V_p$, the required plastic rotation per the 2005 AISC *Seismic Provisions* is ± 0.08 rad.

Until the point where the specimen was loaded up through the cycle at $\gamma = \pm 0.11$ rad, there was no apparent distress at the link-to-column connection or within the link, and no deterioration in strength. Inelastic rotation appeared to be largely confined to the unreinforced portion of the link. From the loading cycle at $\gamma = \pm 0.09$ rad, cracks at the termination of the vertical stiffener welds initiated. After the loading cycle at $\gamma = \pm 0.11$ rad, the stroke of the loading ram was nearly exhausted in one direction of the loading. Loading was then continued by applying additional cycles at $\gamma = + 0.11 / - 0.13$ rad. Failure occurred during the second cycle of loading before the specimen reached $\gamma = + 0.11$ rad, by fracture of the link web at the vertical stiffener farthest from the link-to-column connection, as shown in Figures 3.27 and 3.28. At the end of the experiment there was no significant distress apparent at the link-to-column connection.

Figures 3.25 and 3.26 show specimen AISC-5 after the last full cycle prior to failure. The flaking of the whitewash reveals the extensive yielding that took place in the link web panels. Figure 3.25 also shows that local buckling occurred in the link flanges near the left link end, and the first primary stiffener, away from the link-to-column

connection. Figure 3.26, indicates that yielding was primarily restricted away from the link-to-column connection.

The hysteretic response of Specimen AISC-5 is shown in Figures 3.21 through 3.24. Based on a total link length of $e = 38.6$ inches, the plastic rotation achieved by this specimen was, approximately, $\gamma_p = \pm 0.10$ rad. However, as noted above, inelastic rotation occurred primarily within the 33.1" unreinforced link length. Based on an active link length of 33.1", the plastic rotation achieved by this specimen was approximately $\gamma_p = \pm 0.12$ rad. Thus, it can be concluded that regardless of how the link length is computed, this specimen easily satisfied the plastic rotation requirements of the 2005 AISC *Seismic Provisions*. The overall performance of this link-to-column connection was excellent.

3.3.6 Specimen AISC-6

Specimen AISC-6 had the same reinforced link-to-column connection detail as the previous specimen, but used a W10x68 section for the link. The connection was reinforced using two supplemental stiffeners placed as described above. Each supplemental stiffener was welded to the column flange and to the first vertical web stiffener using CJP groove welds. The supplemental stiffeners were designed based on the procedure discussed in Section 2.3.4.2. According to this design, each supplemental stiffener's thickness was 7/8-inch. The welding of such thick plates to the first vertical stiffeners, with thickness only 3/8-inch, required a large number of weld passes which led to the bending of the first primary stiffeners due to the weld shrinkage. Figure 3.34 shows the bending of the first primary stiffener.

Specimen AISC-6 had a link of length $e = 38.6" = 1.30M_p / V_p$, and an active link length of $e_{active} = 33.2" = 1.13M_p / V_p$. Regardless of how the link length is

calculated, the required, or target plastic rotation per the 2005 AISC *Seismic Provisions* is ± 0.08 rad.

No apparent distress at the link-to-column connection or within the link, and no deterioration in strength of the specimen was observed up through the completion of the loading cycle at $\gamma = \pm 0.11$ rad. The inelastic rotation was limited primarily in the unreinforced portion of the link. After the loading cycle at $\gamma = \pm 0.11$ rad, the stroke of the loading ram was nearly exhausted in one direction of loading. Loading was then continued by applying additional cycles at $\gamma = + 0.12 / - 0.13$ rad, until failure of the specimen. Failure occurred at the beginning of the second loading cycle at $\gamma = + 0.12 / - 0.13$ rad, by fracture of the link web at the vertical stiffener farthest from the link-to-column connection. Figure 3.37 shows the fracture of the link web, initiating from the termination of the stiffener weld. At the end of testing, there was no apparent distress at the link-to-column connection.

Figures 3.35 and 3.36 show specimen AISC-6 after the last full cycle prior to failure. The flaking of the whitewash indicates that extensive yielding took place in the link web panels. Figure 3.35 further demonstrates that the inelastic rotation was largely confined to the unreinforced portion of the link, while the reinforced portion remained primarily elastic. This is also depicted in Figure 3.36 from the flaking of the whitewash at the link bottom flange of the unreinforced part only. Local buckling at the link web was also observed. Finally, it is noted that the welding induced distortion of the first primary stiffeners did not affect the overall performance of the specimen.

The hysteretic response of Specimen AISC-6 is shown in Figures 3.29 through 3.32. Based on a total link length of $e = 38.6$ inches, the plastic rotation achieved by this specimen was approximately $\gamma_p = \pm 0.095$ rad, while based on an active link length of 33.4", the plastic rotation achieved by this specimen was approximately $\gamma_p = \pm 0.11$ rad.

The target plastic rotation angle of 0.08 rad was achieved and in fact exceeded by 20-percent or 38-percent respectively. Thus, it can be concluded that regardless of how the link length is computed, this specimen easily satisfied the plastic rotation requirements of the 2005 AISC *Seismic Provisions*. The overall performance of the link-to-column connection was excellent.

3.3.7 Specimen AISC-7

Specimen AISC-7, constructed using a W10x68 link, was nominally identical to AISC-6, except for the supplemental stiffener thickness and welding details. Specifically, in Specimen AISC-7 the thickness of the supplemental stiffeners was reduced to 3/8", and the supplemental stiffeners were connected to the column flange and the first vertical stiffener using one-side 3/8" fillet welds. The intension of this specimen was to evaluate a less costly reinforced link-to-column connection. Welding the supplemental stiffeners with fillet welds requires that their width will be nearly equal to the actual clear distance of the column flange to the first vertical stiffener. This difficulty was addressed by cutting the supplemental stiffeners after the link was welded to the column flange and the actual distance was measured.

Specimen AISC-7 had a link of length $e = 38.6" = 1.30M_p / V_p$, and an active link length of $e_{active} = 33.2" = 1.13M_p / V_p$. Regardless of how the link length is calculated, the required or target plastic rotation per the 2005 AISC *Seismic Provisions* is ± 0.08 rad.

Up through completion of the loading cycle at $\gamma = \pm 0.11$ rad, no significant distress at the link-to-column connection or within the link was observed, and there was no deterioration in strength. After the loading cycle at $\gamma = \pm 0.05$ rad a larger amount of yielding at the top and bottom flanges of the left side of the link, and a smaller amount of

yielding at the flanges at the location of the first vertical stiffener, outside the link-to-column connection, was observed. Small cracks were observed in the link web at the termination of the fillet welds of the two vertical stiffeners farthest from the column, starting from the loading cycle at $\gamma = \pm 0.07$ rad, as seen in Figure 3.45. After the cycle at $\gamma = \pm 0.11$ rad, the stroke of the loading ram was nearly exhausted in one direction of loading. Loading was then continued by applying an additional cycle at $\gamma = + 0.12 / - 0.13$ rad. Failure occurred before the total rotation of $\gamma = - 0.13$ rad was reached, by fracture of the link web, at the middle vertical stiffener, as shown in Figures 3.46 and 3.47. As seen in Figure 3.48, there was no apparent distress at the link-to-column connection after the completion of the experiment. Figure 3.47 further shows that the yielding occurred primarily in the unreinforced portion of the link. Minor yielding was also observed within the panel zone region of the column.

Figures 3.43 through 3.45 show specimen AISC-7 after the last full cycle prior to failure. The flaking of the whitewash reveals the extensive yielding that took place in the link web panels. During testing, a small amount of web local buckling was also noticed in the link,. No significant flange local buckling was noted.

The hysteretic response of Specimen AISC-7 is shown in Figures 3.38 through 3.41. Based on a total link length of $e = 38.6$ inches, the plastic rotation achieved by this specimen was approximately $\gamma_p = \pm 0.094$ rad, while based on an active link length of 33.4", the plastic rotation achieved by this specimen was approximately $\gamma_p = \pm 0.11$ rad. The target plastic rotation angle of 0.08 rad was achieved, and in fact exceeded by 18-percent or 38-percent respectively. Thus, it can be concluded that regardless of how the link length is computed, this specimen easily satisfied the plastic rotation requirements of the 2005 AISC *Seismic Provisions*. The overall performance of the link-to-column connection was excellent.

3.3.8 Specimen AISC-8

Specimen AISC-8 was the last specimen tested in this research project. It was nominally identical to specimen AISC-5 except for the supplemental stiffener thickness and welding details. Specifically, in specimen AISC-8, the thickness of the supplemental stiffeners was reduced to 3/16", and the supplemental stiffeners were connected to the column flange and the first vertical stiffener using one-sided 3/16" fillet welds. The intention of this specimen was not only to evaluate the performance of a thinner supplemental stiffener, but also to find a lower bound in the thickness and the welding detail of the supplemental stiffeners.

Specimen AISC-8 had a link of length $e = 38.6" = 1.72M_p / V_p$. Based on this link length, the required, or target, plastic rotation per the 2005 AISC *Seismic Provisions* is ± 0.073 rad. However, based on the active link length of the specimen which was $e_{active} = 33.1" = 1.47M_p / V_p$, the required plastic rotation per the 2005 AISC *Seismic Provisions* is ± 0.08 rad.

Up through completion of the loading cycle at $\gamma = \pm 0.07$ rad, no significant distress at the link-to-column connection or within the link was observed and there was no deterioration in strength. From the loading cycle at $\gamma = \pm 0.02$ rad, major yielding of the link flanges at the first vertical stiffener started spreading along the reinforced portion of the link, while there was no significant yielding at the left end of the link. After the loading cycle at $\gamma = \pm 0.05$ rad, yielding at the link flanges was extended between the first and the second vertical stiffeners. However, after the loading cycle at $\gamma = \pm 0.07$ rad, the final complete cycle before failure, yielding at the link flanges also spread to the link-to-column connection. At the last loading cycle at $\gamma = \pm 0.09$ rad, failure occurred before the total rotation of $\gamma = -0.09$ rad was reached, by complete fracture of the link bottom flange adjacent to the weld of the link-to-column connection. In addition, a throat fracture of a

portion of the fillet welds of both secondary stiffeners adjacent to the link-to-column connection occurred. Figures 3.56 through 3.58 and Figure 3.59 show the final failure of this specimen from front and the back views of the specimen, respectively. At the end of the test, no apparent distress at the link top flange was found.

Figures 3.54 and 3.55 show specimen AISC-8 after the last full cycle prior to failure. The flaking of the whitewash shows the extensive yielding that took place in the link web panels. A small amount of flange local buckling was observed at the left end of the link and at the location of the first vertical stiffener. No significant web local buckling was noted. Figure 3.60 illustrates yielding was at the two link ends, indicating that the reinforced portion of the link did not remain elastic. Finally, it is noted that at the end of the test, small cracks at the link web adjacent to the termination of the welds of the vertical stiffeners were observed. However, the specimen failed by fracture of the link-to-column connection before the link web fracture developed significantly.

The hysteretic response of Specimen AISC-8 is shown in Figures 3.49 through 3.52. Based on a total link length of $e = 38.6$ inches, the plastic rotation achieved by this specimen was, approximately, $\gamma_p = \pm 0.056$ rad, while based on an active link length of 33.4", the plastic rotation achieved by this specimen was approximately $\gamma_p = \pm 0.065$ rad. No matter how the link plastic rotation was estimated, the target plastic rotation angles of 0.073 and 0.08 rad, respectively, were not achieved by Specimen AISC-8. Thus, this specimen did not satisfy the performance requirements of the 2005 AISC *Seismic Provisions*. The thickness of the supplemental stiffeners together with their welding detail proved to be inadequate.

3.4 SUMMARY AND DISCUSSION OF TEST RESULTS

A summary of the test results is presented in Tables 3.1 and 3.2. Table 3.1 provides a summary of the results of Specimens AISC-1 through 4 (Phase I). This table lists the failure mode and the maximum link plastic rotation angle developed by each specimen. For comparison, the actual non-dimensional link length and the corresponding target plastic rotation angle are also listed. Similarly, Table 3.2 contains a summary of the results of Specimens AISC-5 through 8 (Phase II). In this table the description of the failure mode of each specimen is accompanied by the maximum link plastic rotation angle calculated based on both the total link length and the active link length. The non-dimensional total and active link lengths of each specimen are also presented along with the corresponding target plastic rotation angles.

A total of eight specimens were tested in this project using two different wide flange link sections. The test program was divided into two phases based on the two proposed link-to-column connections. Phase I evaluated the performance of a simple shop-welded link-to-column connection, while Phase II evaluated a field-welded reinforced link-to-column connection. All the links were designed to be in or near the shear yielding range.

From Tables 3.1 and 3.2, one can observe that only two specimens, AISC-3 and AISC-8, of a total number of eight specimens failed without achieving the target plastic rotation levels specified in the 2005 AISC *Seismic Provisions*. Consequently, six out of eight specimens satisfied the required plastic rotation angles. These specimens showed good overall performance, acquiring plastic rotation angles 19 to 50-percent in excess of the required levels.

The two dominant failure modes observed were:

1. Fracture of the link top or bottom flange base metal, adjacent to the weld of the link-to-column connection,
2. Fracture of the link web initiating at the termination of the stiffener fillet welds.

According to a large number of previous tests conducted by Arce (2002), Ryu (2004), and Galvez (2004) failure of links with length $e < 1.7 M_p / V_p$ is dominated by link web fractures initiating at the termination of the stiffener fillet welds. This observation was also confirmed by these tests. Specifically, in Specimens AISC-4, 6, and 7, which had a total link length of $e = 1.30 M_p / V_p$, the dominant failure mode was link web fracture at the vertical stiffeners.

Specimens AISC-1, 2, 3, and 8 failed due to fracture at the link flange to column connection. In Specimens AISC-1 and 2 when failure occurred, the acquired plastic rotation angle was well in excess of the required (50 and 25-percent respectively). As observed in both specimens, the edge of the link flange was prone to fracture at the toe of the fillet weld. Specimen AISC-2 ultimately failed due to propagation of this fracture. Had an initial flaw been present at this location, such as an undercut, failure of the specimen could have occurred at a much earlier loading stage due to the high stresses and strains. Therefore, it is recommended that the weld tabs be used at the edge of the link flange when placing fillet welds between the link flange and column flange (Preliminary Report, Okazaki; 2004p). It is, also, interesting to point out the better performance of specimen AISC-1, compared to specimen's AISC-2. These two specimens differed only in the welding process used. From the test results, it appears that the SMAW process used in specimen AISC-1 is more beneficial than the GS-FCAW process used in specimen

AISC-2. Nevertheless, Specimen AISC-2, welded with the GS-FCAW process, still achieved the target plastic rotation.

Specimens AISC-3 and 8 failed at the link-to-column connection prior to achieving the required plastic rotation angle. Specimen AISC-3 was nominally identical to AISC-2, except for the size of the fillet welds connecting the link flanges to the column. Because of the similarity of the two specimens, the premature failure of AISC-3 may be attributed to the smaller leg size of the fillet welds. In other words, fillet welds with a leg size approximately equal to the thickness of the connected flange seem to be inadequate for the link-to-column connection. Furthermore, Specimen AISC-8 was nominally identical to specimen AISC-5, except for the thickness of the supplemental stiffeners and the supplemental stiffener welding detail. Because of the similarity of the two specimens, the premature failure of Specimen AISC-8 can be attributed to the smaller thickness of the supplemental stiffeners. That is to say, the size of the supplemental stiffeners was not adequate to make the reinforced portion of the link deform only elastically.

Summarizing, from the limited number of tests conducted in Phase I of this research program, combined with a large number of successful tests on a similar detail by Okazaki et al (2005), it appears that the simple shop-welded link-to-column connection provides a viable connection concept for the seismic resistant EBFs. Particularly, the test results of the first four specimens showed that:

- The use of the FCAW-GS welding process with E70T-9 electrodes, preferred in the shop-welded applications, resulted in a satisfactory performance.
- The simple shop-welded link-to-column connection detail composed of all-around, double-sided fillet welds performed very well. According to the test results, the

fillet welds should have a leg size approximately equal to 1.5-times the thickness of the connected link flange or web.

➤ The use of an alternative link flange weld detail, for shallow links with thick flanges, which combines a partial joint penetration groove weld together with a fillet weld, also demonstrated an excellent performance.

Similarly, from the limited number of tests conducted in Phase II, it appears that the field-welded, reinforced link-to-column connection is a promising connection detail for the seismic resistant EBFs. Specifically, the first two specimens, composed of thick supplemental stiffeners welded to the column flange and the first vertical stiffener using CJP groove welds, showed outstanding performance. In these tests, the reinforced panel of the link remained essentially elastic and at the end of the testing no apparent distress at the link-to-column connection was observed. On the other hand, the other two specimens were composed of thinner supplemental stiffeners connected to the column flange and the first vertical stiffener using one-side fillet welds, with a leg size equal to the thickness of the supplemental stiffeners. However, the results from these two tests were inconclusive. While specimen AISC-7 showed excellent performance keeping the reinforced panel of the link elastic and the link-to-column connection undamaged, specimen AISC-8 failed prematurely without performing as intended. These test results indicate that further analytical research and testing is needed to confirm the successful performance of the reinforced connection detail. Further research could concentrate on determining a simple rule for calculating the supplemental stiffener thickness and its welding detail.

Table 3.1: Summary of Test Results (Phase I)

Specimen No.	Section	Link Length $e / (M_p / V_p)$	Target γ_p (rad)	Test Results	
				Measured γ_p (rad)	Failure Mode
AISC-1	W18x40	1.72	± 0.073	+ 0.109 / - 0.118	Fracture at link flange to column connection (fracture primarily in link flange base metal near the fillet weld)
AISC-2	W18x40	1.72	± 0.073	\pm 0.093	Fracture at link flange to column connection (fracture primarily in link flange base metal near the fillet weld)
AISC-3	W18x40	1.72	± 0.073	\pm 0.057	Fracture at link flange to column connection (fracture primarily in link flange base metal near the fillet weld)
AISC-4	W10x68	1.30	± 0.08	\pm 0.095	Fracture of link web at stiffeners (no distress at the link-to-column connection)

Table 3.2: Summary of Test Results (Phase II)

Specimen No	Section	Total Link Length $e / (M_p / V_p)$	Active Link Length $e_{active} / (M_p / V_p)$	Target γ_p (rad) based on		Test Results		
				e	e_{active}	Measured γ_p (rad) based on		Failure Mode
						e	e_{active}	
AISC-5	W18x40	1.72	1.47	± 0.073	± 0.08	± 0.10	± 0.12	Fracture of link web at stiffener farthest from the connection (no distress at the link-to-column connection)
AISC-6	W10x68	1.30	1.13	± 0.08	± 0.08	± 0.095	± 0.11	Fracture of link web at stiffener farthest from the connection (no distress at the link-to-column connection)
AISC-7	W10x68	1.30	1.13	± 0.08	± 0.08	± 0.094	± 0.11	Fracture of link web at the middle stiffener (no distress at the link-to-column connection)
AISC-8	W18x40	1.72	1.47	± 0.073	± 0.08	± 0.056	± 0.065	Fracture at link bottom flange to column connection (fracture primarily in link flange base metal near the weld)

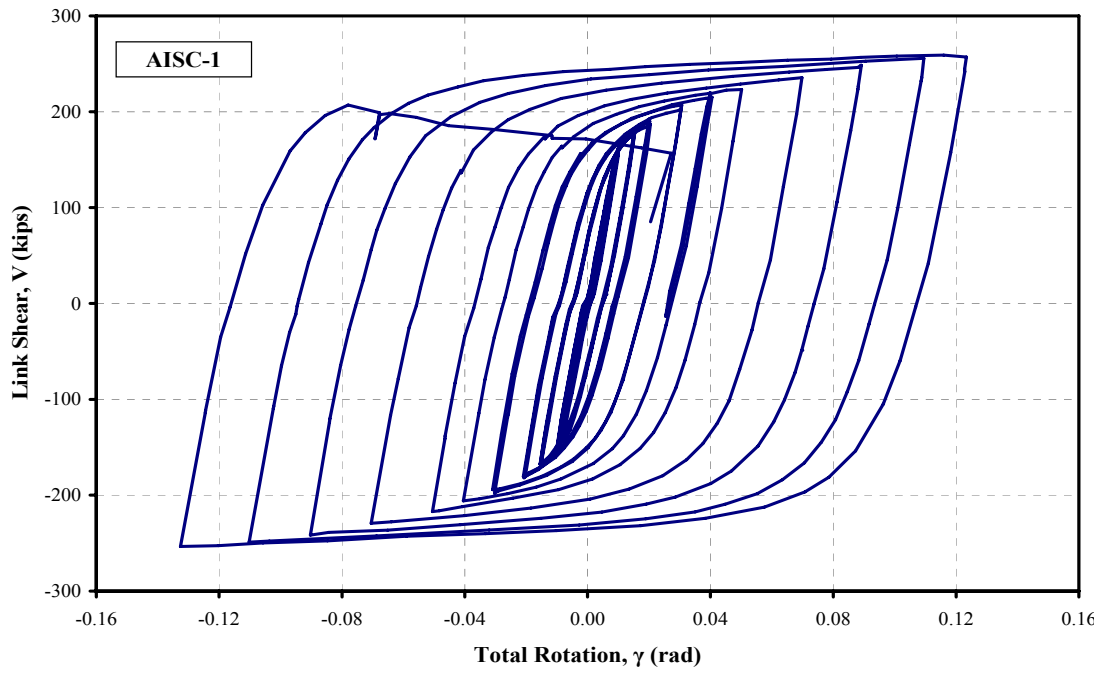


Figure 3.1: Link Shear vs. Total Rotation for Specimen AISC-1

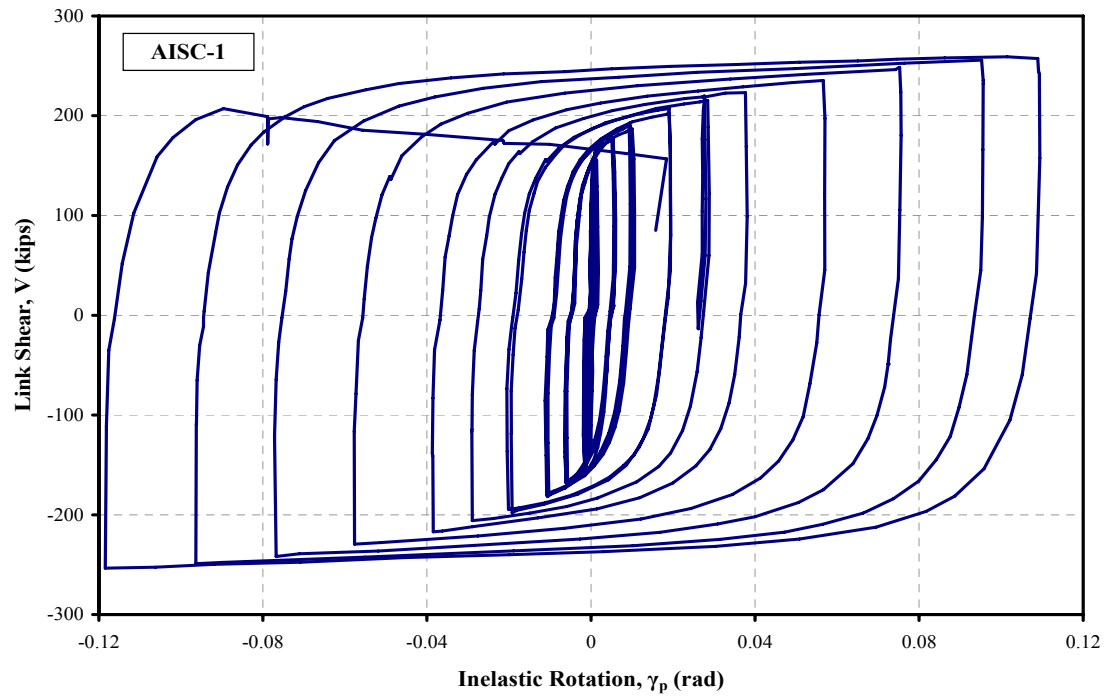


Figure 3.2: Link Shear vs. Inelastic Rotation for Specimen AISC-1

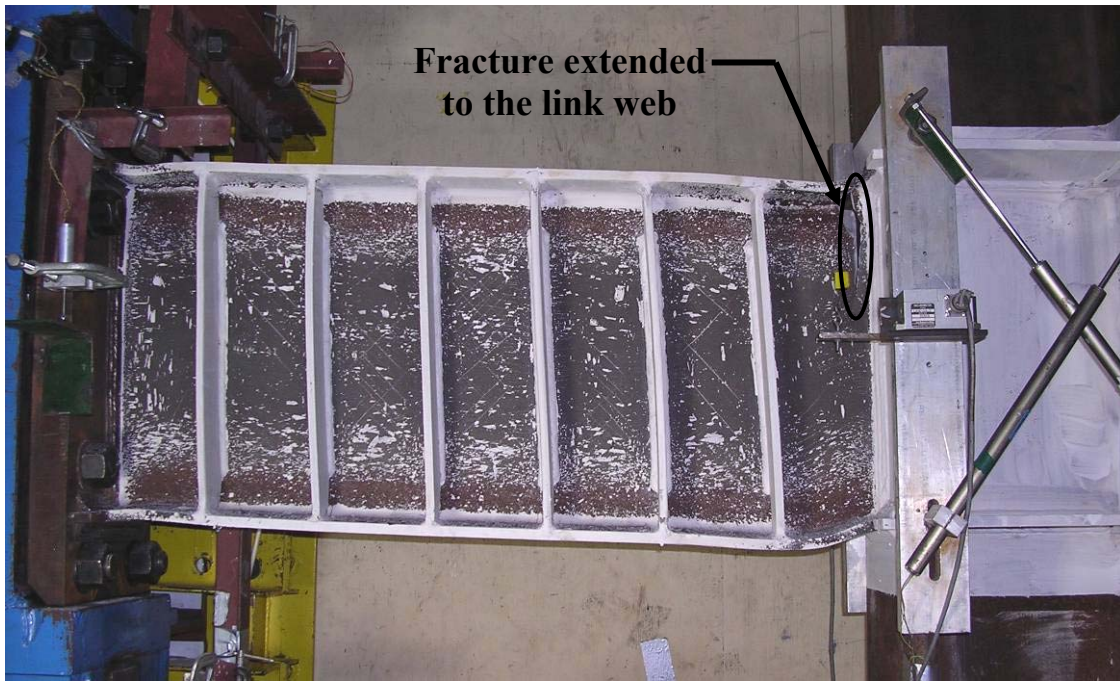


Figure 3.3: Failure of Specimen AISC-1

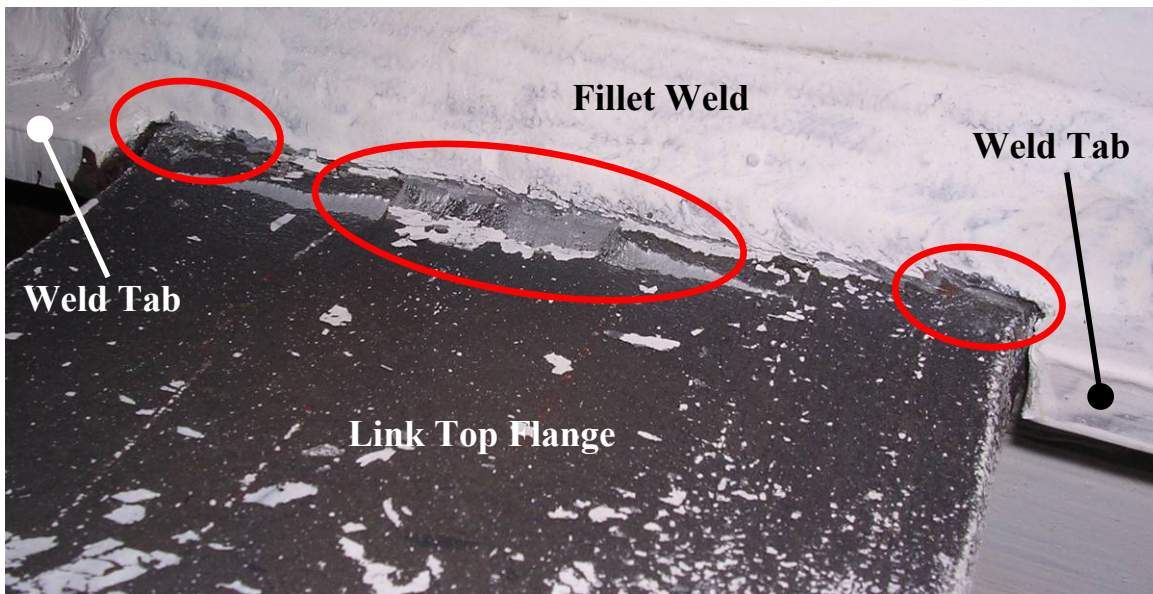


Figure 3.4: Link Flange Fracture in Specimen AISC-1



Figure 3.5: Extension of link flange fracture to the link web – AISC-1

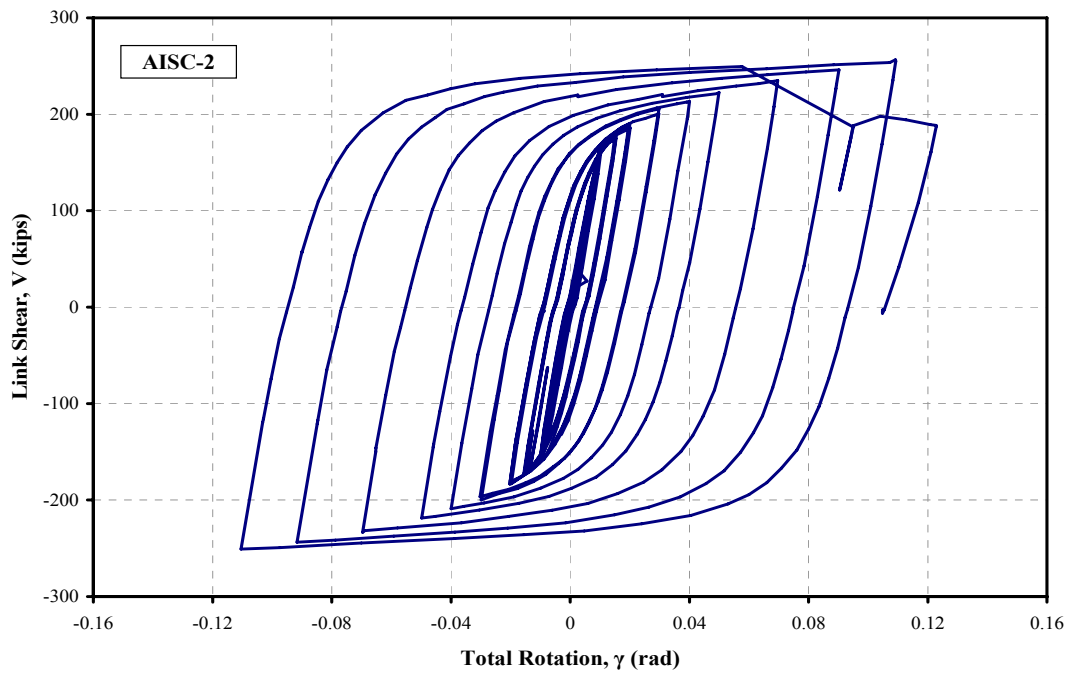


Figure 3.6: Link Shear vs. Total Rotation for Specimen AISC-2

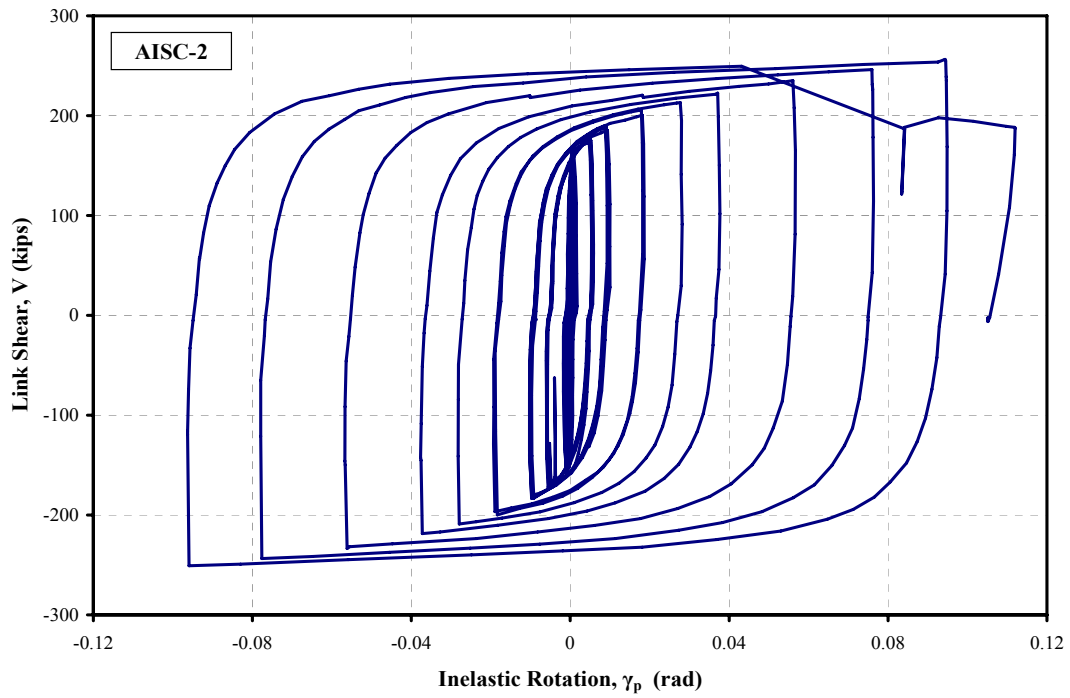


Figure 3.7: Link Shear vs. Inelastic Rotation for Specimen AISC-2

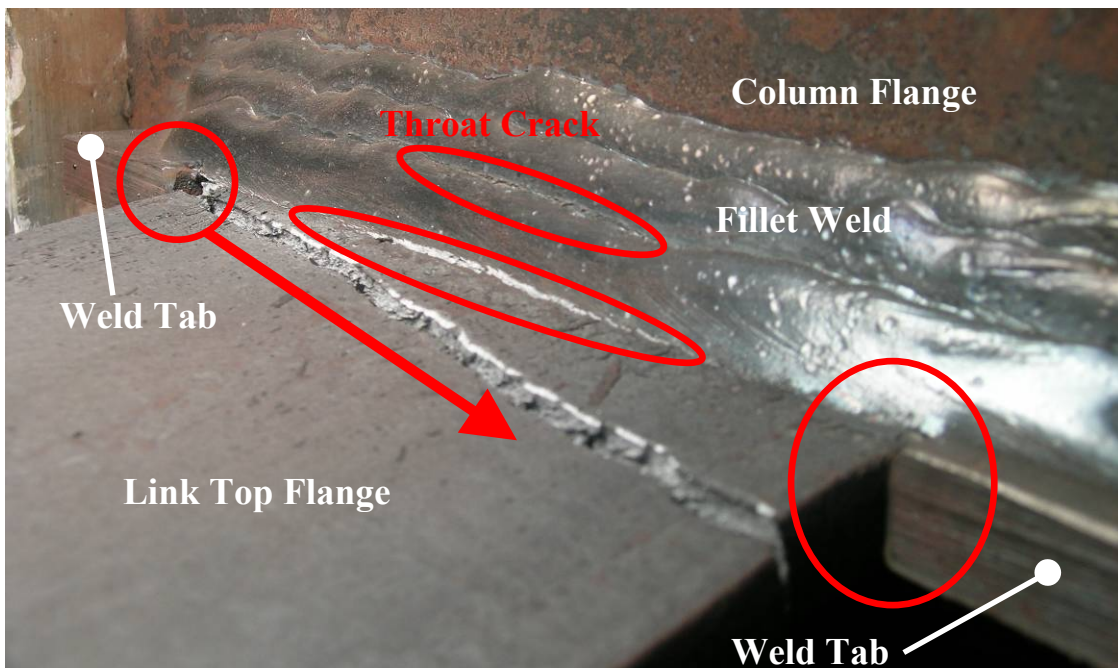


Figure 3.8: Link Flange Fracture in Specimen AISC-2

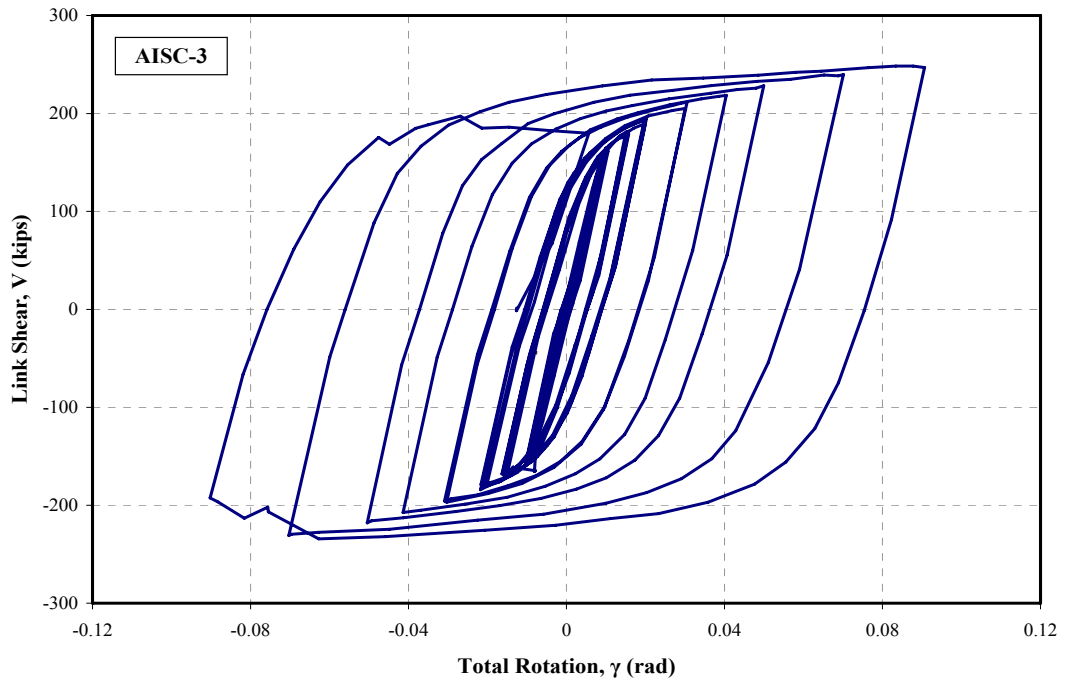


Figure 3.9: Link Shear vs. Total Rotation for Specimen AISC-3

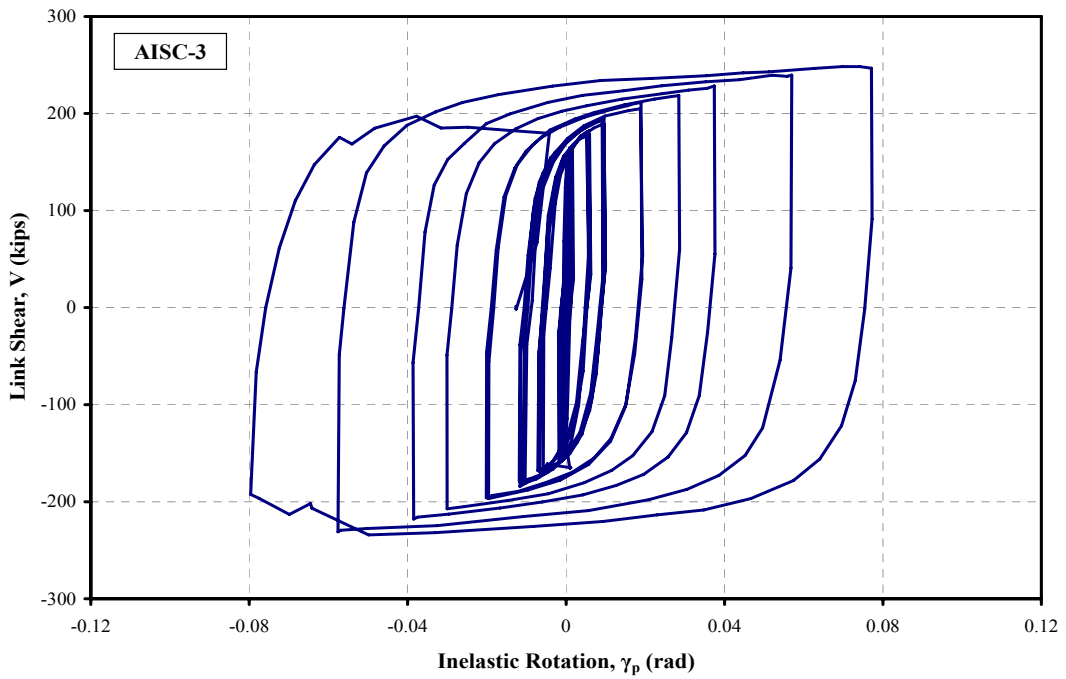


Figure 3.10: Link Shear vs. Inelastic Rotation for Specimen AISC-3



Figure 3.11: Failure of Specimen AISC-3 during loading cycle at $\gamma = + 0.11$ rad



Figure 3.12: AISC-3 – Fracture of the Bottom Link Flange during loading cycle at $\gamma = - 0.09$ rad

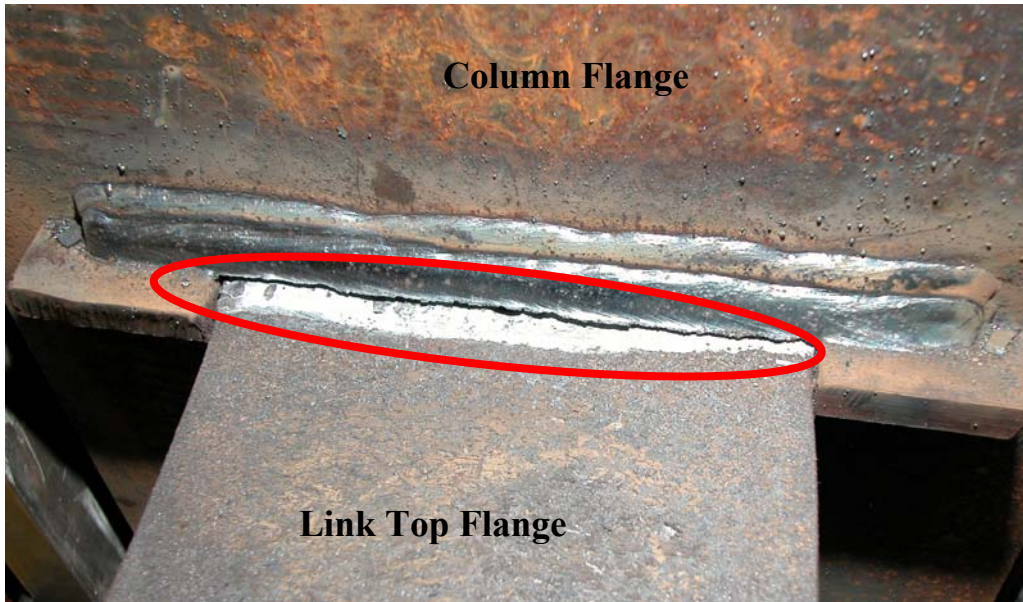


Figure 3.13: AISC-3 – Fracture of the Top Link Flange during loading cycle at $\gamma = +0.11$ rad

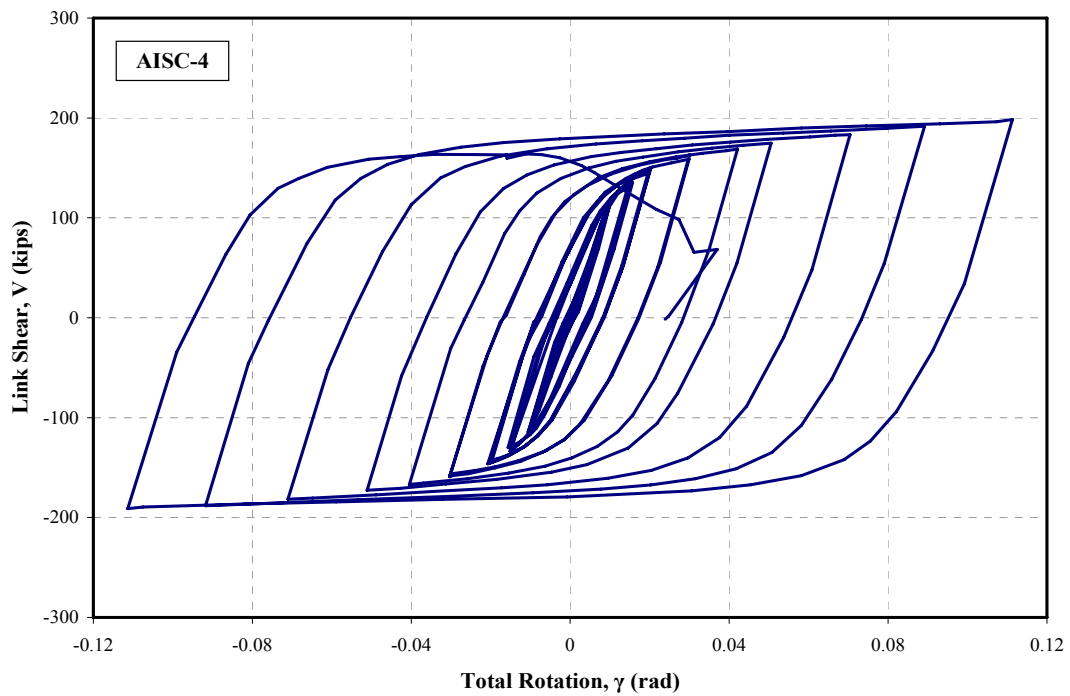


Figure 3.14: Link Shear vs. Total Rotation for Specimen AISC-4

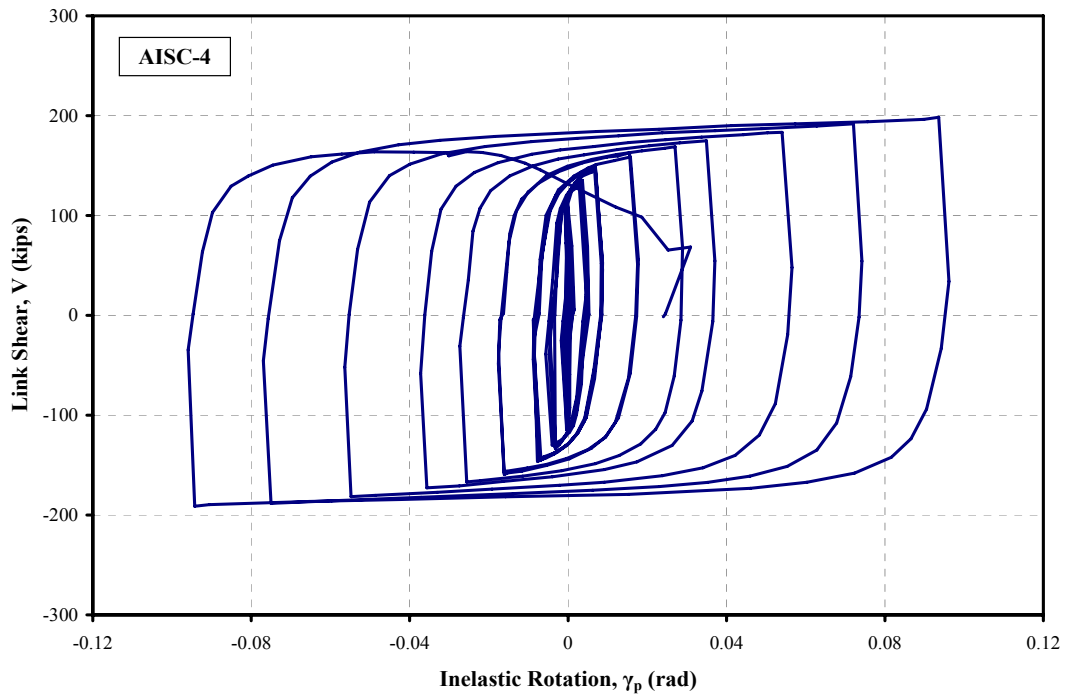


Figure 3.15: Link Shear vs. Inelastic Rotation for Specimen AISC-4



Figure 3.16: Specimen AISC-4 after Loading Cycle at $\gamma = \pm 0.11$ rad (Last full loading cycle prior failure)



Figure 3.17: Specimen AISC-4 – Web Cracks adjacent to stiffener welds after loading cycle at $\gamma = \pm 0.11$ rad



Figure 3.18: Fracture of Link Web adjacent to stiffener's weld during loading cycle of $\gamma = + 0.13$ rad



Figure 3.19: Failure of Specimen AISC-4 during loading cycle of $\gamma = + 0.13$ rad

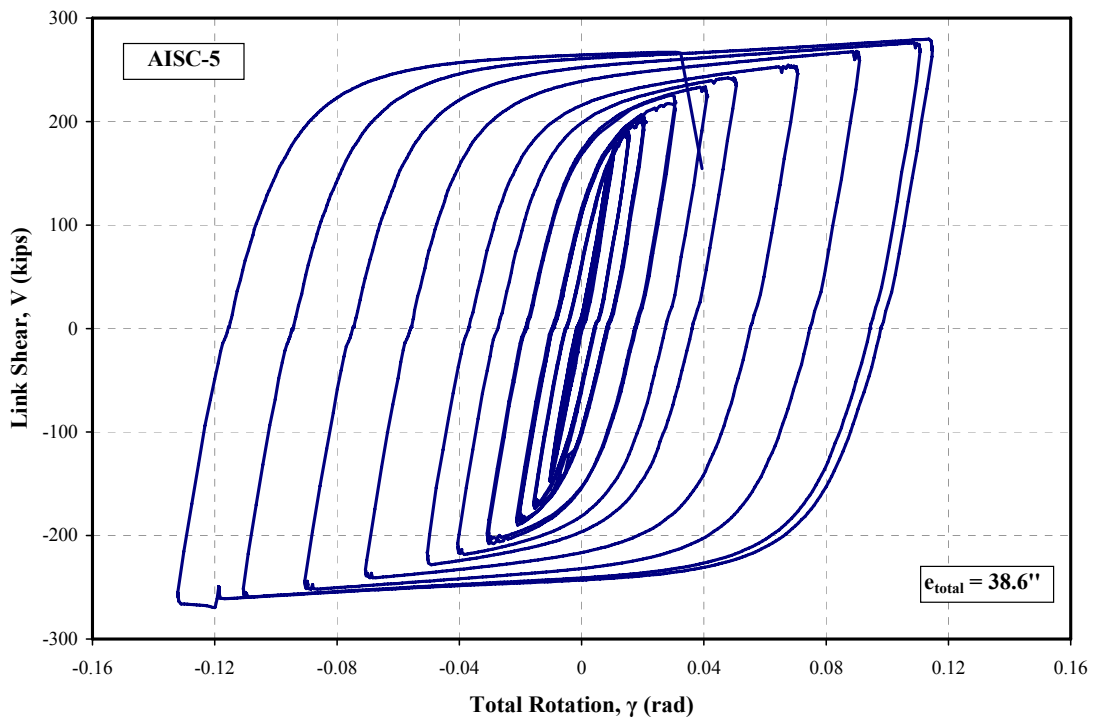


Figure 3.20: Link Shear vs. Total Rotation (rotation based on $e_{total} = 38.6''$) – AISC-5

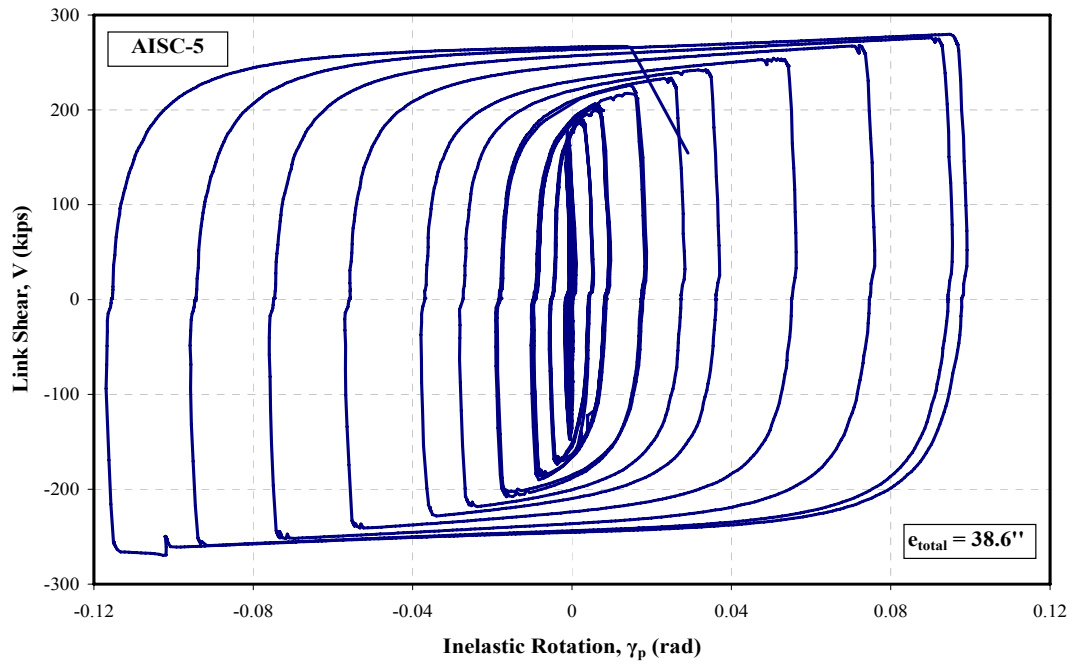


Figure 3.21: Link Shear vs. Inelastic Rotation (rotation based on $e_{total} = 38.6''$) – AISC-5

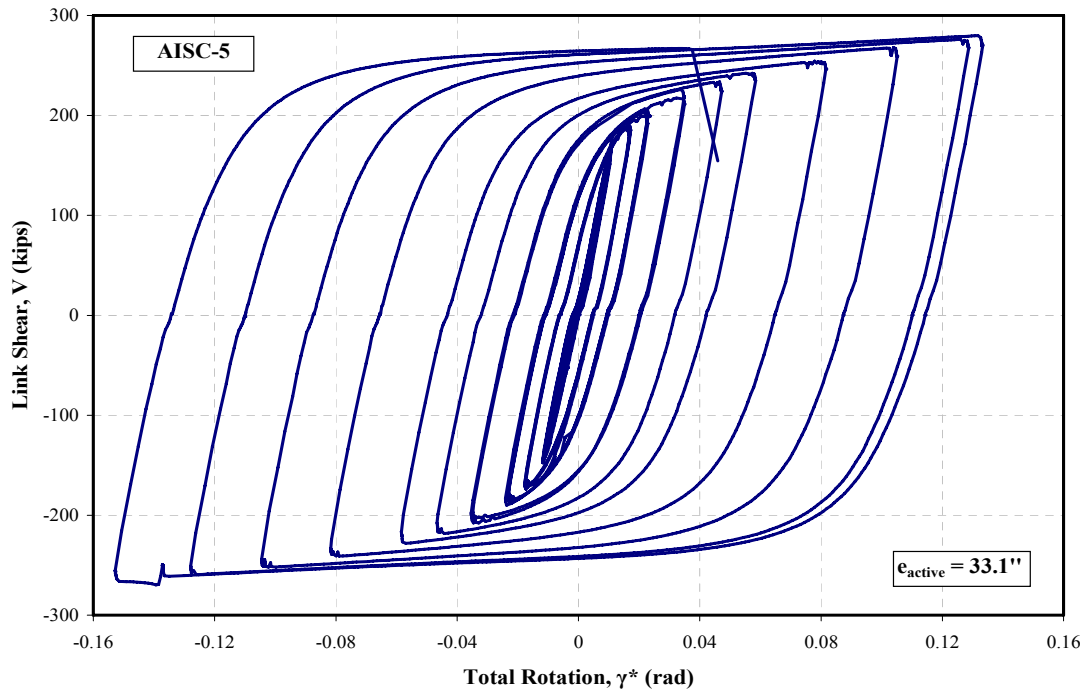


Figure 3.22: Link Shear vs. Total Rotation (rotation based on $e_{active} = 33.1''$) – AISC-5

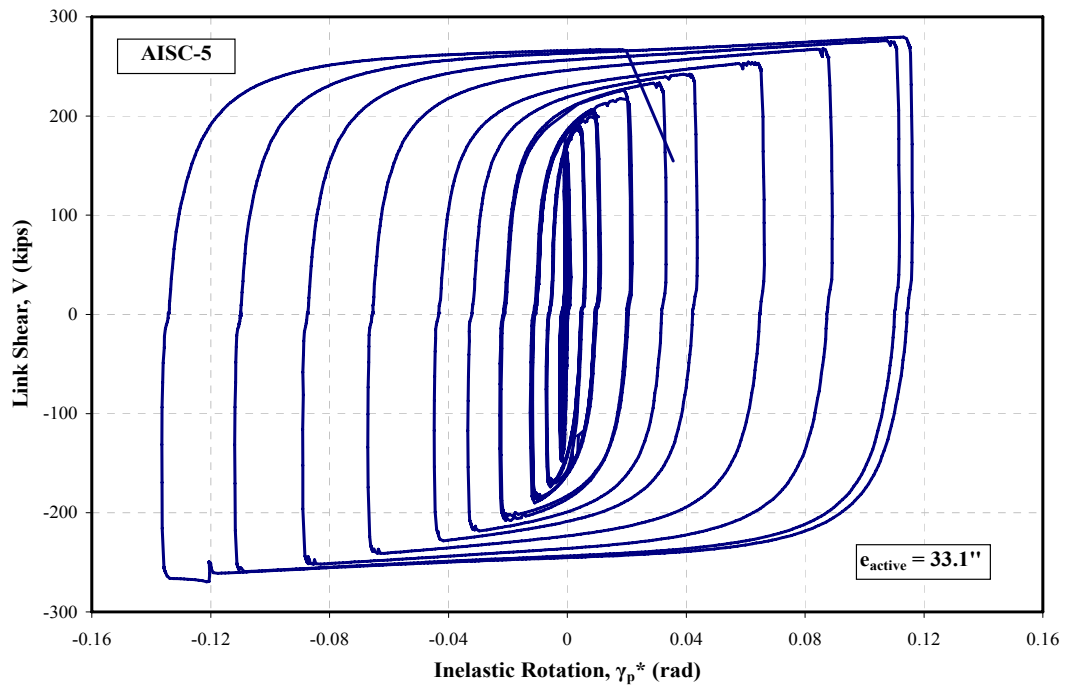


Figure 3.23: Link Shear vs. Inelastic Rotation (rotation based on $e_{\text{active}} = 33.1''$)—AISC-5



Figure 3.24: Specimen AISC-5 prior to Testing and Whitewash



Figure 3.25: Specimen AISC-5 after First Loading Cycle at $\gamma = + 0.11 / -0.13$ rad (Last full loading cycle prior to failure)



Figure 3.26: Yielding restricted primarily away from the link-to-column connection (Last full loading cycle prior to failure)

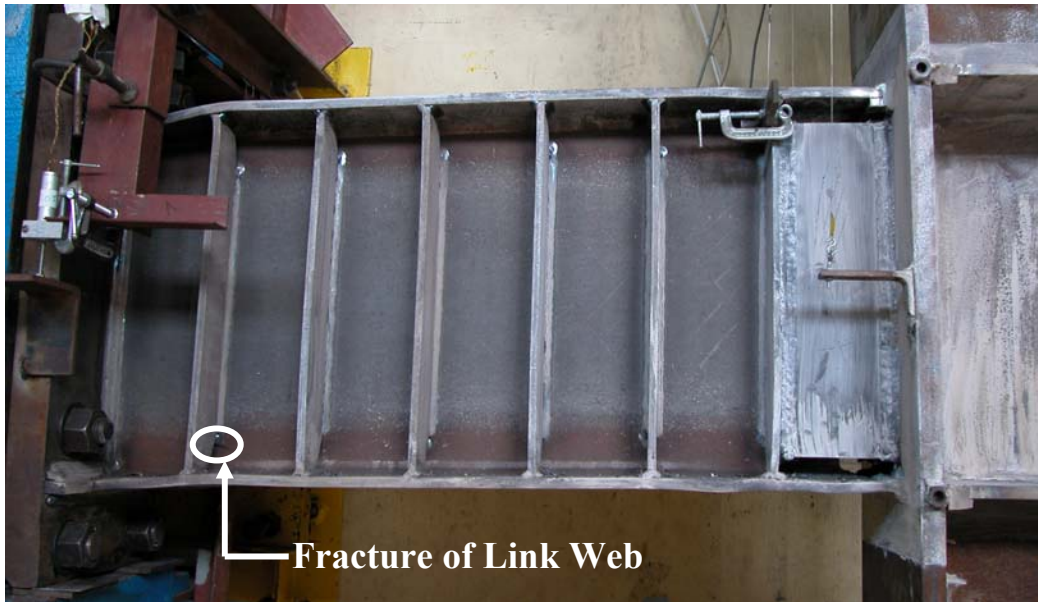


Figure 3.27: Failure of Specimen during 2nd Loading Cycle at $\gamma = + 0.11 / - 0.13$ rad
(Failure by fracture of the link web at the termination of the stiff. weld)

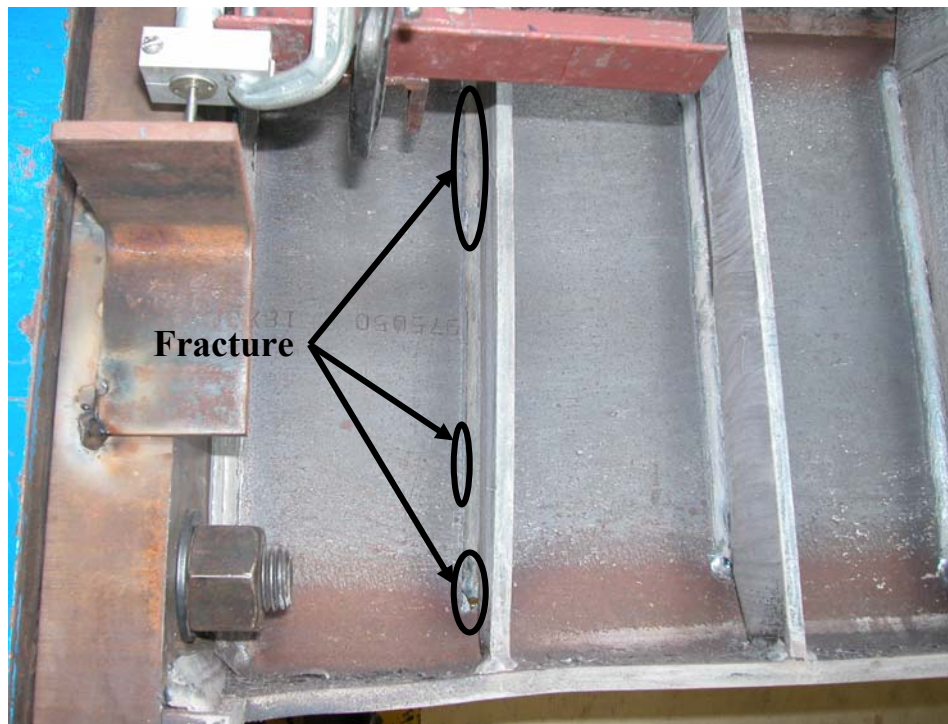


Figure 3.28: Specimen AISC-5 – Fracture of the Link Web

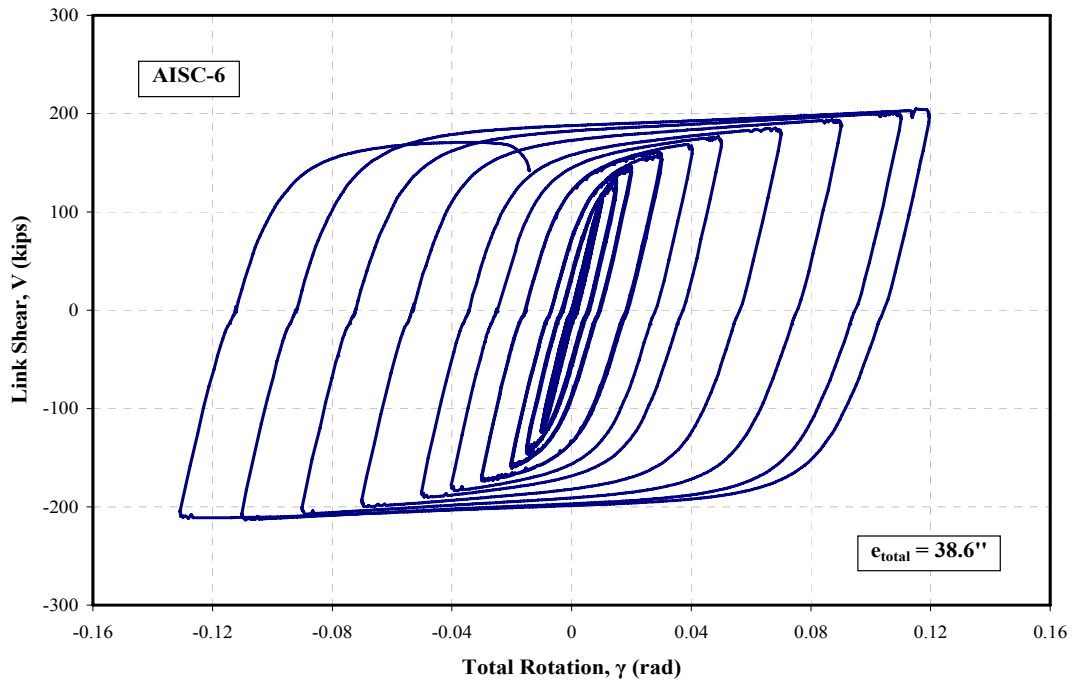


Figure 3.29: Link Shear vs. Total Rotation (rotation based on $\epsilon_{total} = 38.6''$) – AISC-6

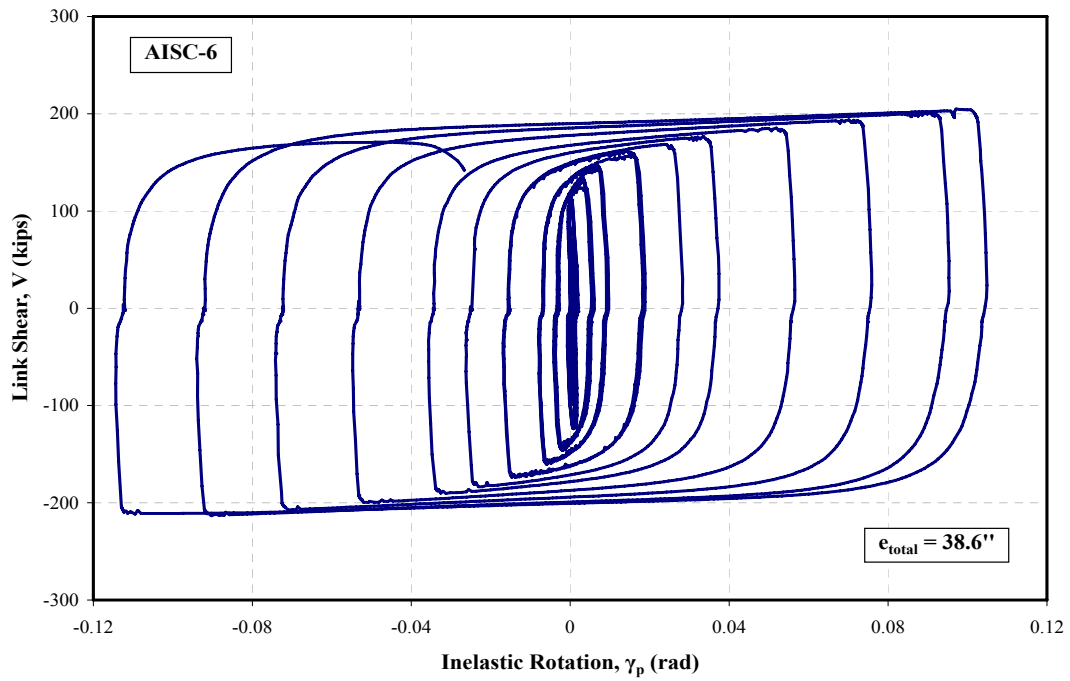


Figure 3.30: Link Shear vs. Inelastic Rotation (rotation based on $\epsilon_{total} = 38.6''$) – AISC-6

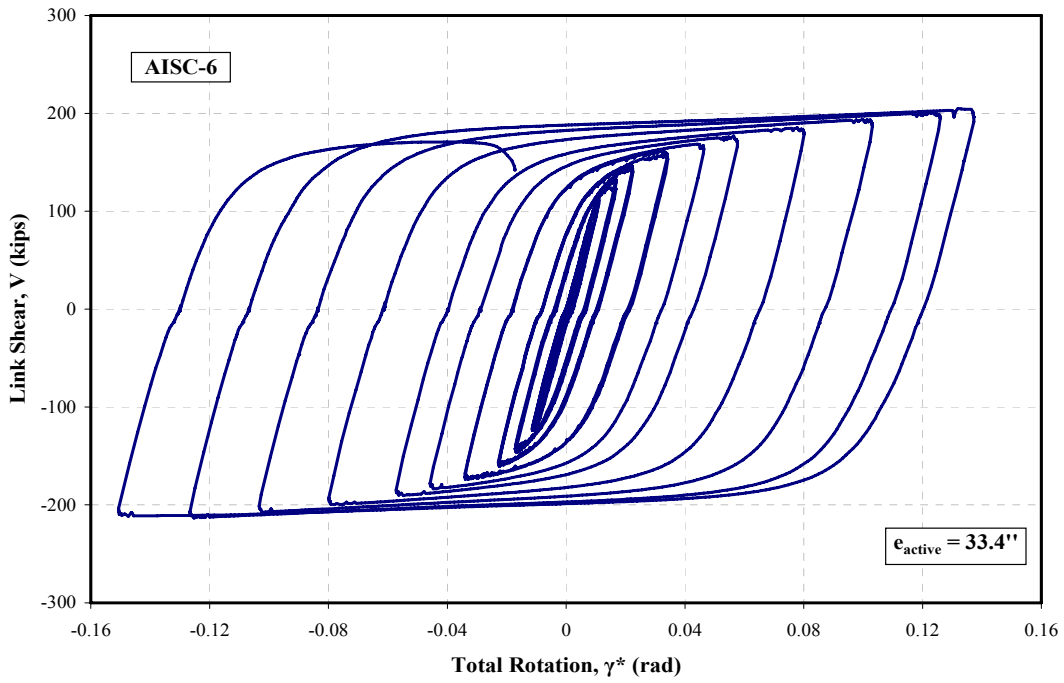


Figure 3.31: Link Shear vs. Total Rotation (rotation based on $e_{\text{active}} = 33.4''$) – AISC-6

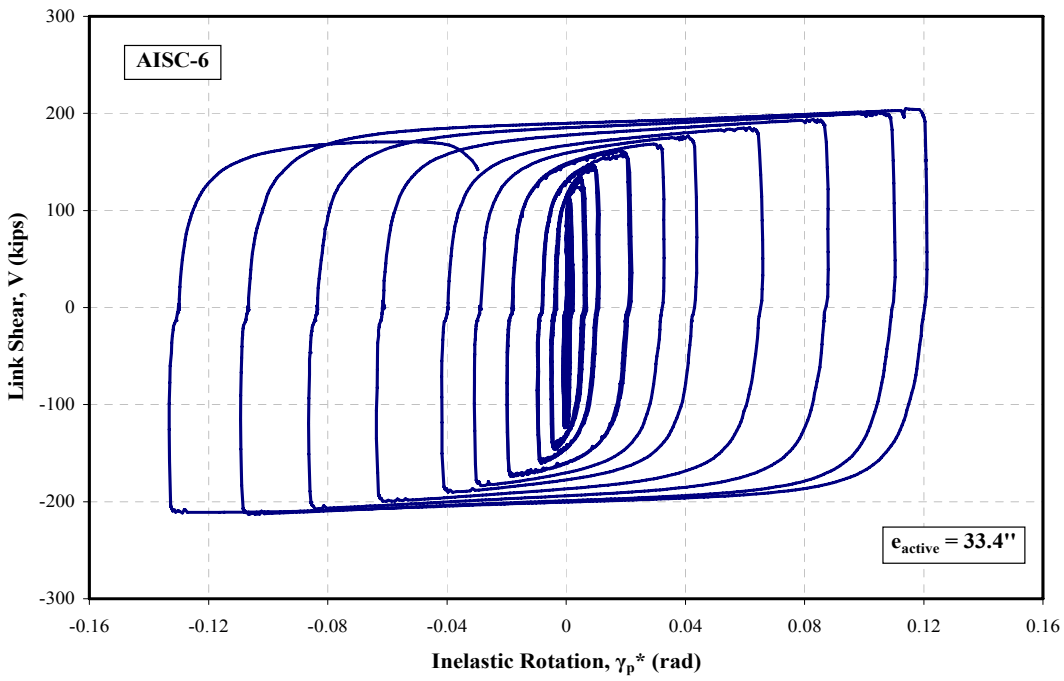


Figure 3.32: Link Shear vs. Inelastic Rotation (rotation based on $e_{\text{active}} = 33.4''$)–AISC-6



Figure 3.33: Specimen AISC-6 prior to Testing and Whitewash



Figure 3.34: Specimen AISC-6 – Link-to-Column Connection

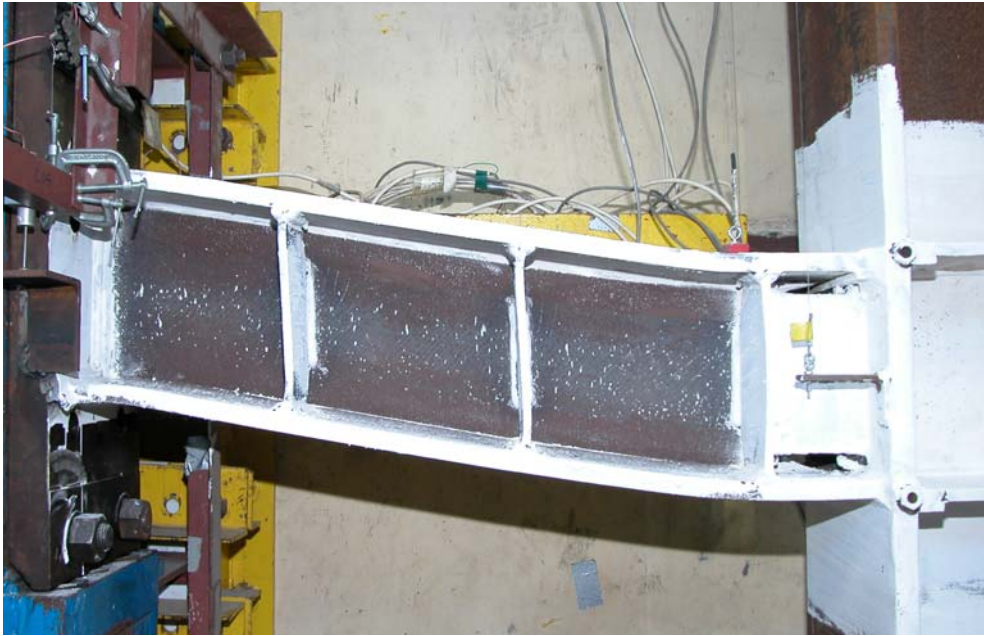


Figure 3.35: Specimen AISC-6 after First Loading Cycle of $\gamma = + 0.12 / - 0.13$ rad
(Last full loading cycle prior to failure)



Figure 3.36: Specimen AISC-6 – Yielding confined in the Unreinforced portion
(Last full loading cycle prior to failure)



Figure 3.37: Failure of Specimen AISC-6 during 2nd loading cycle of $\gamma=+0.12/-0.13$ rad (Failure by fracture of the link web adjacent to vertical stiffener)

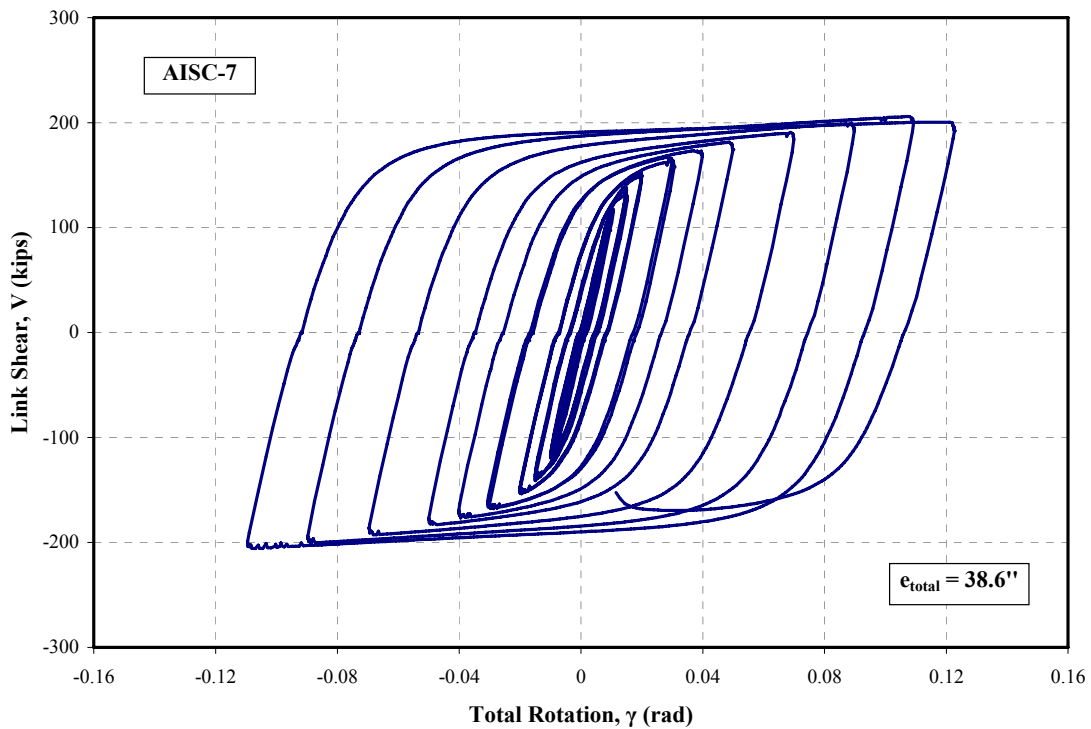


Figure 3.38: Link Shear vs. Total Rotation (rotation based on $e_{total} = 38.6''$) – AISC-7

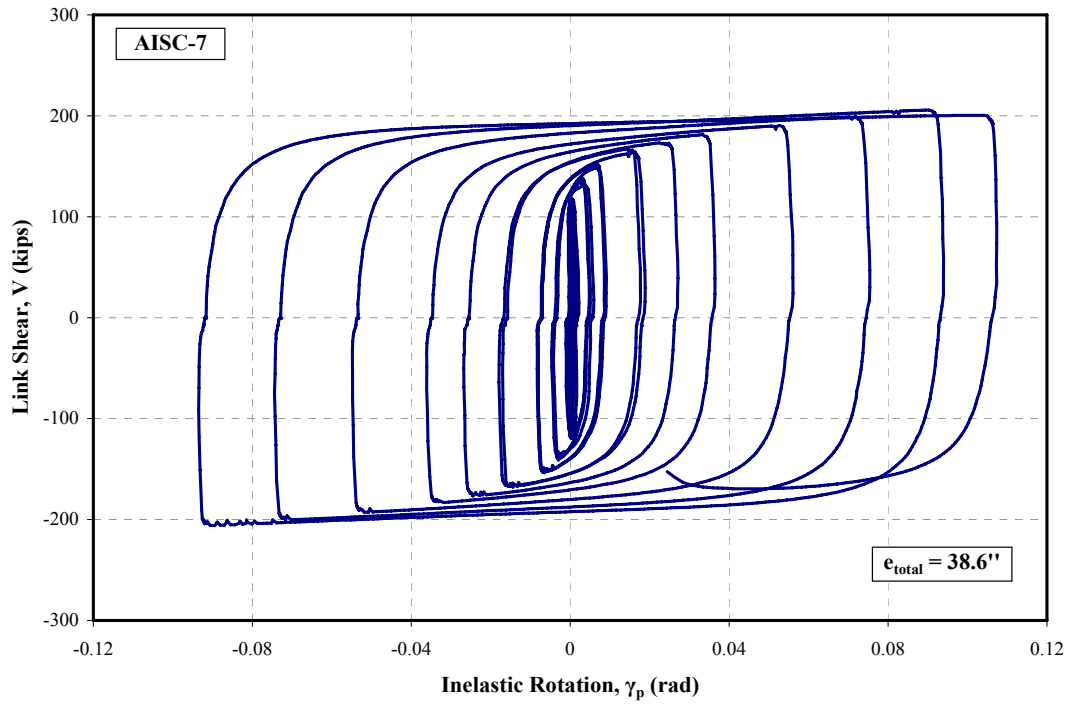


Figure 3.39: Link Shear vs. Inelastic Rotation (rotation based on $e_{total} = 38.6''$) – AISC-7

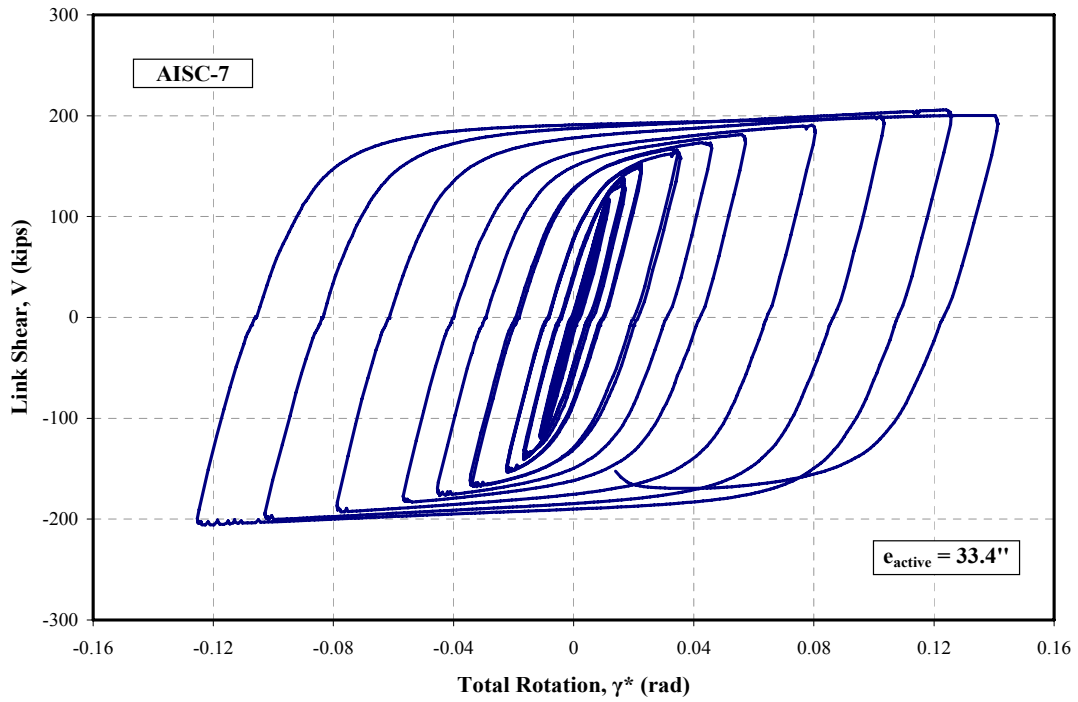


Figure 3.40: Link Shear vs. Total Rotation (rotation based on $e_{active} = 33.4''$) – AISC-7

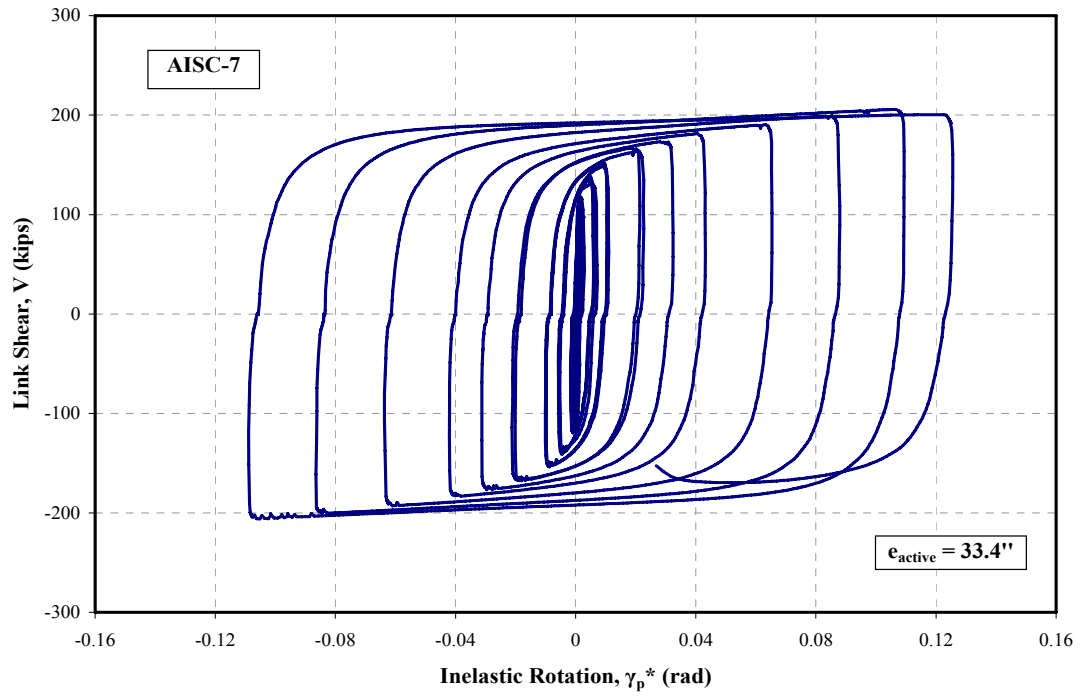


Figure 3.41: Link Shear vs. Inelastic Rotation (rotation based on $e_{\text{active}} = 33.4''$)–AISC-7



Figure 3.42: Specimen AISC-7 prior to Testing



Figure 3.43: Specimen AISC-7 after loading cycle of $\gamma = \pm 0.11$ rad
(Last full loading cycle prior to failure)



Figure 3.44: Link Bottom Flange at the Link-to-Column Connection after cycle of $\gamma = \pm 0.11$ rad (Last full loading cycle prior to failure)

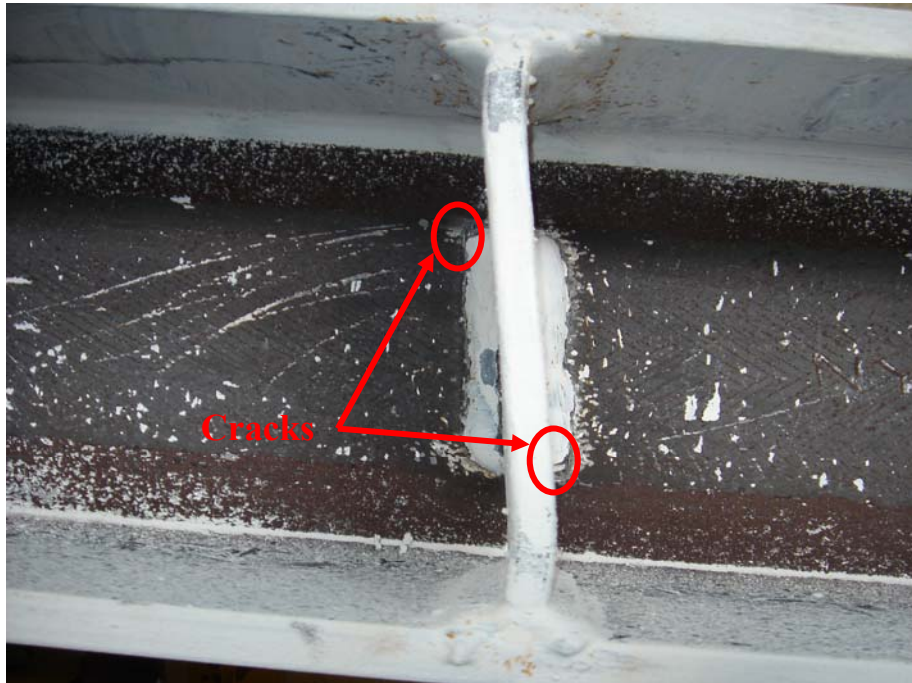


Figure 3.45: Cracks at the termination of the fillet welds of the two vertical stiffeners furthest from the connection (Last full loading cycle prior to failure)

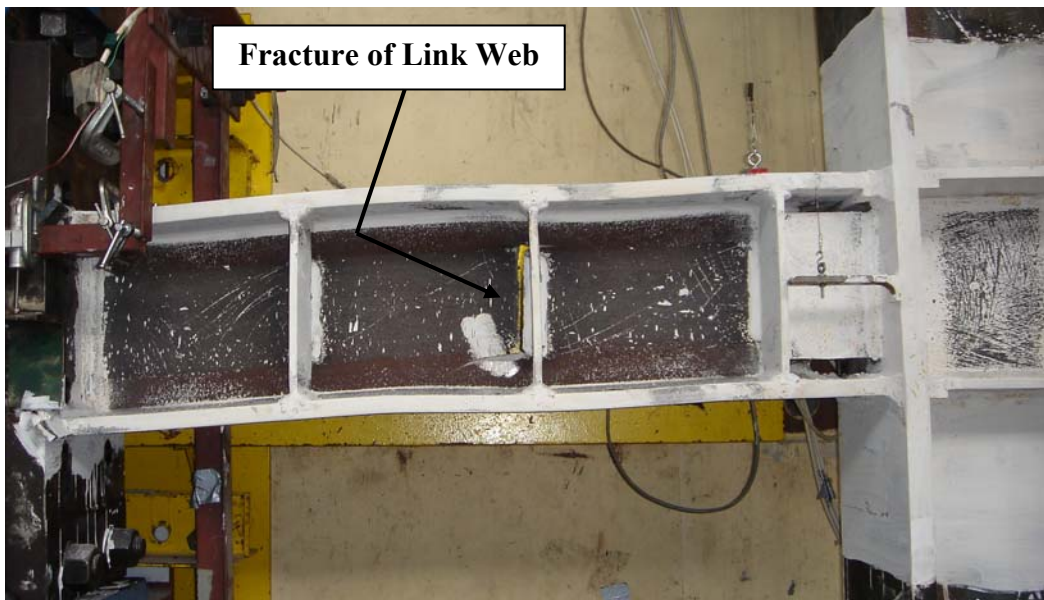


Figure 3.46: Failure of Specimen AISC-7 during Loading Cycle of $\gamma = + 0.12 / -0.13$ rad (Failure by Fracture of Link Web adjacent to middle vertical stiffener)

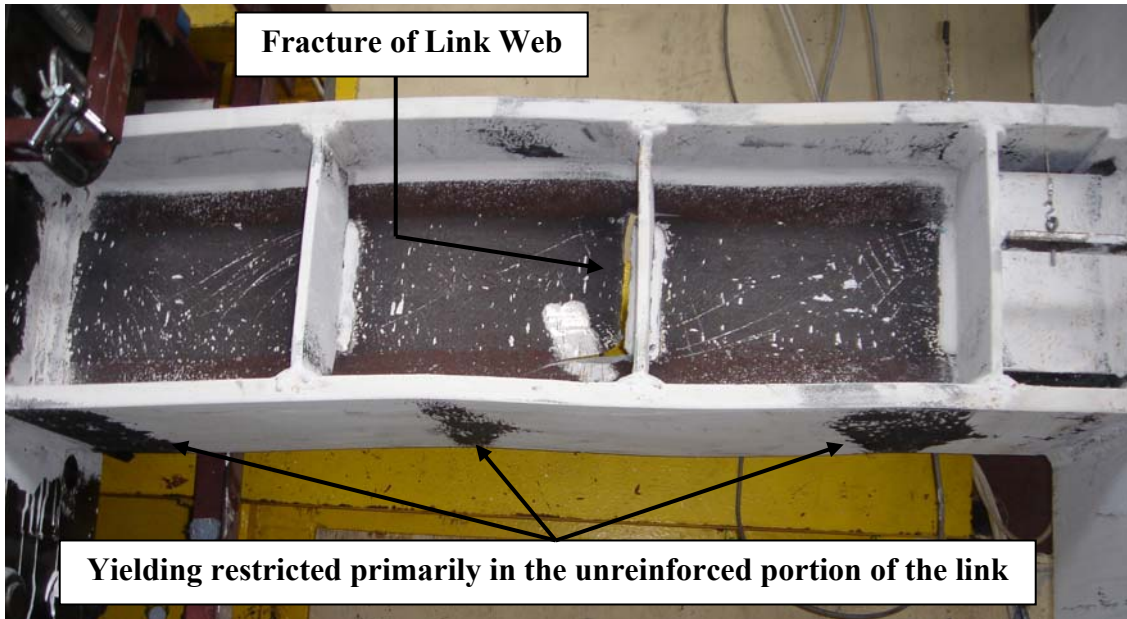


Figure 3.47: Yielding restricted primarily in the unreinforced portion of the Link after Failure of Specimen AISC-7 during Loading Cycle of $\gamma = + 0.12/-0.13$ rad



Figure 3.48: No apparent distress in the Link-to-Column Connection after Failure of Specimen AISC-7 during Loading Cycle of $\gamma = + 0.12 / - 0.13$ rad

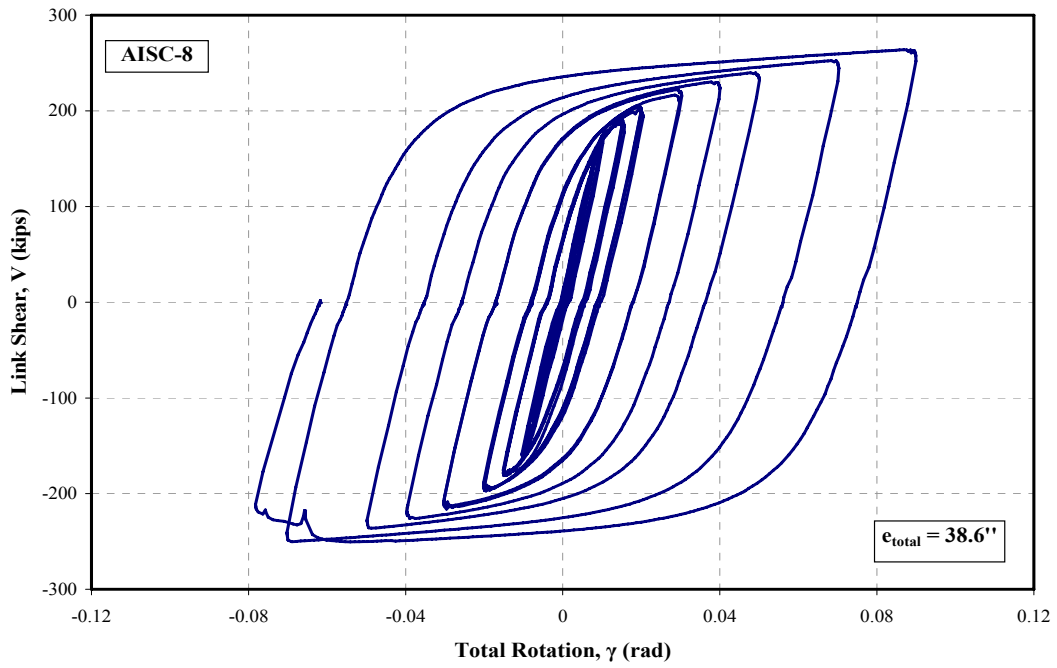


Figure 3.49: Link Shear vs. Total Rotation (rotation based on $e_{total} = 38.6''$) – AISC-8

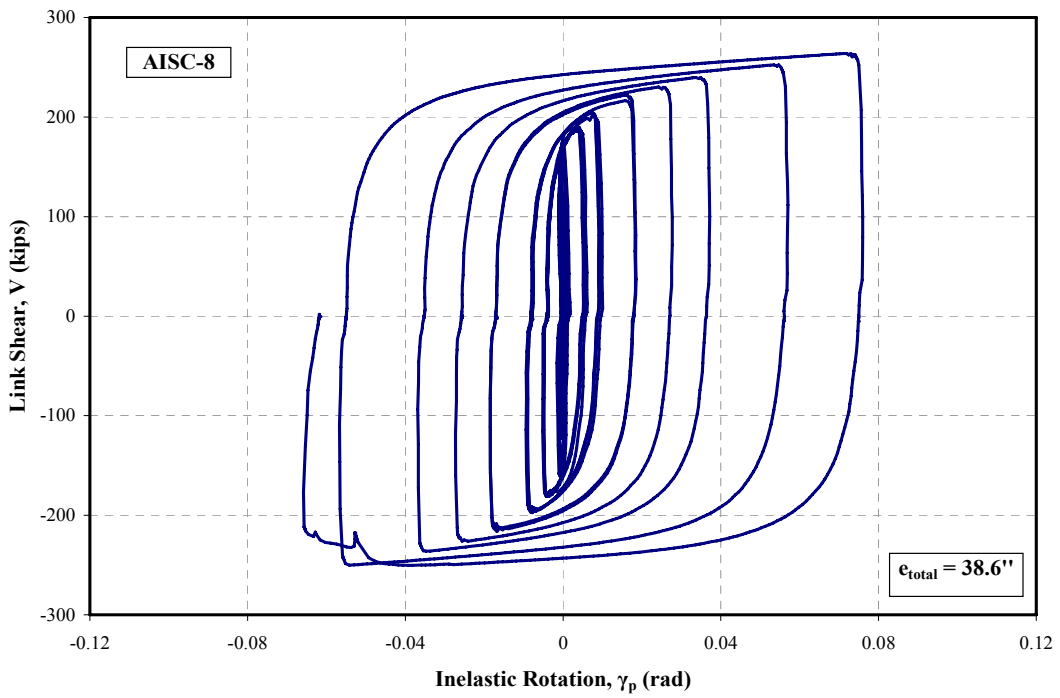


Figure 3.50: Link Shear vs. Inelastic Rotation (rotation based on $e_{total} = 38.6''$) – AISC-8

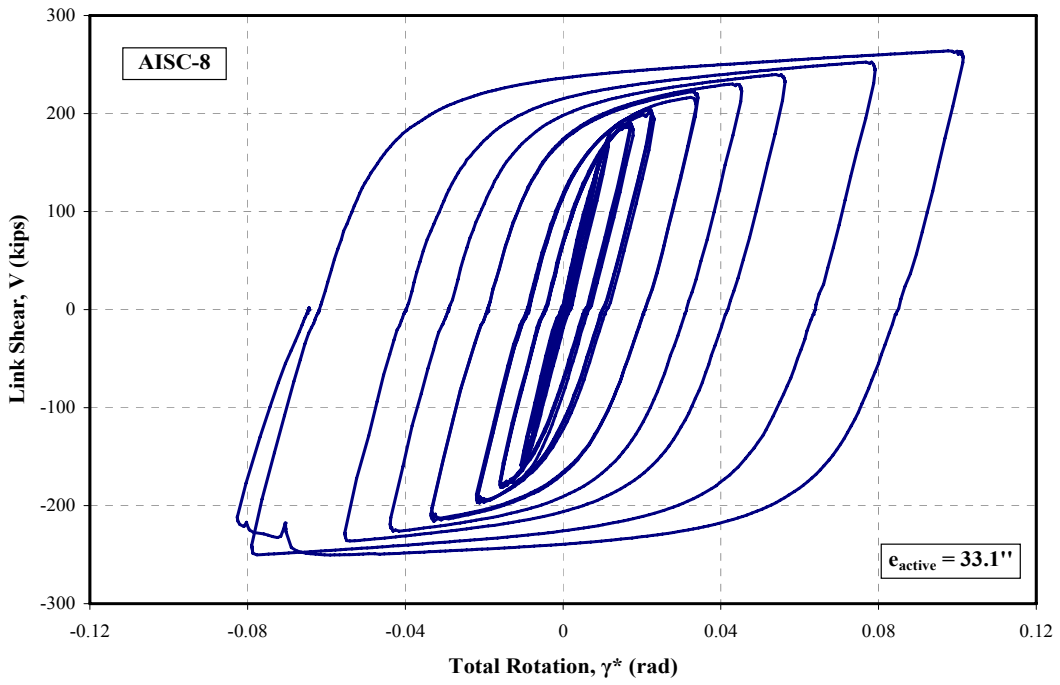


Figure 3.51: Link Shear vs. Total Rotation (rotation based on $e_{\text{active}} = 33.1''$) – AISC-8

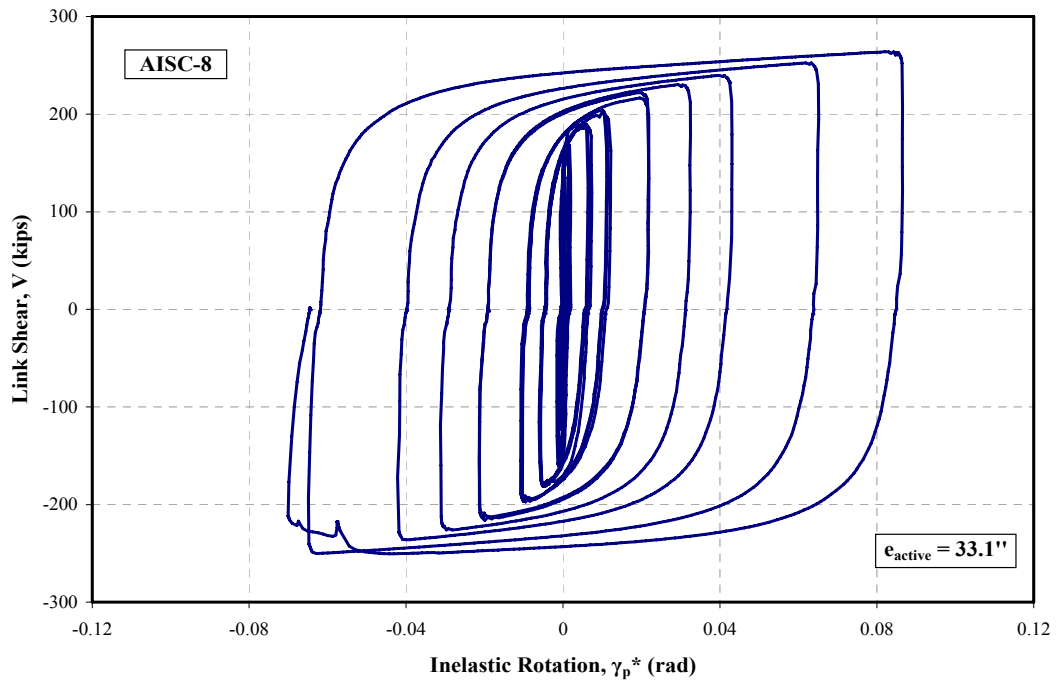


Figure 3.52: Link Shear vs. Inelastic Rotation (rotation based on $e_{\text{active}} = 33.1''$) – AISC-8



Figure 3.53: Specimen prior to Whitewash and Testing



Figure 3.54: Specimen AISC-8 after Loading Cycle of $\gamma = \pm 0.07$ rad
(Last full loading cycle prior to failure)



Figure 3.55: AISC-8 Link Bottom Flange at the Link-to-Column Connection after Loading Cycle of $\gamma = \pm 0.07$ rad (Last full loading cycle prior to failure)

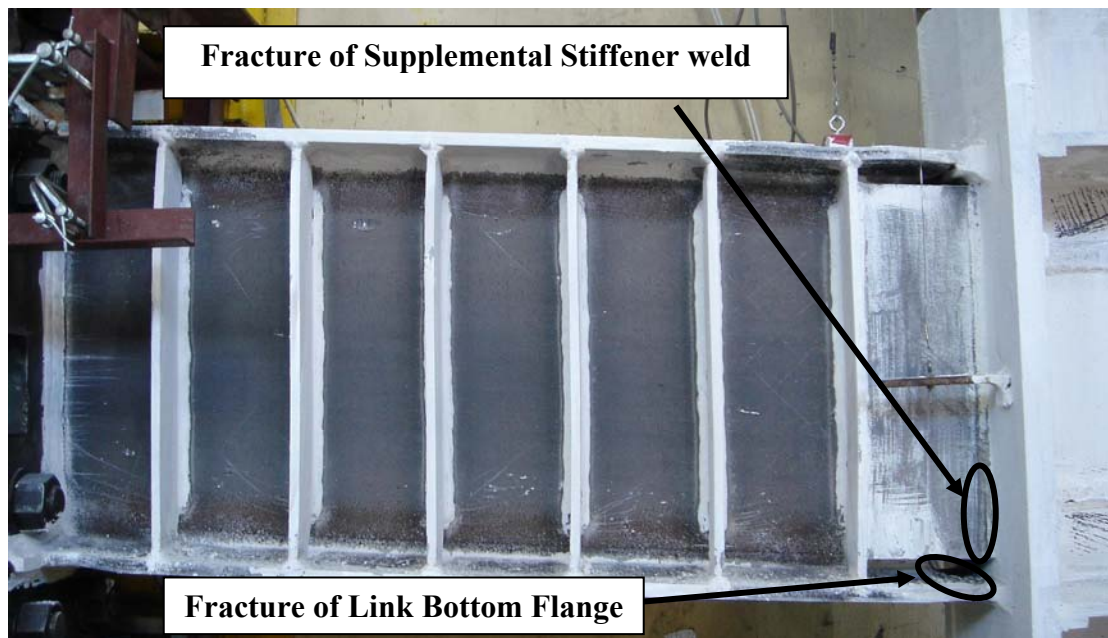


Figure 3.56: Failure of Specimen AISC-8 during Loading Cycle of $\gamma = \pm 0.09$ rad (Failure by Fracture of Link Bottom Flange)

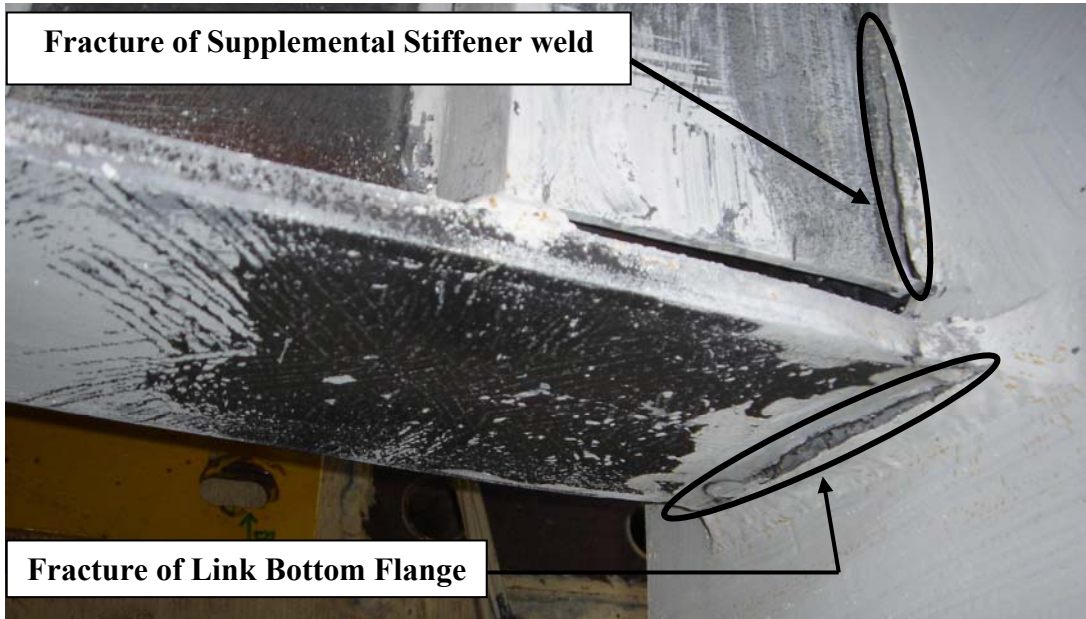


Figure 3.57: Link-to-Column Connection after Failure of Specimen AISC-8 during Loading Cycle of $\gamma = \pm 0.09$ rad

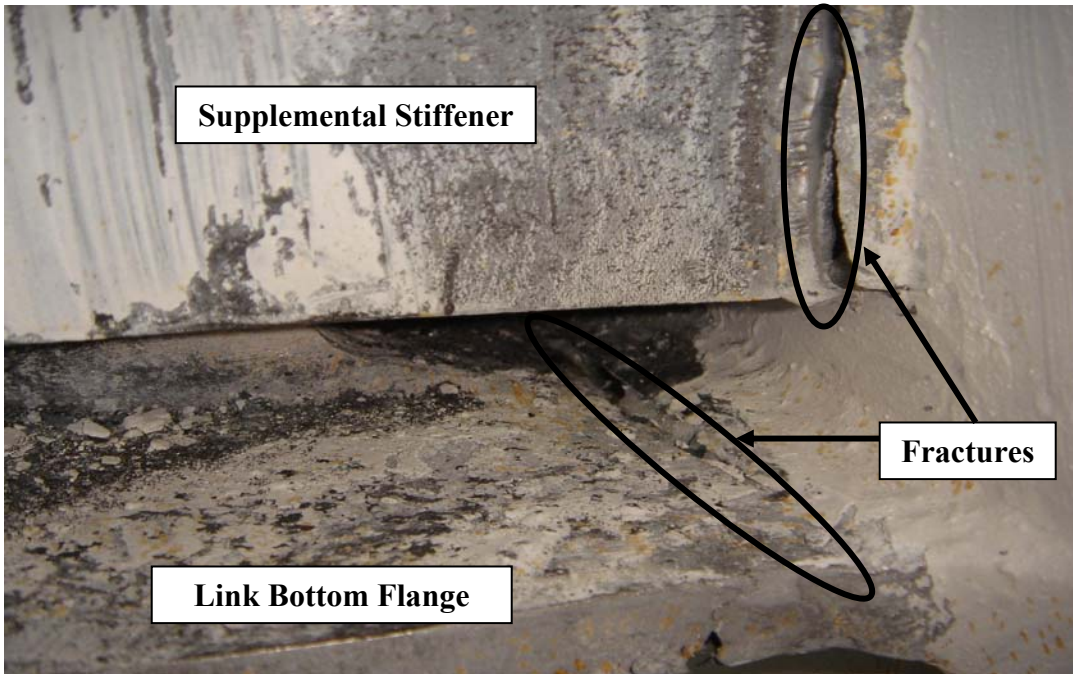


Figure 3.58: Link-to-Column Connection after Failure of Specimen AISC-8 during Loading Cycle of $\gamma = \pm 0.09$ rad (Front View)

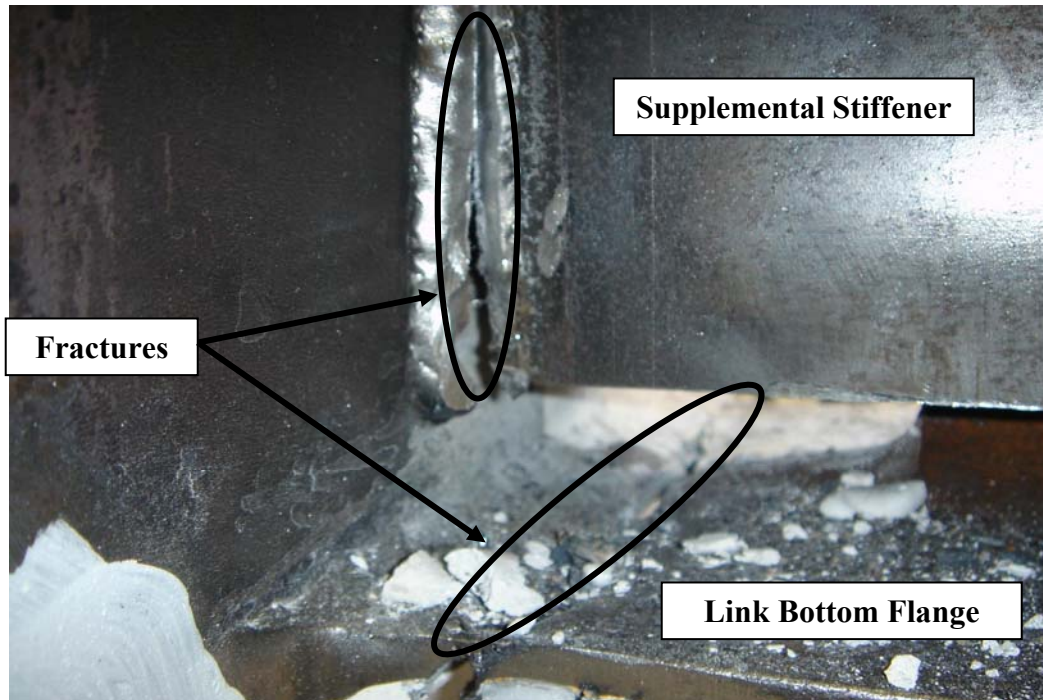


Figure 3.59: Link-to-Column Connection after Failure of Specimen AISC-8 during Loading Cycle of $\gamma = \pm 0.09$ rad (Back View)



Figure 3.60: Location of Yielding at the Link Flanges after Failure of Specimen AISC-8 during Loading Cycle of $\gamma = \pm 0.09$ rad

CHAPTER 4

Additional Experimental Data

4.1 GENERAL

This chapter presents some additional data from this test program that contributes to the understanding the performance of links in EBFs. First, link overstrength is discussed and overstrength factors derived from these experiments are presented. In addition, the end moments developed at the two ends of each link specimen are compared.

4.2 LINK OVERSTRENGTH DATA

For purposes of evaluating link overstrength, the nominal shear strength V_n , of a link is defined as the lesser of V_p or $2 M_p / e$, where V_p and M_p are calculated based on the actual measured dimensions and the actual measured yield stresses of the W-sections used for the link specimens. For all specimens tested in this program, the plastic shear capacity, V_p , controls and thus for the specimens of this project $V_n = V_p$.

Tables 4.1 and 4.2 list overstrength factors for the specimens of Phases I and II, respectively. The link overstrength is a term used to estimate the maximum forces that can be generated by a fully yielded and strain hardened link and it is defined as the maximum shear force developed by a link divided by its nominal shear strength, V_n . That is, the link overstrength factor is specified as the ratio of V_{max} / V_p , where V_{max} is the absolute value of the largest shear force reported in each test. Link overstrength, mainly, occurs due to strain hardening exhibited by the steel sections, and due to shear resistance developed by the link flanges. Link overstrength is a key parameter in the design

procedure used in EBFs. As described in Chapter 1, EBFs follow the “Capacity Design” concept, according to which all members outside the link must be designed for the forces generated by the fully yielded and strain hardened links. That is to say, the braces, the beam segments outside the links and the columns are designed to remain essentially elastic under the maximum forces developed in the links. Similarly, link-to-column connections must also be capable of sustaining the maximum forces generated by the link. Therefore, an estimate of the maximum forces generated by the links is needed in many aspects of EBF design. The maximum forces can be estimated by multiplying the nominal shear strength, V_n , of the link by an overstrength factor. Consequently, a safe and economical EBF design requires on a realistic approximation of the overstrength exhibited by the links.

As used in the *AISC Seismic Provisions*, the link overstrength factor is defined as the ratio V_{max}/V_n . Note that overstrength does not include any increases in link strength due to a material yield strength that is in excess of the minimum specified value. In the *AISC Seismic Provisions*, this effect is accounted for separately by using the *expected yield stress* for the link. Thus, in Tables 4.1 and 4.2,, overstrength is computed with respect to V_n using actual measured yield stress.

Table 4.1 also lists the ratio of M_{max}/M_p for specimens AISC-1 through 4, where M_{max} denotes the absolute value of the maximum link end moments developed at the column end of each link, and M_p the plastic moment capacity of the link based on measured yield stress values. Table 4.2 lists two different moment ratios; the first is the ratio of $M_{stiff,max}/M_p$ and the second is the ratio of M_{max}/M_{pr} . $M_{stiff,max}$ is the absolute value of the maximum link moment developed at the location of the first vertical stiffener and it was computed as $M_{stiff} = M_c - V(e_{total} - e_{active})$. M_{max} is the maximum link moment at the column face. Finally, M_p is the plastic moment capacity of the link and M_{pr} is the

estimated actual plastic moment capacity of the reinforced portion of the link, computed as $M_{pr} = M_{p,W-section} + Z_{stiff}(F_y)$. The plastic moment capacity of the W-shape link, $M_{p,W-section}$, is based on measured dimensions and yield stress values. The plastic moment capacity of the stiffeners, $Z_{stiff}(F_y)$ is based on the minimum specified yield stress of 50 ksi for the stiffeners material, as coupon data was not available for this material.

The moment ratios in Table 4-2 indicate what percentage of the link moment capacity is reached at two critical locations of interest on the link. For the Phase II specimens, the ratio $M_{stiff,max} / M_p$ can be used for the design of the supplemental stiffeners. The ratio M_{max} / M_{pr} provides an indication of whether the reinforced portion of the link remained elastic, as intended.

Recent tests on rolled wide-flange links constructed of A992 steel (Okazaki et al; 2005) showed strength increases due to strain hardening ranging from 1.11 to 1.47, with an average of 1.35. When considering only shear yielding links, the average overstrength factor was 1.41. Further tests done on shear yielding links (Galvez; 2004) demonstrated link overstrength factors ranging from 1.25 to 1.55, with an average of 1.36.

In this research project, links experienced strength increases ranging from 1.35 to 1.52, with an average value of 1.42. That is, on average, the maximum shear force developed by these specimens was 1.42-times the link nominal strength, based on actual section and material properties. These results further confirm the observed overstrength in shear links of previous test programs.

The EBF design requirements, as stated in the 2005 AISC *Seismic Provisions*, are based on an assumed link overstrength of 1.5. However, the *Seismic Provisions* specify a link overstrength factor of 1.25 for the design of the diagonal braces, and an overstrength factor of 1.1 for the design of the beam segments outside of the link and for the columns. As described in the commentary of the *Seismic Provisions*, these factors are less than 1.5

for a number of reasons, including the use of the R_y factor to account for material overstrength in the link but not in the beam or the brace, the use of resistance factors when computing the strength of the brace and other members outside of the link, and the ability of members outside the link to sustain limited yielding among others. Concluding, the results of this experimental project indicate that the overstrength factor of 1.5, which forms the basis for EBF design requirements in the 2005 AISC *Seismic Provisions*, appears reasonable for shear links tested in this program.

Specimens AISC-4, 6, and 7, fabricated using W10x68 links, did not experience unusually high link overstrength despite the fact that they have a high ratio of flange to web area. This may indicate that these specimens did not develop significant shear resistance in the link flanges which, in turn, could lead to greater link overstrength. On the other hand, specimens AISC-1, 2, 3, 5, and 8, fabricated using W18x40 links developed high and in some cases higher link overstrength than the W10x68 specimens.

In Phase I, the highest link overstrength, 1.41, was obtained by specimen AISC-1 and the lowest, 1.35, by specimen AISC-3. Specimens AISC-2 and 4 achieved somewhat less overstrength; 1.39 and 1.38, respectively. The smaller overstrength of AISC-2 compared to AISC-1 can be explained due to the better performance and the higher inelastic link rotation achieved by the latter, which was credited to the different welding process and electrodes used since these two specimens were otherwise identical. Similarly, specimen AISC-3 developed the lowest link overstrength due to the premature failure which did not allow the specimen to achieve its full capacity.

In Phase II, the highest link overstrength, 1.52, was obtained by specimen AISC-5 and the lowest, 1.43, by specimens AISC-7 and 8. Specimen AISC-6 achieved a link overstrength of 1.48. The high overstrength observed in specimens AISC-5 and 6 may be attributed to the very large inelastic link rotation developed by these links. On the other

hand, the observed link overstrength of specimens AISC-7 and 8 was somewhat less since the failure of these specimens occurred in an earlier stage which did not allow them to develop as large a degree of strain hardening. Nevertheless, it is interesting to note that despite the fact that specimen AISC-8 failed prematurely by fracture of the link bottom flange, its achieved link overstrength was 1.43, very close to the overstrength obtained by the other specimens.

Table 4.1: Overstrength Factors for Specimens of Phase I

Specimen	V_p (kips)	M_p (in-k)	$2 M_p / e$ (kips)	V_n (kips)	V_{max} (kips)	M_{max} (in-kips)	V_{max} / V_p	M_{max} / M_p
AISC-1	184	4137	214	184	259	4697	1.41	1.14
AISC-2	184	4137	214	184	256	4888	1.39	1.18
AISC-3	184	4137	214	184	248	4633	1.35	1.12
AISC-4	144	4264	221	144	198	4000	1.38	0.94

Note: V_p , M_p , and V_n in this table are based on measured section dimensions and measured static yield stress values

Table 4.2: Overstrength Factors for Specimens of Phase II

Specimen	V_p (kips)	M_p (in-k)	M_{pr} (in-k)	$2 M_p / e$ (kips)	V_n (kips)	V_{max} (kips)	$M_{stiff,max}$ (in-k)	M_{max} (in-k)	V_{max} / V_p	$M_{stiff,max} / M_p$	M_{max} / M_{pr}
AISC-5	184	4137	6204	214	184	280	4262	5800	1.52	1.03	0.93
AISC-6	144	4264	5305	221	144	213	3300	4366	1.48	0.77	0.82
AISC-7	144	4264	4710	221	144	206	2983	4053	1.43	0.70	0.86
AISC-8	184	4137	5171	214	184	264	3878	5250	1.43	0.94	1.02

Note: V_p , M_p , and V_n in this table are based on measured section dimensions and measured static yield stress values

4.3 LINK END MOMENTS

The test setup was originally designed to provide greater rotational restraint at the column end of the link than at the beam end of the link in the elastic range of behavior (Okazaki; 2004), in order to realistically represent the environment of an EBF with one link end connected to the column. Therefore, with this configuration the initial elastic end moment at the column end of the link is expected to be larger than that at the beam end of the link, as shown in Figure 2.2. As the test proceeds and the link yields, there is a tendency for the end moments to equalize, due to redistribution of the link moment from the column end to the beam end. Nonetheless, according to the 2005 *AISC Seismic Provisions*, complete equalization of the link end moments is not expected to occur in shear yielding links attached to columns.

This section provides plots of the hysteretic relation between the column face moment of the link, denoted as M_c , and the beam face moment of the link, denoted as M_b . Specifically these plots illustrate:

- The largest initial elastic end moment,
- The redistribution of the link moment during the test, as the link yields,
- The degree to which the link end moments equalize,
- The effect of the rapid loss in strength in the $M_c - M_b$ relation, after the development of fractures in the link-to-column connection, or the link web, and
- The magnitude of the developed link end moments.

Figures 4.1 through 4.8 present the hysteretic relation between M_c and M_b . Furthermore, Figures 4.9 through 4.12 demonstrate the hysteretic relation between M_c and M_{stiff} of specimens AISC-5 through 8. As noted above, M_{stiff} represents the link moment at the location of the first vertical stiffener. These plots are intended to examine the end moments of the active portion of the link. The bending moments at the link ends

were calculated following the sign convention shown on Figure 1.3. The dotted line in Figures 4.1 through 4.12 represents the condition where the link end moments are equal.

The plots of all specimens confirm that the highest initial elastic link moment occurred at the column end of the link, as intended. Furthermore, the plots indicate a large redistribution of the link moment from the column end to the beam end of the link, as it enters the strain hardening.

In specimen AISC-8 the link end moments M_c and M_b equalized at the end of the experiment. Nevertheless, in all other specimens, despite the fact that at some point during the test the moments equalized, a few cycles prior to fracture, the moment at the beam end of the link became bigger. It is also interesting to note that in many specimens the $M_c - M_b$ relation was different in the two directions of the loading. This may be attributed to the application of different link rotation angles between the loading and the reverse loading, due to the exhaustion of the loading ram stroke in the one direction. This observation is more obvious in specimens AISC-4 through 7.

In specimens AISC-1, 2, 3, and 8 the M_c vs. M_b plots exhibited some irregular behavior during their final cycle. Specifically, a very large redistribution of the moment from the column end to the beam end of the link occurred rapidly. This behavior results from the failure of the specimens by the occurrence of fracture at the link-to-column connection. This failure resulted in a dramatic loss of flexural stiffness at the column end of the link which, in turn, led to the large redistribution of the moment to the beam end of the link. As a result of this large moment redistribution, the beam end of the link developed a very large moment. On the other hand, specimens AISC-4, 5, 6, and 7 exhibited milder link moment redistribution, as a result of the failure being in the link web away from the link-to-column connection.

At this point it has to be noted that the links of all specimens except AISC-5 developed larger moment at the beam end than at the column end, even prior to the occurrence of any kind of fracture at the link. This behavior may be an artifact of the test setup, reflecting the high flexural stiffness of the reinforced portion of the beam in the region adjacent to the link.

Finally, after observing the M_{stiff} vs. M_b plots of specimens AISC-5 through 8, it can be concluded that the initial elastic moments of both ends of the active link were close to being equal. However, as the link yielded, the moment of the beam end became greater than the moment of the link at the location of the first vertical stiffener.

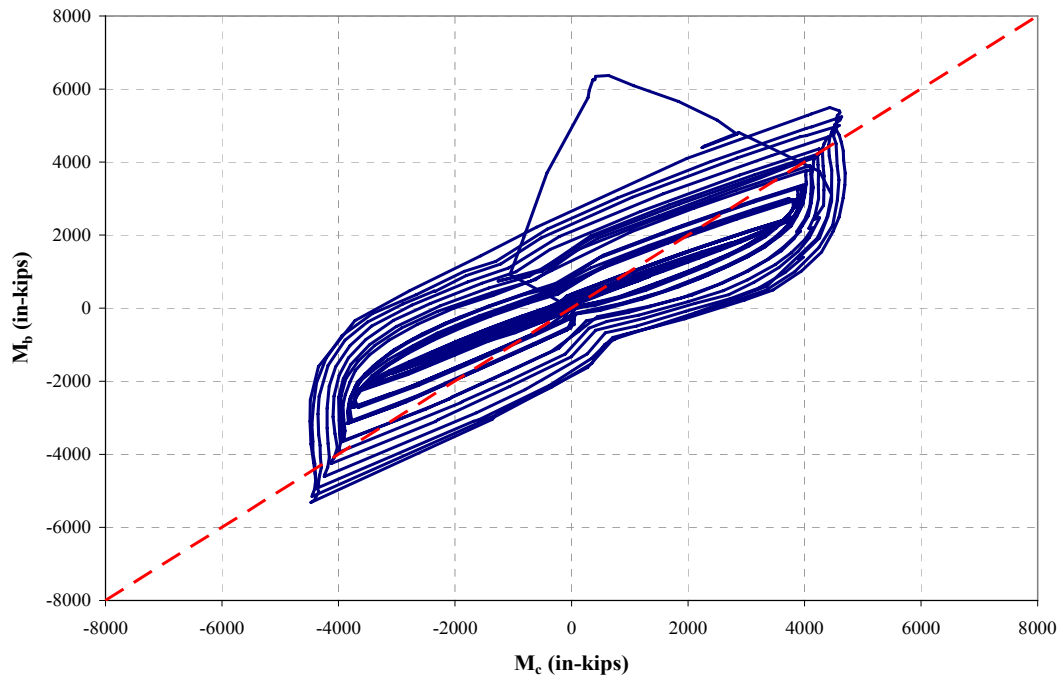


Figure 4.1: Link end moment relationship of Specimen AISC-1

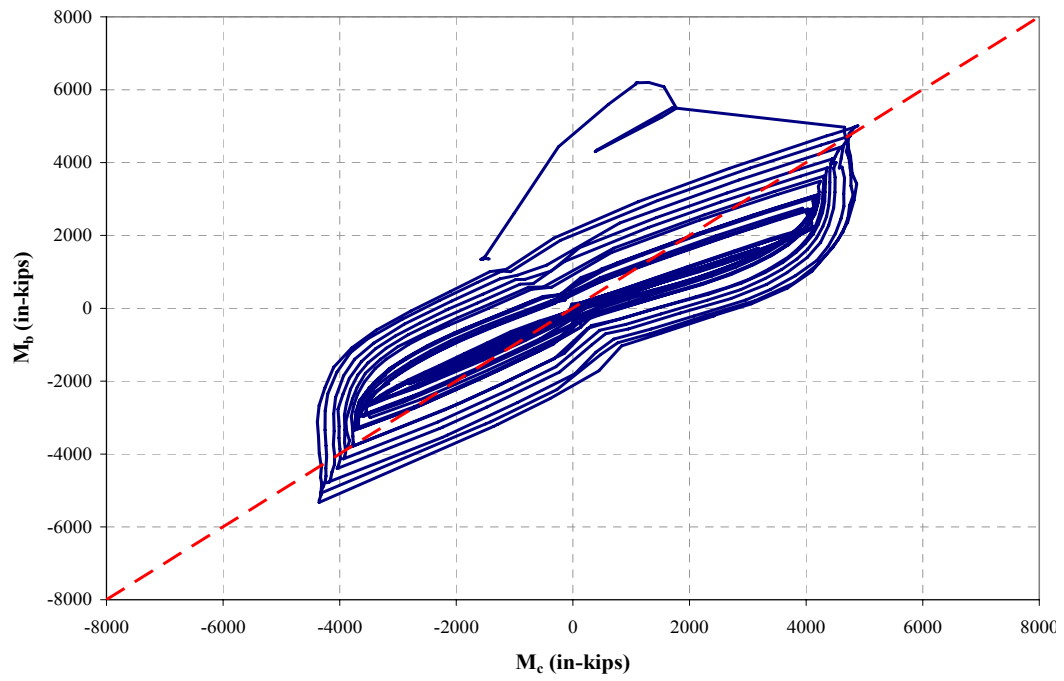


Figure 4.2: Link end moment relationship of Specimen AISC-2

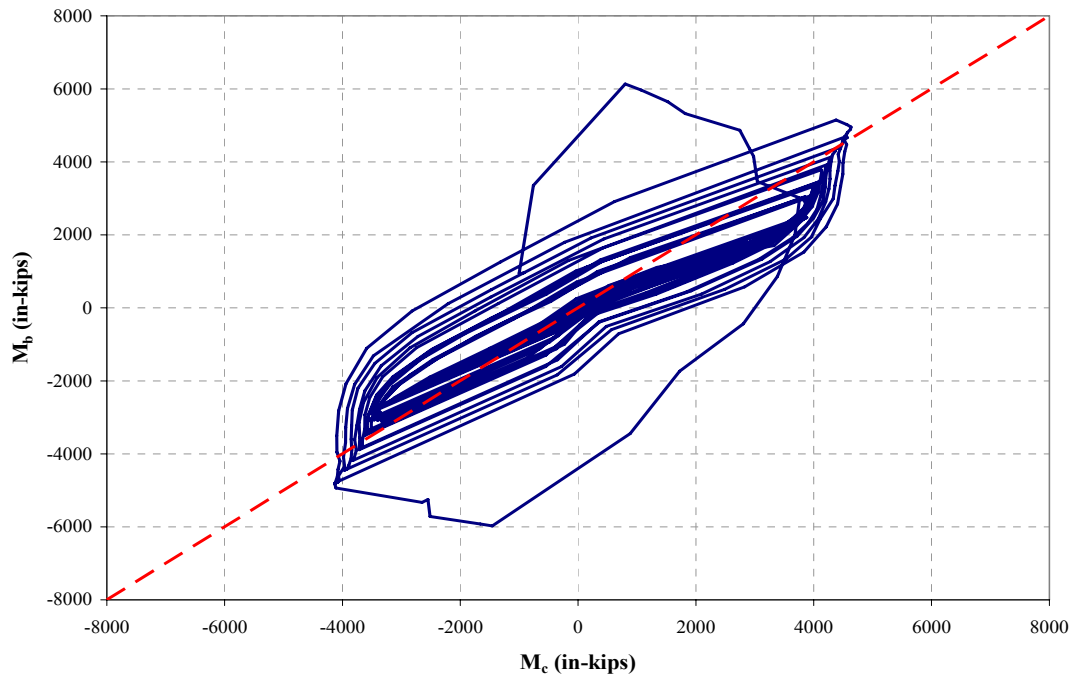


Figure 4.3: Link end moment relationship of Specimen AISC-3

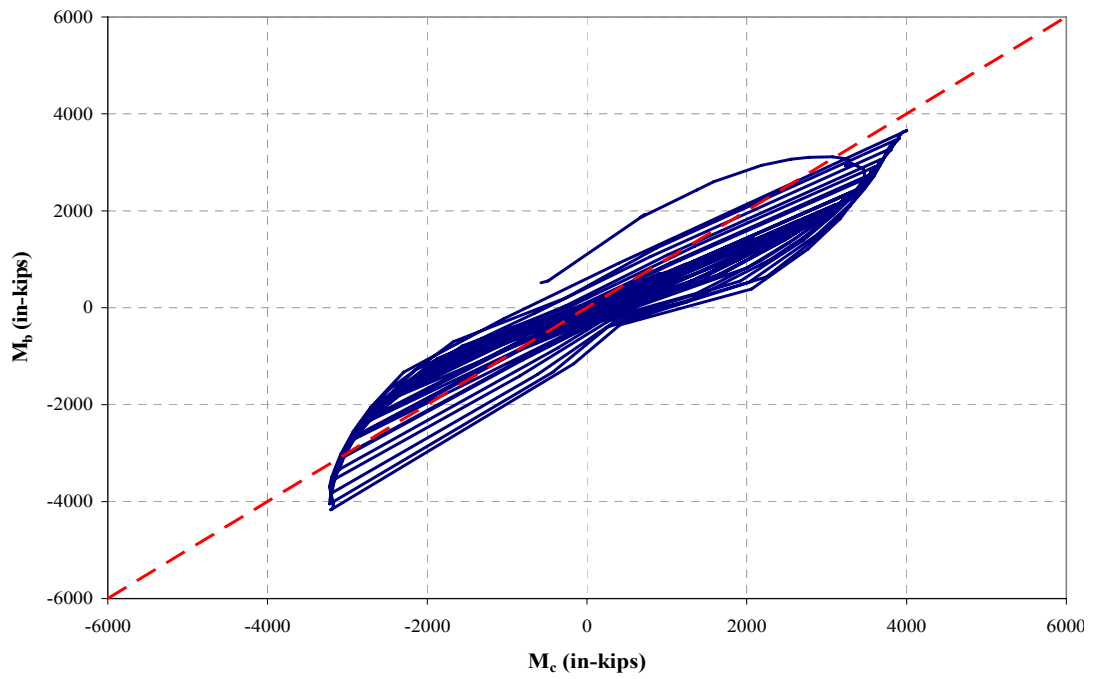


Figure 4.4: Link end moment relationship of Specimen AISC-4

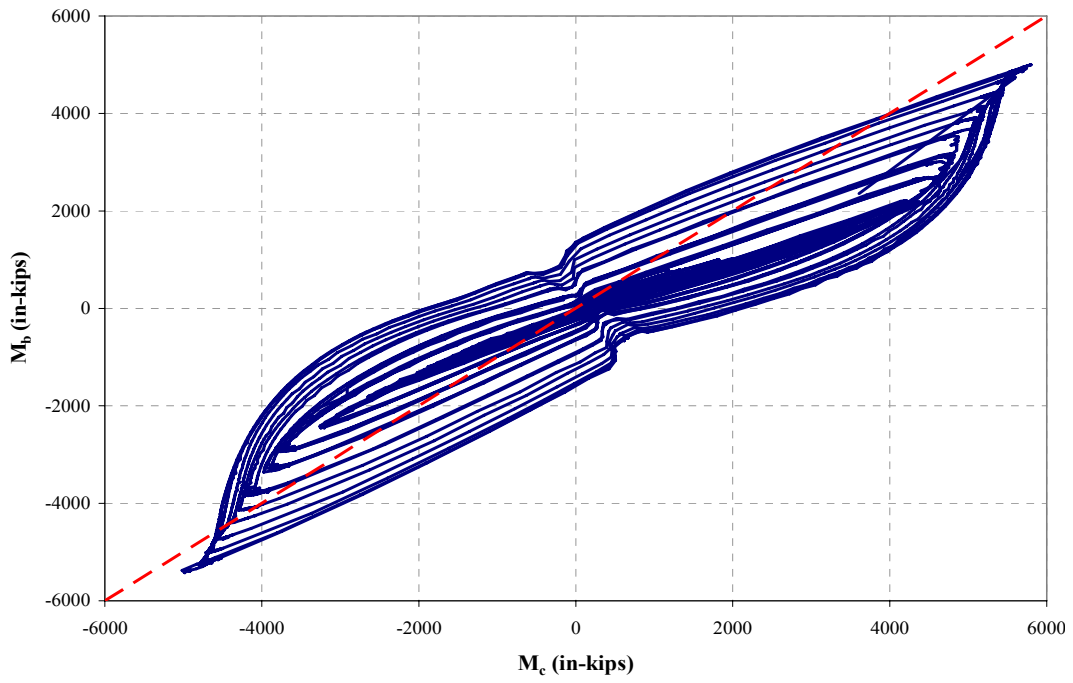


Figure 4.5: Link end moment relationship of Specimen AISC-5

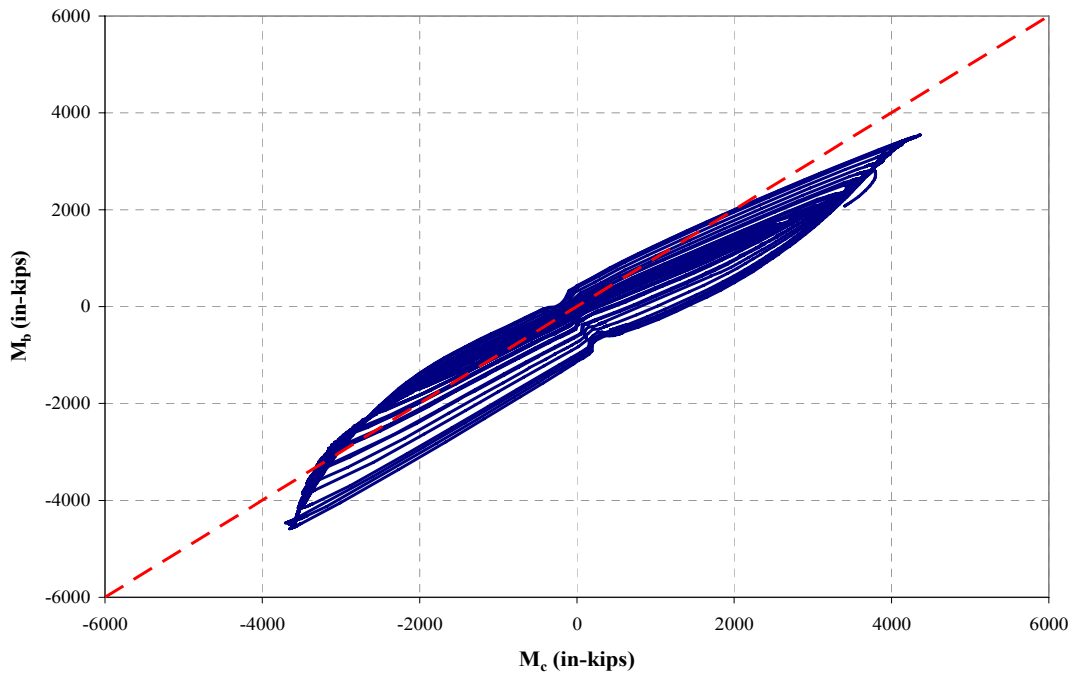


Figure 4.6: Link end moment relationship of Specimen AISC-6

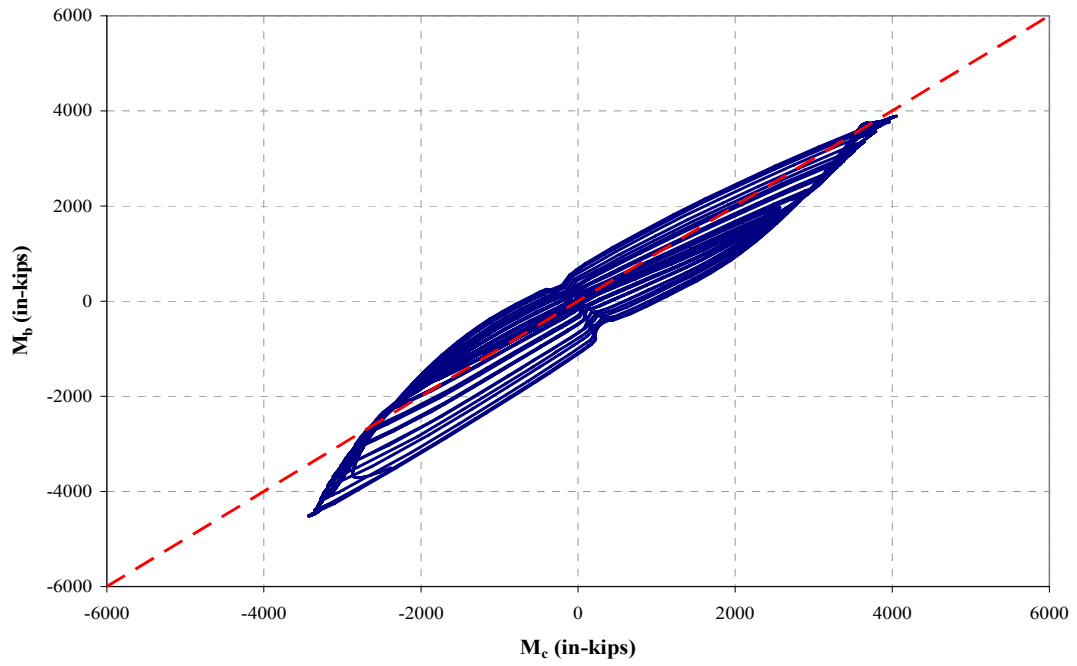


Figure 4.7: Link end moment relationship of Specimen AISC-7

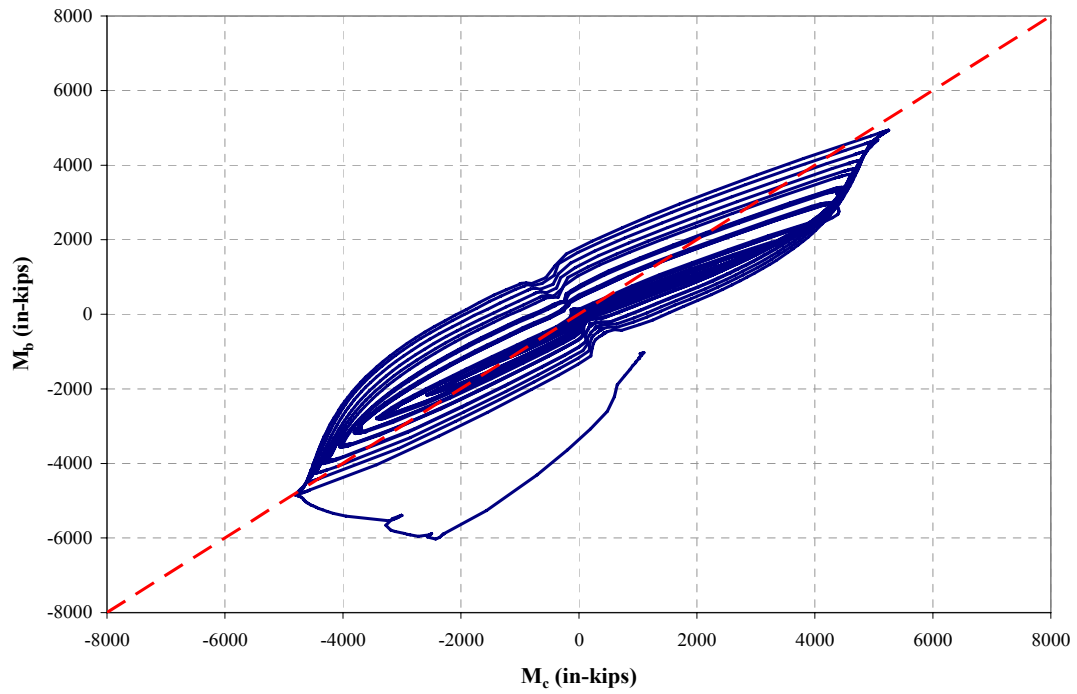


Figure 4.8: Link end moment relationship of Specimen AISC-8

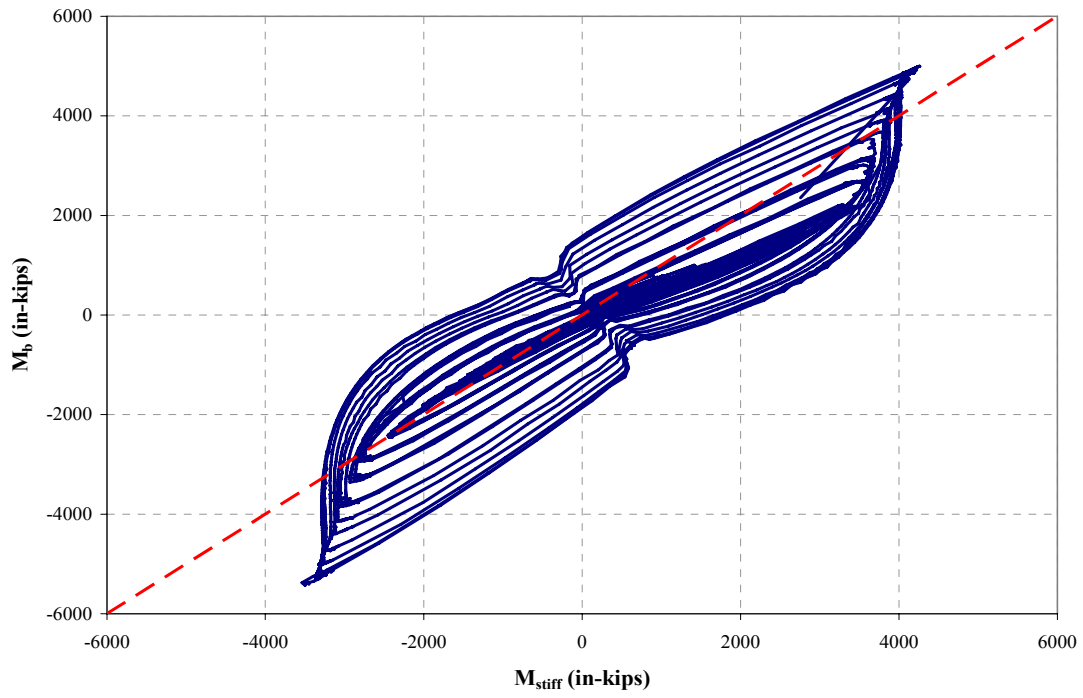


Figure 4.9: Active Link end moment relationship of Specimen AISC-5

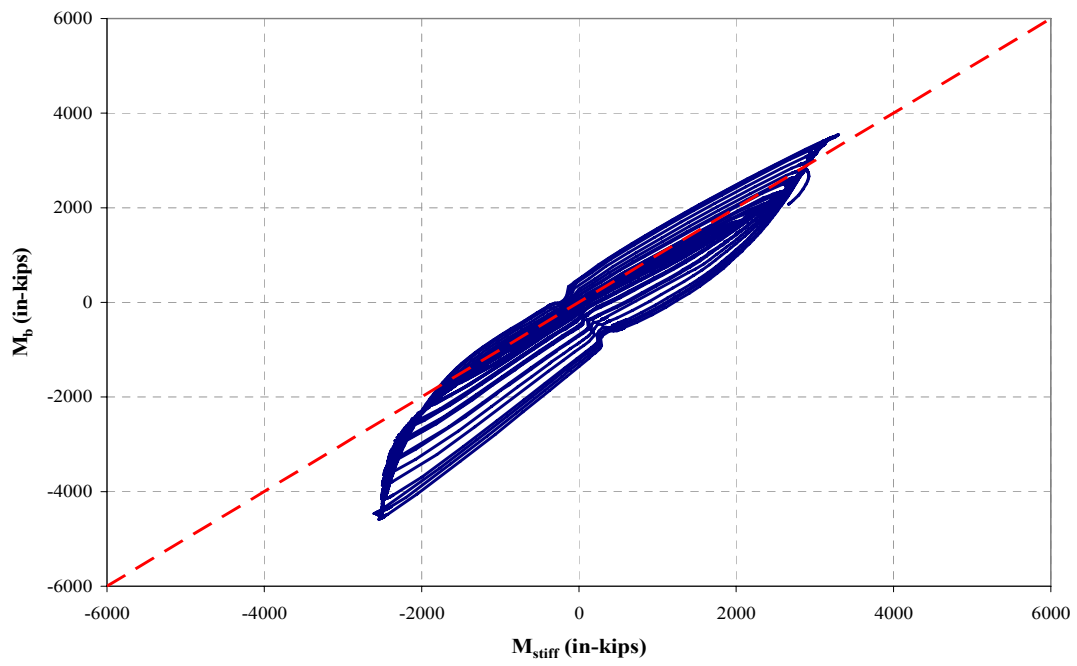


Figure 4.10: Active Link end moment relationship of Specimen AISC-6

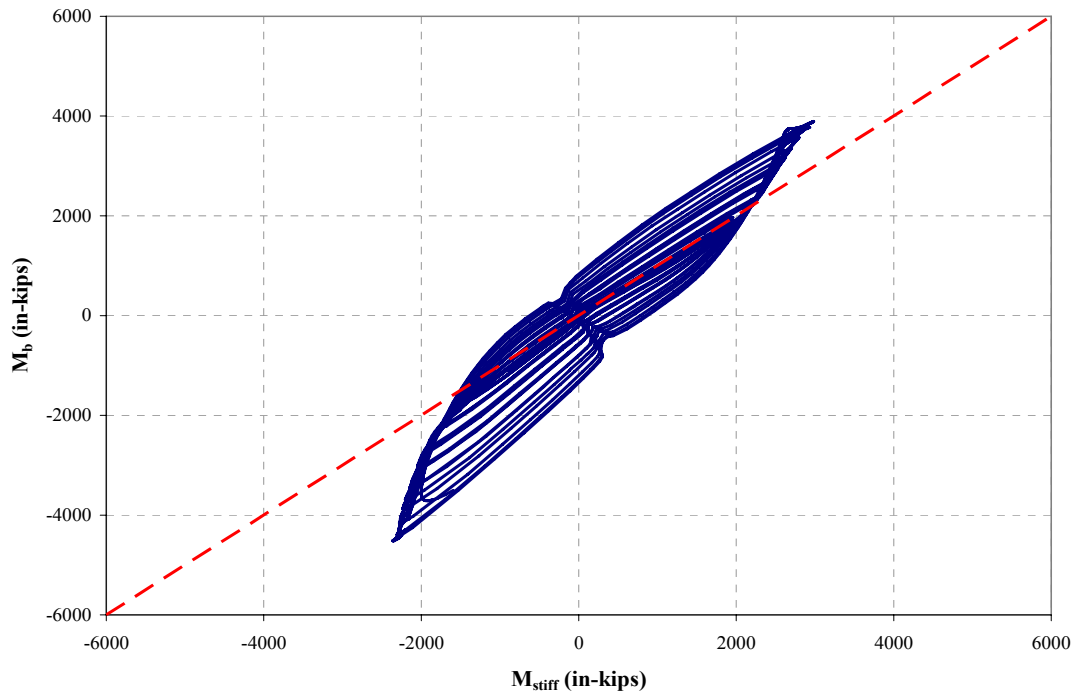


Figure 4.11: Active Link end moment relationship of Specimen AISC-7

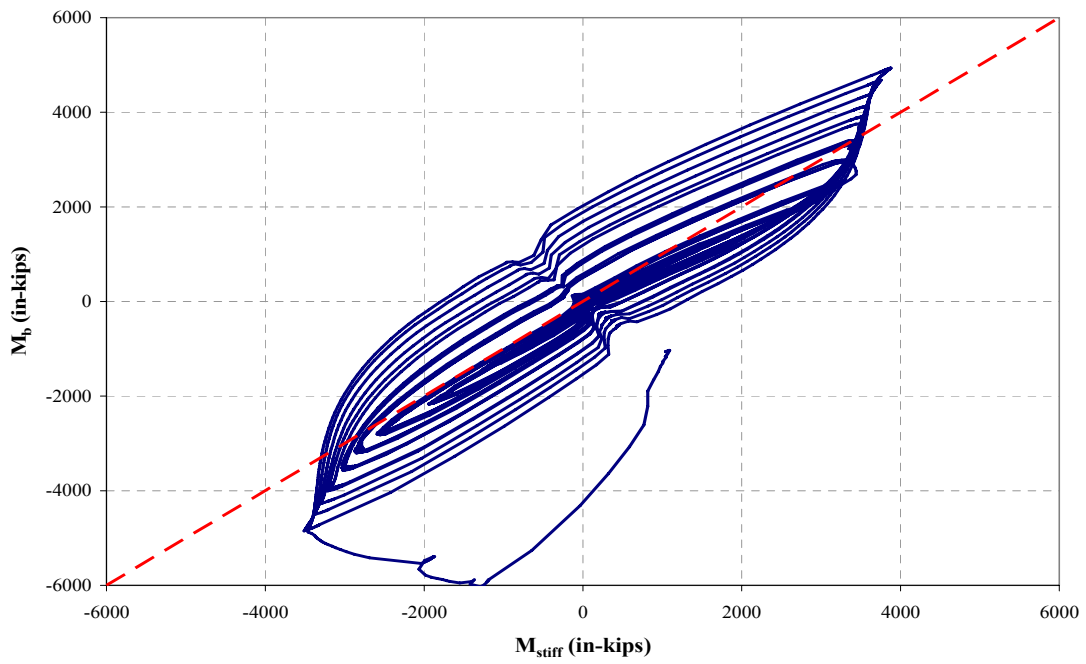


Figure 4.12: Active Link end moment relationship of Specimen AISC-8

CHAPTER 5

Summary and Conclusions

5.1 SUMMARY

This thesis has documented the results of an experimental project on the cyclic loading performance of link-to-column connections in seismic-resistant steel Eccentrically Braced Frames. Previous research in this area has highlighted the very large force and deformation demands on link-to-column connections and the difficulty in identifying economical and practical details that can provide satisfactory performance. Therefore, the main objective of this experimental project, which has built upon recent work in this area by others, was to conduct pilot tests on two proposed link-to-column connections details to evaluate their potential to satisfy the connection performance requirements of the 2005 AISC *Seismic Provisions*.

A total of eight specimens, designated as AISC-1 to AISC-8, were tested in this program to evaluate two different link-to-column connection details. In the first detail, used in specimens AISC-1 through 4, the link was welded to the face of the column using either double-sided fillet welds, or a combination of PJP groove welds and fillet welds. This detail uses no weld access holes in the link. Because of fit-up tolerances, this detail is not likely to be suitable for field welding. Rather, this detail is envisioned to be most appropriate as a shop welded link-to-column connection. In this “column tree” approach, columns with shop attached links would be shipped to the field, where the brace and beam segment outside of the link are then attached with bolted or welded splices. This connection type was motivated by successful tests of a similar detail in an investigation by Arce and Okazaki (Arce et al; 2003, Okazaki et al; 2005).

The second link-to-column connection detail, used in specimens AISC-5 through 8, was constructed with reinforcement, in the form of two supplemental stiffeners in the first panel of the link adjacent to the column. The link flanges and web are connected to the column flange using CJP groove welds. The supplemental stiffeners, placed parallel to the link web, are then welded to the column flange and the first vertical stiffener using either CJP groove welds or fillet welds. This detail is expected to be suitable for field welding, and was developed in a joint study with Hong and Uang (2005, 2006) at the University of California at San Diego (UCSD).

The eight specimens tested in this program were built from A992 steel. The links were constructed using W18x40 and W10x68 sections, while W12x120 sections were used for all the columns. The length of each link was 38.6-inches, and all links were in or near the shear yielding range. The test setup used for this program was originally designed and constructed by Okazaki (2004) and Arce (2002), and replicates the forces and deformations imposed on a link for EBF configurations with the links attached to columns.

All specimens were tested by applying increasing levels of cyclic link rotation following the link loading protocol specified in Appendix S of the 2005 AISC *Seismic Provisions*. Failure of the specimen was assumed to occur, as specified in the *Seismic Provisions*, when the shear resistance of the specimen dropped below the nominal shear strength of the link, V_p .

The primary parameter used to assess the performance of each specimen was the maximum plastic rotation angle, γ_p , developed by the link and sustained for at least one full cycle of loading prior to failure. The measured value of γ_p was compared to a target plastic rotation angle, specified depending on the length of the link, per the 2005 AISC *Seismic Provisions*.

5.2 RESULTS AND CONCLUSIONS

The performance of the eight specimens tested in this experimental program was presented in Chapter 3, accompanied by a discussion about the key events that characterized this performance. Chapter 4 provided some additional data on the specimen behavior. The most important observations made from this research program can be summarized in the following:

- Six of the eight specimens achieved the target plastic rotation requirements of the 2005 AISC *Seismic Provisions*. These specimens showed good overall performance, acquiring plastic rotation angles 19 to 50-percent in excess of the required levels.
- All specimens failed ultimately either by fracture of the link top or bottom flange base metal, adjacent to the weld of the link-to-column connection, or by fracture of the link web initiating at the termination of the stiffener fillet welds.
- The three specimens constructed using W10x68 sections as links, with a link length of $e = 1.30 M_p / V_p$ confirmed the observation that the dominant failure mode of links with length $e < 1.7 M_p / V_p$ is link web fracture initiating at the termination of the stiffener fillet welds. This observation was made by Arce (2002), Ryu (2004), and Galvez (2004) after a large number of tests conducted on shear yielding links.
- The specimen constructed with all-around fillet welds at the link-to-column connection using the SMAW welding process showed marginally better performance than the specimen with the same link-to-column detail fabricated using the FCAW-GS

welding process. Nonetheless, the specimen with the FCAW-GS process still achieved the link target plastic rotation required by the 2005 AISC *Seismic Provisions*.

➤ The limited number of tests conducted in Phase I of this research program, together with a large number of successful tests on a similar detail by Okazaki et al (2005) suggests that the simple shop-welded link-to-column connection provides a viable connection concept for the seismic resistant EBFs. Specifically, the test results of the first four specimens demonstrated that:

1. The use of the FCAW-GS welding process with E70T-9 electrodes, preferred in the shop-welded applications, resulted in a satisfactory performance.
2. The simple shop-welded link-to-column connection detail composed of all-around, double-sided fillet welds performed very well. According to the test results, the fillet welds with a leg size approximately equal to 1.5-times the thickness of the connected link flange or web provide satisfactory performance.
3. The use of an alternative link flange weld detail, for shallow links with thick flanges, which combines a partial joint penetration groove weld together with a fillet weld, also demonstrated an excellent performance.

➤ From the limited number of tests conducted in Phase II, it appears that the field-welded, reinforced link-to-column connection is a promising connection detail for the seismic resistant EBFs. Specifically, the test results demonstrated that:

1. Links reinforced at the first panel adjacent to the column with thick supplemental stiffeners welded to the column flange and the first vertical stiffener using CJP groove welds exhibited excellent performance. In these specimens, the reinforced

- panel of the link remained essentially elastic and at the end of the testing no apparent distress at the link-to-column connection was observed.
2. Links reinforced at the first panel adjacent to the column with thin supplemental stiffeners connected to the column flange and the first vertical stiffener using one-side fillet welds, with a leg size equal to the thickness of the supplemental stiffeners exhibited somewhat inconclusive results. Therefore, further analytical research and testing is needed to evaluate the lower limit of stiffener thickness and weld size needed for satisfactory performance.
- In this research project, links experienced strength increases ranging from 1.35 to 1.52, with an average value of 1.42. That is, on average, the maximum shear force developed by these specimens was 1.42-times the link nominal strength, based on actual section and material properties. These results are in accordance with recent tests on rolled wide-flange shear yielding links constructed of A992 steel (Okazaki et al; 2005) which showed strength increases due to strain hardening ranging from 1.34 to 1.47, with an average of 1.41. Furthermore, the results of this experimental project indicate that the overstrength factor of 1.5, which forms the basis for EBF design requirements in the 2005 *AISC Seismic Provisions*, appears reasonable for shear links constructed of typical rolled W-sections.

In conclusion, this experimental research program conducted at the University of Texas at Austin combined with the analytical studies done at the University of California at San Diego has identified two very promising link-to-column connection details; one intended primarily for shop welding application and the other intended primarily for field welding application. Both details showed the potential for outstanding performance, with

the capability of developing the link's full plastic rotation capacity without connection failure, and the capability of satisfying the link-to-column connection performance requirements of the 2005 AISC *Seismic Provisions*.

Only a small number of tests were conducted in this pilot program. Nonetheless, the excellent performance of the connections in these tests justifies further work on these details. Additional analytical and large-scale experimental studies are recommended to further confirm the performance of these connections, identify appropriate limits of application for these details, and to further refine the preliminary design approaches that have been developed for these connections.

APPENDIX A

Welding/Fabrication Sequence and Welding Procedures

A.1 GENERAL

This appendix lists the welding/fabrication sequence and the welding procedures used to construct the specimens of Phase II, AISC-5 through AISC-8. These procedures include the description of all the fabrication and welding steps followed for the construction of the left end connection of the link, as well as for the link-to-column connection.

A.2 SPECIFIED PROCEDURES

The welding procedures include a detailed description of the welding of the vertical stiffeners to the link, the welding of the left link end to the 2-inch thick end plate, the welding of the right link end to the column flange, and the welding of the supplemental stiffeners to the column flange and the first vertical stiffener. Each description includes the citation of the welding process and electrodes used, accompanied by fabrication details and a reference to the appropriate pre-qualified welding procedure specification.

Two different welding procedures were prepared. The first one was followed for the construction of specimens AISC-5 and AISC-8. These two specimens had the same link sections and differed only in the design of the supplemental stiffeners. Therefore, in this procedure, there is a difference in the welding detail of the supplemental stiffeners. Step 11 was divided in 11A and 11B denoting the supplemental stiffener procedure for specimen AISC-5 and AISC-8, respectively. The second welding procedure was followed

for the construction of specimens AISC-6 and AISC-7. Similarly, these two specimens had the same link sections and differed only in the design of the supplemental stiffeners. Therefore, Step 11 was again divided in 11A and 11B denoting the supplemental stiffener procedure for specimen AISC-6 and AISC-7, respectively.

The two welding procedures differed only in the welding detail of the link left end to the thick end plate. Specifically, for the thick flanges of specimens AISC-6 and 7, it was decided to make partial penetration groove welds between the outside face of the link flanges and the end plate, and fillet welds between the inside faces of the link flanges and the end plate, and between the link web and the end plate. On the other hand, specimens AISC-5 and AISC-8 were connected to the thick end plate using simple all-around fillet welds.

Detailed welding procedures were not documented for Specimens AISC-1 to AISC-4. However, the welding details, processes, procedures and electrodes used for the left end of the links for AISC-5 to AISC-8 (to connect to the 2-inch thick end plates) described below were identical to the welding details, processes, procedures and electrodes used to weld the link-to-column connections in Specimens AISC-1 to AISC-4.

Specimens AISC-5 & AISC-8 – Welding/Fabrication Sequence and Welding Procedures

1. Weld vertical stiffeners to link (fillet welds).
For each stiffener – weld stiffener to link flanges first, then weld stiffener to link web.
Use gas-shielded FCAW with E70T-9 electrode (Lincoln OS-70 or OS-70H; 3/32”). Orient link so that welds are made in a flat position.
Use Schuff Steel Co. WPS No. F 105-70T-9.
No preheat required.
2. Weld link to 2" thick end plate.
Use gas-shielded FCAW with E70T-9 electrode (Lincoln OS-70 or OS-70H; 3/32”). Orient link so that welds are made in a flat position.
Use Schuff Steel Co. WPS No. F 105-70T-9.
Preheat end plate to at least 150⁰ F.
3. Weld shear tab to column flange.
Use self-shielded FCAW with E71T-8 electrode (Lincoln 0.072" NR-232).
Orient column so that welds are made in a flat position.
Use WPS No. EBF5-1.
4. Bolt link web to shear tab. Fully tension bolts using turn-of-nut method.
5. Place specimen in upright position (i.e. same position as it would be in the field). Make all remaining welds with specimen in this position.
6. Weld link flanges to column flange. Use self-shielded FCAW with E70T-6 electrode (Lincoln 3/32" NR-305). No preheat is required. Make welds as follows:

- a. Tack weld 3/8" x 1" backing bars to link flange and to column flange. Length of backing bars should be adequate so that they extend approximately 2-inches beyond end of link flange. Tack welds should be located so that they will be incorporated inside the groove weld.
- b. Attach weld tabs. Weld tabs should extend groove approximately 2-inches beyond edge of link flange. Tack welds should be located so that they will be incorporated inside the groove weld.
- c. Make groove weld between link top flange and column flange using WPS # EBF5-2. Each weld bead should start on a weld tab and end on the opposite weld tab.
- d. Make groove weld between link bottom flange and outside face of column flange using WPS # EBF5-2. Welding at the bottom flange should be in accordance with the following:
 - i. Weld one bead on one side of the bottom flange, starting at the weld access hole. After arc is initiated, travel should progress toward the edge of the flange. The bead should be terminated on the weld tab. The start of the bead in the weld access hole should be visually inspected to ensure fusion, soundness, freedom from slag inclusions, and excess porosity. The resulting bead profile should be suitable for obtaining good fusion by the subsequent pass to be initiated on the opposite side of the beam web. If the profile is not conducive to good fusion, the start of the weld bead should be gouged, chipped, or otherwise prepared to ensure good fusion.
 - ii. Weld one bead on the other side of the bottom flange. Follow same instructions as in (i) above.

- iii. Continue placing beads on alternate sides of the link web in accordance with (i) and (ii) above until weld is completed.
7. Using carbon air arc gouge, remove the backing bar at the beam bottom flange groove weld and backgouge root of CJP groove weld to sound metal. Care should be taken so as not to damage the base metal when removing the backing bar and during backgouging. Any pits, gouges, discontinuities and slag pockets discovered at the root of the groove weld should be grounded out. Reweld root of CJP groove weld from underneath the weld and place a 5/16" fillet weld using WPS # EBF5-3. (Lincoln 0.072" NR-232 electrode).
8. Place a 5/16" fillet weld between the backing bar and the column flange at the top beam flange groove weld using WPS # EBF5-4. (Lincoln 0.072" NR-232 electrode). No preheat is required.
9. Using carbon air arc gouge, remove weld tabs from both the top and bottom beam flange groove welds. Grind smooth and inspect ground surfaces for discontinuities. Inclusions 1/16" or less in depth shall be removed by grinding. Deeper indications should be removed and replaced by welding.
10. Make groove weld between link web and column flange (shear tab serves as backing). Use self-shielded FCAW with E71T-8 electrode (Lincoln 0.072" NR-232). Weld should extend full depth of the link web, from access hole to access hole.
Use WPS # EBF5-5. No preheat is required.
- 11A Weld secondary stiffeners to column flange and to vertical stiffener. For each of the two stiffeners, use the following procedure:
 - a. Tack weld 3/8" x 1" backing bars to face of column flange and to vertical stiffener. Length of backing bars should be adequate so that they extend approximately 1/2-inches beyond ends of the secondary stiffener. Tack

welds should be located so that they will be incorporated inside the groove weld.

- b. Do not use weld tabs.
- c. Weld the secondary stiffener to the column flange. Use self-shielded FCAW with E71T-8 electrode (Lincoln 0.072" NR-232). Use WPS #EBF5-5. No preheat is required.
- d. Weld the secondary stiffener to the vertical stiffener. Use self-shielded FCAW with E71T-8 electrode (Lincoln 0.072" NR-232). Use WPS #5-5. No preheat is required.

11B Weld secondary stiffeners to column flange and to vertical stiffener. For each of the two stiffeners, use the following procedure:

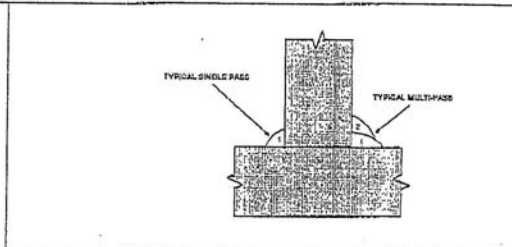
- a. Place secondary stiffeners in the correct position.
- b. Tack secondary stiffeners to face of column flange and to vertical stiffener. Tack welds should be located so that they will be incorporated inside the groove weld.
- c. Weld the secondary stiffener to the column flange. Use self-shielded FCAW with E71T-8 electrode (Lincoln 0.072" NR-232). No preheat is required.
- d. Weld the secondary stiffener to the vertical stiffener. Use self-shielded FCAW with E71T-8 electrode (Lincoln 0.072" NR-232). No preheat is required.



SCHUFF STEEL CO.
Welding Procedure Specification

WPS No. F 105-70 T9 Revision 0 Date 7/11/2002 By JIM MURRAY
 Authorized By JIM MURRAY Date 7/11/2002 Prequalified
 Welding Process(es) FCAW Type: Manual Machine Semi-Auto Auto
 Supporting PQR(s) _____

JOINT
 Type FILLET WELD
 Backing Yes No Single Weld Double Weld
 Backing Material NA
 Root Opening NA Root Face Dimension NA
 Groove Angle NA Radius (J-U) NA
 Back Gouge Yes No
 Method NA



BASE METALS
 Material Spec. SEE NOTES to SEE NOTES
 Type or Grade _____ to _____
 Thickness: Groove () _____ - _____
 Fillet (in) 1/8 - Unlimited
 Diameter (Pipe,) _____ - _____

POSITION
 Position of Groove _____ Fillet 1F, 2F
 Vertical Progression: Up Down

FILLER METALS
 AWS Specification A5.20
 AWS Classification E70T-9 LINC.(OS 70)

ELECTRICAL CHARACTERISTICS
 Transfer Mode (GMAW):
 Short-Circuiting Globular Spray
 Current: AC DCEP DCEN Pulsed
 Other CONSTANT VOLTAGE
 Tungsten Electrode (GTAW):
 Size NA Type NA

SHIELDING
 Flux Gas CO-2
 NA Composition 100%
 Electrode-Flux (Class) Flow Rate 45 CFH
 NA Gas Cup Size 1/2"

TECHNIQUE
 Stringer or Weave Bead Stringer*
 Multi-pass or Single Pass (per side) Either*
 Number of Electrodes 1
 Electrode Spacing: Longitudinal NA
 Lateral NA
 Angle NA
 Contact Tube to Work Distance 1 1/8"
 Peening NONE
 Interpass Cleaning HAND TOOL

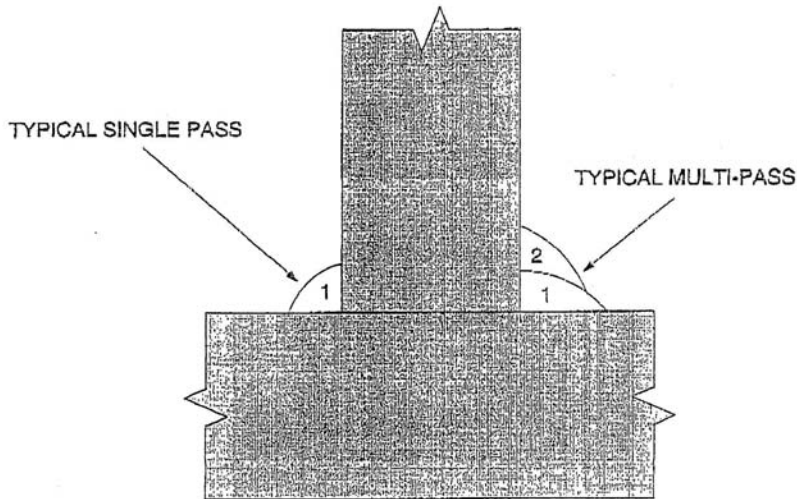
PREHEAT
 Preheat Temp., Min. NONE ****
 Thickness Up to 3/4" Temperature NONE ****
 Over 3/4" to 1-1/2" 50°
 Over 1-1/2" to 2-1/2" 150°
 Over 2-1/2" 225°
 Interpass Temp., Min. NONE **** Max. NONE

POSTWELD HEAT TREATMENT PWHT Required
 Temp. NA Time NA

WELDING PROCEDURE								
Layer/Pass	Process	Filler Metal Class	Diameter	Cup Type	Amps or WFS	Volts	Travel Speed	Other Notes
ALL	FCAW	E70T-9(O.S.70)	3/32	DCEP	455/200ipm	30	20 IPM	NOTE**



SCHUFF STEEL CO.
Welding Procedure Specification



MEMO

NOTES:

*AWS D1.1; TABLE 3.7:
IN FLAT, HORIZONTAL SPLIT LAYERS WHEN THE LAYER WIDTH > 5/8". MAX BEAD THK=1/4"

MAXIMUM SINGLE PASS FILLET WELD SIZE: FLAT= 1/2"; HORIZONTAL= 3/8".

**AWS D1.1; TABLE 4.5:

ALLOWABLE RANGE VARIANCES:

VOLTS: ± 7%

AMPS: ± 10%

WIRE FEED SPEED: ± 10%

TRAVEL SPEED: ± 25%

APPLICABLE MATERIAL FOR THIS PROCEDURE:

A36; A572 GR-50; A992; A913 GR-50; A500 GR-B; A53, TYPE E or S, GR-B.

***AWS D1.1 TABLE 3.2 NOTE 1:

1. When the base metal temperature is below 32°F (0°C), the base metal shall be preheated to at least 70°F (21°C) and this minimum temperature maintained during welding.

PRE-QUALIFIED WELDING PROCEDURE SPECIFICATION

FILLET WELD FLAT POSITION WELD BETWEEN LINK WEB AND SHEAR TAB

WPS # EBF5-1

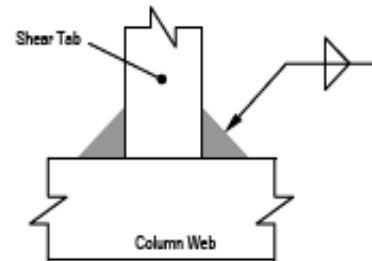
Material Specification: ASTM A36, A572-Gr. 50, A992
 Welding Process: Flux Cored Arc Welding – Self Shielded
 Position of Welding: 2G
 Filler Metal: AWS Specification: 5.20
 AWS Classification: E71T-8
 Brand Designation: Lincoln NR-232
 Diameter: 0.072"
 Current: DC - Electrode Negative

Minimum Preheat and Interpass Temperature:

Thickness	Temperature (deg F)
Up to 3/4"	50
Over 3/4" to 1-1/2"	50
Over 1-1/2" to 2-1/2"	150
Over 2-1/2"	225

Maximum Interpass Temperature: 550° F

Joint Detail:



Welding Procedure

Pass No.	Electrode Diameter	Wire Feed Speed (in / min)	Volts	Approx. Current (amps)	Travel Speed (in / min)
All as Req'd	0.072"	155 - 170	19 - 23	240 - 255	8 - 12
Distance from contact tube to work = 0.5 to 1"					

PRE-QUALIFIED WELDING PROCEDURE SPECIFICATION

COMPLETE JOINT PENETRATION SINGLE BEVEL GROOVE WELD FLAT POSITION WELD BETWEEN LINK FLANGE AND COLUMN FLANGE

WPS # EBF5-2

Material Specification: ASTM A36, A572-Gr. 50, A992
 Welding Process: Flux Cored Arc Welding – Self Shielded
 Position of Welding: 1G
 Filler Metal: AWS Specification: 5.20
 AWS Classification: E70T-6
 Brand Designation: Lincoln NR-305
 Diameter: 3/32"
 Current: DC – Electrode Positive

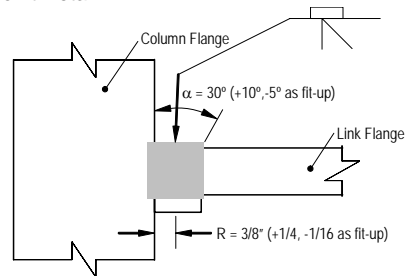
Minimum Preheat and Interpass Temperature:

Thickness	Temperature (deg F)
Up to 3/4"	50
Over 3/4" to 1-1/2"	50
Over 1-1/2" to 2-1/2"	150
Over 2-1/2"	225

Maximum Interpass Temperature: 550° F

Joint Designation: TC-U4a-GF

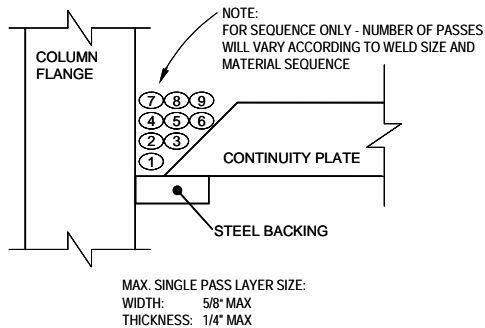
Joint Detail:



Welding Procedure

Pass No.	Electrode Diameter	Wire Feed Speed (in / min)	Volts	Approx. Current (amps)	Travel Speed (in / min)
All as Req'd	3/32"	240 - 300	25 - 29	390 - 475	9 - 15
Distance from contact tube to work = 1-1/2 to 2-1/2"					

Weld Pass Sequence and Size



Weld Pass Technique

- Stringer passes only. No weaving or wash passes.
- Weld stringer passes using sequence shown above. Start the first stringer pass in each layer against the face of the column.
- Slag each pass thoroughly.
- Each stringer pass to melt at least 1/3 of the preceding pass for good fusion between passes and to prevent valley between passes which are hard to clean.

PRE-QUALIFIED WELDING PROCEDURE SPECIFICATION

OVERHEAD REINFORCING FILLET WELD FOR BACKGROUGED CJP GROOVE WELD

WPS # EBF5-3

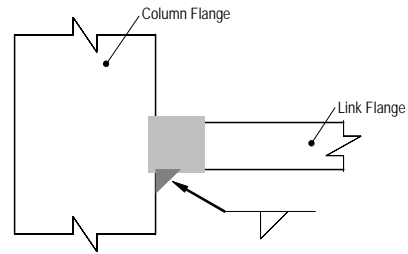
Material Specification: ASTM A36, A572-Gr. 50, A992
 Welding Process: Flux Cored Arc Welding – Self Shielded
 Position of Welding: 4F
 Filler Metal: AWS Specification: 5.20
 AWS Classification: E71T-8
 Brand Designation: Lincoln NR-232
 Diameter: 0.072"
 Current: DC – Electrode Negative

Minimum Preheat and Interpass Temperature:

Thickness	Temperature (deg F)
Up to 3/4"	50
Over 3/4" to 1-1/2"	50
Over 1-1/2" to 2-1/2"	150
Over 2-1/2"	225

Maximum Interpass Temperature: 550° F

Joint Detail:



Welding Procedure

Pass No.	Electrode Diameter	Wire Feed Speed (in / min)	Volts	Approx. Current (amps)	Travel Speed (in / min)
All as Req'd	0.072"	155 - 170	19 - 23	240 - 275	8 - 12

Distance from contact tube to work = 0.5 to 1"

PRE-QUALIFIED WELDING PROCEDURE SPECIFICATION

OVERHEAD FILLET WELD FOR WELDING BACKING BAR TO COLUMN FLANGE

WPS # EBF5-4

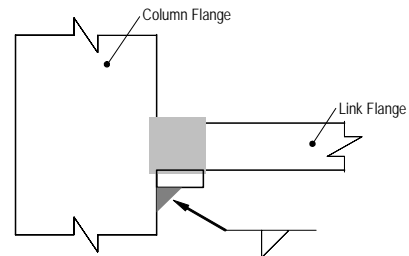
Material Specification: ASTM A36, A572-Gr. 50, A992
 Welding Process: Flux Cored Arc Welding – Self Shielded
 Position of Welding: 4F
 Filler Metal: AWS Specification: 5.20
 AWS Classification: E71T-8
 Brand Designation: Lincoln NR-232
 Diameter: 0.072"
 Current: DC – Electrode Negative

Minimum Preheat and Interpass Temperature:

Thickness	Temperature (deg F)
Up to 3/4"	50
Over 3/4" to 1-1/2"	50
Over 1-1/2" to 2-1/2"	150
Over 2-1/2"	225

Maximum Interpass Temperature: 550° F

Joint Detail:



Welding Procedure

Pass No.	Electrode Diameter	Wire Feed Speed (in / min)	Volts	Approx. Current (amps)	Travel Speed (in / min)
All as Req'd	0.072"	155 - 170	19 - 23	240 - 255	8 - 12
Distance from contact tube to work = 0.5 to 1"					

PRE-QUALIFIED WELDING PROCEDURE SPECIFICATION

COMPLETE JOINT PENETRATION SINGLE BEVEL GROOVE WELD:
VERTICAL POSITION WELD BETWEEN LINK WEB AND COLUMN FLANGE
AND VERTICAL POSITION WELDS FOR SECONDARY STIFFENERS

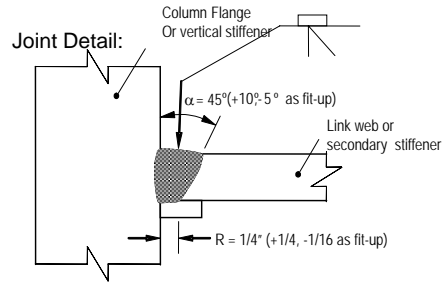
WPS # EBF5-5

Material Specification: ASTM A36, A572-Gr. 50, A992
 Welding Process: Flux Cored Arc Welding – Self Shielded
 Position of Welding: 3G
 Filler Metal: AWS Specification: 5.20
 AWS Classification: E71T-8
 Brand Designation: Lincoln NR-232
 Diameter: 0.072"
 Current: DC - Electrode Negative

Minimum Preheat and Interpass Temperature:

Thickness	Temperature (deg F)
Up to 3/4"	50
Over 3/4" to 1-1/2"	50
Over 1-1/2" to 2-1/2"	150
Over 2-1/2"	225

Maximum Interpass Temperature: 550° F



Welding Procedure

Pass No.	Electrode Diameter	Wire Feed Speed (in / min)	Volts	Approx. Current (amps)	Travel Speed (in / min)
All as Req'd	0.072"	155 - 170	19 - 23	240 - 255	8 - 12
Distance from contact tube to work = 0.5 to 1"					

Specimens AISC-6 & AISC-7 – Welding/Fabrication Sequence and Welding Procedures

1. Weld vertical stiffeners to link (fillet welds).
For each stiffener – weld stiffener to link flanges first, then weld stiffener to link web.
Use gas-shielded FCAW with E70T-9 electrode (Lincoln OS-70 or OS-70H; 3/32”). Orient link so that welds are made in a flat position.
Use Schuff Steel Co. WPS No. F 105-70T-9.
No preheat required.

2. Weld link to 2" thick end plate.
Use gas-shielded FCAW with E70T-9 electrode (Lincoln OS-70 or OS-70H; 3/32”). Orient link so that welds are made in a flat position.
 - a. Make partial penetration groove welds between link flange and end plate.
Provide weld tabs at each end of groove weld. Preheat end plate to at least 150⁰ F. Use WPS EBF 6-1.
 - b. Make fillet welds between inside faces of link flanges and end plate, and between link web and end plate.
Use Schuff Steel Co. WPS No. F 105-70T-9.
Preheat end plate to at least 150⁰ F.
For fillet welds at inside face of link flange, run welds over the weld tabs.
Leave weld tabs in-place at completion of welding.

3. Weld shear tab to column flange.
Use self-shielded FCAW with E71T-8 electrode (Lincoln 0.072" NR-232).
Orient column so that welds are made in a flat position.
Use WPS No. EBF6-2.

4. Bolt link web to shear tab. Fully tension bolts using turn-of-nut method.

5. Place specimen in upright position (i.e. same position as it would be in the field). Make all remaining welds with specimen in this position.
6. Weld link flanges to column flange. Use self-shielded FCAW with E70T-6 electrode (Lincoln 3/32" NR-305). No preheat is required. Make welds as follows:
 - a. Tack weld 3/8" x 1" backing bars to link flange and to column flange. Length of backing bars should be adequate so that they extend approximately 2-inches beyond end of link flange. Tack welds should be located so that they will be incorporated inside the groove weld.
 - b. Attach weld tabs. Weld tabs should extend groove approximately 2-inches beyond edge of link flange. Tack welds should be located so that they will be incorporated inside the groove weld.
 - c. Make groove weld between link top flange and column flange using WPS # EBF6-3. Each weld bead should start on a weld tab and end on the opposite weld tab.
 - d. Make groove weld between link bottom flange and outside face of column flange using WPS # EBF6-3. Welding at the bottom flange should be in accordance with the following:
 - i. Weld one bead on one side of the bottom flange, starting at the weld access hole. After arc is initiated, travel should progress toward the edge of the flange. The bead should be terminated on the weld tab. The start of the bead in the weld access hole should be visually inspected to ensure fusion, soundness, freedom from slag inclusions, and excess porosity. The resulting bead profile should be suitable for obtaining good fusion by the subsequent pass to be initiated on the opposite side of the beam web. If the

profile is not conducive to good fusion, the start of the weld bead should be gouged, chipped, or otherwise prepared to ensure good fusion.

- ii. Weld one bead on the other side of the bottom flange. Follow same instructions as in (i) above.
 - iii. Continue placing beads on alternate sides of the link web in accordance with (i) and (ii) above until weld is completed.
7. Using carbon air arc gouge, remove the backing bar at the beam bottom flange groove weld and backgouge root of CJP groove weld to sound metal. Care should be taken so as not to damage the base metal when removing the backing bar and during backgouging. Any pits, gouges, discontinuities and slag pockets discovered at the root of the groove weld should be ground out. Reweld root of CJP groove weld from underneath the weld and place a 5/16" fillet weld using WPS # EBF6-4. (Lincoln 0.072" NR-232 electrode).
8. Place a 5/16" fillet weld between the backing bar and the column flange at the top beam flange groove weld using WPS # EBF6-5. (Lincoln 0.072" NR-232 electrode). No preheat is required.
9. Using carbon air arc gouge, remove weld tabs from both the top and bottom beam flange groove welds. Grind smooth and inspect ground surfaces for discontinuities. Inclusions 1/16" or less in depth shall be removed by grinding. Deeper indications should be removed and replaced by welding.
10. Make groove weld between link web and column flange (shear tab serves as backing). Use self-shielded FCAW with E71T-8 electrode (Lincoln 0.072" NR-232). Weld should extend full depth of the link web, from access hole to access hole.
Use WPS # EBF6-6. No preheat is required.

11A Weld secondary stiffeners to column flange and to vertical stiffener. For each of the four stiffeners, use the following procedure:

- a. Tack weld 3/8" x 1" backing bars to face of column flange and to vertical stiffener. Length of backing bars should be adequate so that they extend approximately 1/2-inches beyond ends of the secondary stiffener. Tack welds should be located so that they will be incorporated inside the groove weld.
- b. Do not use weld tabs.
- c. Weld the secondary stiffener to the column flange. Use self-shielded FCAW with E71T-8 electrode (Lincoln 0.072" NR-232). Use WPS #EBF6-6. No preheat is required.
- d. Weld the secondary stiffener to the vertical stiffener. Use self-shielded FCAW with E71T-8 electrode (Lincoln 0.072" NR-232). Use WPS #6-6. No preheat is required.

11B Weld secondary stiffeners to column flange and to vertical stiffener. For each of the two stiffeners, use the following procedure:

- a. Place secondary stiffeners in the correct position.
- b. Tack secondary stiffeners to face of column flange and to vertical stiffener. Tack welds should be located so that they will be incorporated inside the groove weld.
- c. Weld the secondary stiffener to the column flange. Use self-shielded FCAW with E71T-8 electrode (Lincoln 0.072" NR-232). No preheat is required.

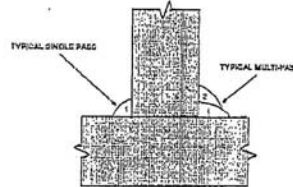
- d. Weld the secondary stiffener to the vertical stiffener. Use self-shielded FCAW with E71T-8 electrode (Lincoln 0.072" NR-232). No preheat is required.



SCHUFF STEEL CO.
Welding Procedure Specification

WPS No. F 105-70 T9 Revision 0 Date 7/11/2002 By JIM MURRAY
 Authorized By JIM MURRAY Date 7/11/2002 Prequalified
 Welding Process(es) FCAW Type: Manual Machine Semi-Auto Auto
 Supporting PQR(s) _____

JOINT
 Type FILLET WELD
 Backing Yes No Single Weld Double Weld
 Backing Material NA
 Root Opening NA Root Face Dimension NA
 Groove Angle NA Radius (J-U) NA
 Back Gouge Yes No
 Method NA



BASE METALS
 Material Spec. SEE NOTES to SEE NOTES
 Type or Grade _____ to _____
 Thickness: Groove () _____ - _____
 Fillet (in) 1/8 - Unlimited
 Diameter (Pipe,) _____ - _____

POSITION
 Position of Groove _____ Fillet 1F, 2F
 Vertical Progression: Up Down

FILLER METALS
 AWS Specification A5.20
 AWS Classification E70T-9 LINC.(OS 70)

ELECTRICAL CHARACTERISTICS
 Transfer Mode (GMAW):
 Short-Circuiting Globular Spray
 Current: AC DCEP DCEN Pulsed
 Other CONSTANT VOLTAGE
 Tungsten Electrode (GTAW):
 Size NA Type NA

SHIELDING
 Flux Gas CO-2
 NA Composition 100%
 Electrode-Flux (Class) Flow Rate 45 CFH
 NA Gas Cup Size 1/2"

TECHNIQUE
 Stringer or Weave Bead Stringer*
 Multi-pass or Single Pass (per side) Either*
 Number of Electrodes 1
 Electrode Spacing: Longitudinal NA
 Lateral NA
 Angle NA
 Contact Tube to Work Distance 1 1/8"
 Peening NONE
 Interpass Cleaning HAND TOOL

PREHEAT
 Preheat Temp., Min. NONE ****
 Thickness Up to 3/4" Temperature NONE ****
 Over 3/4" to 1-1/2" 50°
 Over 1-1/2" to 2-1/2" 150°
 Over 2-1/2" 225°
 Interpass Temp., Min. NONE **** Max. NONE

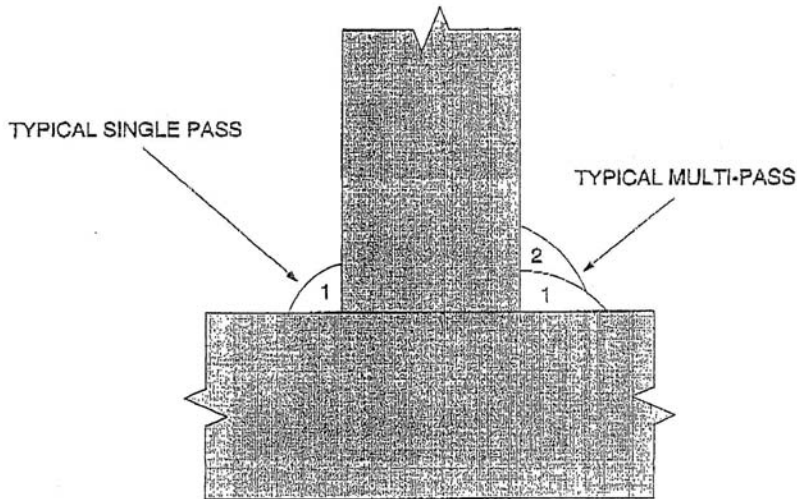
POSTWELD HEAT TREATMENT PWHT Required
 Temp. NA Time NA

WELDING PROCEDURE

Layer/Pass	Process	Filler Metal Class	Diameter	Cup Type	Amps or WFS	Volts	Travel Speed	Other Notes
ALL	FCAW	E70T-9(O.S.70)	3/32	DCEP	455/200ipm	30	20 IPM	NOTE**



SCHUFF STEEL CO.
Welding Procedure Specification



MEMO

NOTES:

*AWS D1.1; TABLE 3.7:
IN FLAT, HORIZONTAL SPLIT LAYERS WHEN THE LAYER WIDTH > 5/8". MAX BEAD THK=1/4"

MAXIMUM SINGLE PASS FILLET WELD SIZE: FLAT= 1/2"; HORIZONTAL= 3/8".

**AWS D1.1; TABLE 4.5:

ALLOWABLE RANGE VARIANCES:

VOLTS: ± 7%

AMPS: ± 10%

WIRE FEED SPEED: ± 10%

TRAVEL SPEED: ± 25%

APPLICABLE MATERIAL FOR THIS PROCEDURE:

A36; A572 GR-50; A992; A913 GR-50; A500 GR-B; A53, TYPE E or S, GR-B.

***AWS D1.1 TABLE 3.2 NOTE 1:

1. When the base metal temperature is below 32°F (0°C), the base metal shall be preheated to at least 70°F (21°C) and this minimum temperature maintained during welding.

PRE-QUALIFIED WELDING PROCEDURE SPECIFICATION

Partial Joint Penetration Single Bevel Groove Weld
Flat Position Weld between Link Flange and End Plate

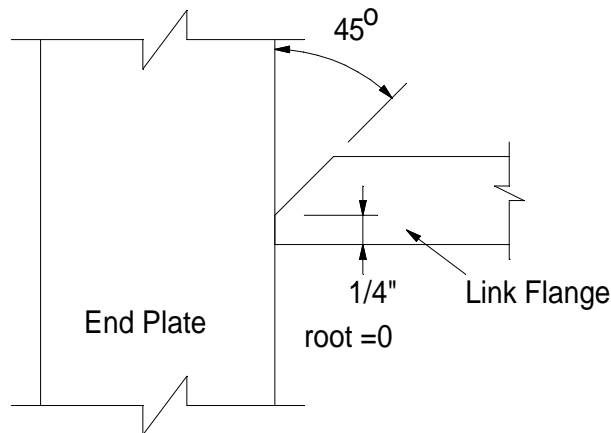
WPS # EBF6-1

Material Specification: ASTM A36, A572 Gr. 50, A992
Welding Position: Flat Position 1G
Welding Process: Flux Cored Arc Welding – Gas Sheilded
Filler Metal: AWS Specification A5.20
AWS Classification: E70T-9
Brand Designation: Lincoln OS 70H
Diameter: 3/32"

Current: DC – Electrode Positive

Minimum Preheat Temperature: 150 deg F

Joint Detail



Shielding: Gas 100% CO₂ - Flow rate: 45 CFH

Welding Procedure: All Passes
Electrical Stickout: 1-1/8"
Current Type: DC Electrode +
Volts: 28 – 31
Wire feed Speed: 200 inches/minute
Approx. Current: 455 amps
Travel Speed: 20 inches/minute

PRE-QUALIFIED WELDING PROCEDURE SPECIFICATION

COMPLETE JOINT PENETRATION SINGLE BEVEL GROOVE WELD FLAT POSITION WELD BETWEEN LINK FLANGE AND COLUMN FLANGE

WPS # EBF6-3

Material Specification: ASTM A36, A572-Gr. 50, A992
 Welding Process: Flux Cored Arc Welding – Self Shielded
 Position of Welding: 1G
 Filler Metal: AWS Specification: 5.20
 AWS Classification: E70T-6
 Brand Designation: Lincoln NR-305
 Diameter: 3/32"

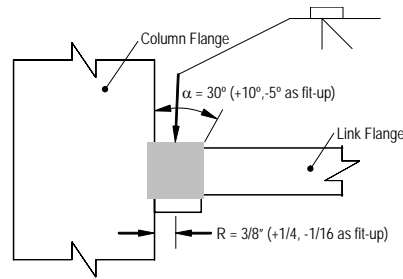
Current: DC – Electrode Positive Joint Detail:

Minimum Preheat and Interpass Temperature:

Thickness	Temperature (deg F)
Up to 3/4"	50
Over 3/4" to 1-1/2"	50
Over 1-1/2" to 2-1/2"	150
Over 2-1/2"	225

Maximum Interpass Temperature: 550° F

Joint Designation: TC-U4a-GF

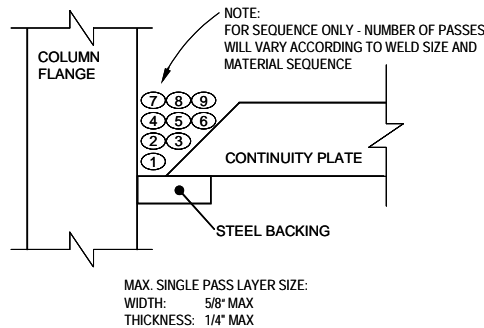


Welding Procedure

Pass No.	Electrode Diameter	Wire Feed Speed (in / min)	Volts	Approx. Current (amps)	Travel Speed (in / min)
All as Req'd	3/32"	240 - 300	25 - 29	390 - 475	9 - 15

Distance from contact tube to work = 1-1/2 to 2-1/2"

Weld Pass Sequence and Size



Weld Pass Technique

- Stringer passes only. No weaving or wash passes.
- Weld stringer passes using sequence shown above. Start the first stringer pass in each layer against the face of the column.
- Slag each pass thoroughly.
- Each stringer pass to melt at least 1/3 of the preceding pass for good fusion between passes and to prevent valley between passes which are hard to clean.

PRE-QUALIFIED WELDING PROCEDURE SPECIFICATION

OVERHEAD FILLET WELD FOR WELDING BACKING BAR TO COLUMN FLANGE

WPS # EBF6-5

Material Specification: ASTM A36, A572-Gr. 50, A992
 Welding Process: Flux Cored Arc Welding – Self Shielded
 Position of Welding: 4F
 Filler Metal: AWS Specification: 5.20
 AWS Classification: E71T-8
 Brand Designation: Lincoln NR-232
 Diameter: 0.072"

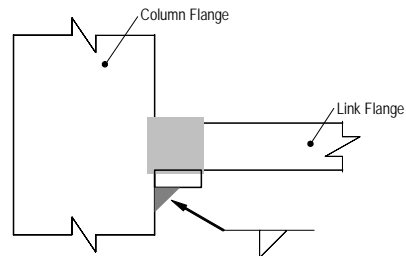
Current: DC – Electrode Negative

Joint Detail:

Minimum Preheat and Interpass Temperature:

Thickness	Temperature (deg F)
Up to 3/4"	50
Over 3/4" to 1-1/2"	50
Over 1-1/2" to 2-1/2"	150
Over 2-1/2"	225

Maximum Interpass Temperature: 550° F



Welding Procedure

Pass No.	Electrode Diameter	Wire Feed Speed (in / min)	Volts	Approx. Current (amps)	Travel Speed (in / min)
All as Req'd	0.072"	155 - 170	19 - 23	240 - 255	8 - 12
Distance from contact tube to work = 0.5 to 1"					

REFERENCES

- AISC (2005), "Manual of Steel Construction", Thirteenth Edition, American Institute of Steel Construction, Inc., Chicago.
- AISC (2005), "Seismic Provisions for Structural Steel Buildings", American Institute of Steel Construction, Inc., Chicago.
- Arce, Gabriela (2002), "Impact of higher strength steels on local buckling and overstrength of links in eccentrically braced frames", Master's Thesis, University of Texas at Austin, TX.
- Arce, G., Okazaki, T. and Engelhardt, M. D. (2003), "Experimental behavior of shear and flexural yielding links of ASTM A992 steel", Proceedings: STESSA 2003 – Behavior of Steel Structures in Seismic Areas – June 9-12, 2003, Naples, Italy.
- Choi, J.-H., Stojadinovic, B. and Goel, S. C. (2000), "Parametric tests on the free flange moment connections", Report No. SAC/BD-00/02, SAC Joint Venture, Sacramento, CA.
- Engelhardt, M. D. and Popov, E. P. (1989a), "Behavior of Long Links in Eccentrically Braced Frames", *Report No. UCB/EERC-89/01*, Earthquake Engineering Research Center, University of California at Berkeley, Richmond, CA.
- Engelhardt, M. D. and Popov, E. P. (1989b), "On Design of Eccentrically Braced Frames", *Earthquake Spectra*, Volume 5, No. 3, pp. 495-511.
- Engelhardt, M. D. and Popov, E. P. (1992), "Experimental performance of long links in eccentrically braced frames", *Journal of Structural Engineering*, ASCE, Vol. 118, No.11, pp. 3067-3088.
- Engelhardt, M. D. and Sabol, T. A. (1997), "Seismic-resistant Steel Moment Connections: Developments since the 1994 Northridge Earthquake", *Construct. Res. Comm. Ltd. ISSN 1365-0556*: 68-77.
- FEMA, 2000, Recommended Seismic Design Criteria for New Steel Moment-Frame Buildings, prepared by the SAC joint venture for the Federal Emergency Management Agency (FEMA), Washington, DC.
- Galvez, Pedro (2004), Investigation of Factors affecting Web Fractures in Shear Links", Master's Thesis, University of Texas at Austin, TX.

- Hjelmstad, K. D. and Popov, E. P. (1983), "Seismic Behavior of Active Beam Links in Eccentrically Braced Frames", Report No. UCB/EERC-83/24, Earthquake Engineering Research Center, University of California at Berkeley, CA.
- Hong, J.-K., and Uang, C.- M. (2005), "Analytical Studies on Link-to-Column Connections in EBFs", Unpublished Report, University of California at San Diego, October 4, 2005.
- Hong, J.-K., and Uang, C.- M. (2006), "Basis of Supplemental Stiffeners design for EBF Links", Unpublished Report, University of California at San Diego, May 25, 2006.
- Johnson, M. (2000), "State of the art report on welding and inspection", Report No. FEMA 355B, Federal Emergency Management Association, Washington, DC.
- Kasai, K. and Popov, E.P. (1986), "A study of seismically resistant eccentrically braced steel frame systems, *Report No. UCB/EERC-86/01*. Earthquake Engineering Research Center, University of California at Berkeley, Richmond, CA.
- Malley, J. O. and Popov, E. P. (1983), "Design considerations for shear links in eccentrically braced frames", Report No. UCB/EERC-83/24, Earthquake Engineering Research Center, University of California at Berkeley, Richmond, CA.
- Malley, J. O. and Popov, E. P. (1984), "Shear links in eccentrically braced frames", *Journal of the Structural Division, American Society of Civil Engineers*, Vol. 110, No. 9, pp. 2275-2295.
- Okazaki, Taichiro (2004), "Seismic performance of link-to-column connections in steel eccentrically braced frames", PhD Dissertation, University of Texas at Austin, TX.
- Okazaki, T. (2004p), "Preliminary Report – EBF link-to-column connection tests 1 and 2", Unpublished Report, University of Texas at Austin, November 22, 2004.
- Okazaki, T., Engelhardt, M. D., Nakashima, M., Suita, K. and Tsai, K. (2003), "Behavior of link-to-column connections in steel eccentrically braced frames", *Proceedings: STESSA 2003-Behavior of Steel Structures in Seismic Areas – June 9-12, 2003, Naples, Italy*.
- Okazaki, T., Engelhardt, M. D., Nakashima, M. and Suita, K. (2004), "Experimental study of link-to-column connections in steel eccentrically braced frames", *Proceedings – 13th World Conference on Earthquake Engineering – Vancouver, August 1-6, 2004*.

- Okazaki, T., Arce, G., Ryu, H. and Engelhardt, M. D. (2005), “ Experimental study of local buckling, overstrength and fracture of links in EBFs”, *Journal of Structural Engineering*, ASCE, Vol. 131, No. 10, pp. 1526-1535.
- Okazaki, T., Engelhardt, M. D., Nakashima, M., and Suita, K. (2006a), “Experimental performance of link-to-column connections in eccentrically braced frames”, *Journal of Structural Engineering*, ASCE, Vol. 132, No. 8, pp. 1201-1211.
- Okazaki, T., Schell, E. and Engelhardt, M. D. (2006b), “Experimental investigation of shop welded link-to-column connections in eccentrically braced frames”, *Proceedings: STESSA 2006*.
- Popov, E. P. and Engelhardt, M. D. (1988), “Seismic Eccentrically Braced Frames,” *Journal of Constructional Steel Research*, Vol. 10, pp. 321-354.
- Richards, P. and Uang, C. M. (2003), “Development of testing protocol for short links in eccentrically braced frames”, Report No. SSRP-2003/08, Department of Structural Engineering, University of California at San Diego, CA.
- Richards, P. and Uang, C. M. (2004), “Testing protocol for short links in eccentrically braced frames”, *Journal of Structural Engineering*, American Society of Civil Engineers.
- Suita, K., Tamura, T., Morita, S., Nakashima, M. and Engelhardt, M. D. (1999), “Plastic rotation capacity of steel beam-to-column connections using a reduced beam section and no weld access hole design – Full scale tests for improved steel beam-to-column subassemblages – Part 1-”, *Journal of Structural Construction Engineering*, Architectural Institute of Japan, 526, 177-184 (in Japanese).
- Tsai, K. C. and Popov E. P. (1988), “Steel beam-column joints in seismic moment resisting frames.”, Report No. UCB/EERC-88/19, Earthquake Engineering Research Center, University of California at Berkeley, CA.
- Tsai, K. C., Engelhardt, M. D. and Nakashima, M. (2000), “Cyclic performance of link-to-box column connections in steel eccentrically braced frames”, *The First International Conference on Structural Stability and Dynamics*, Taipei, Taiwan.
- Uang, C.- M., and Hong J.-K. (2007), “ABAQUS analysis of specimen AISC-7”, Unpublished Report, University of California at San Diego, March 14, 2007.

VITA

Apostolos Drolias was born in Athens, Greece on January 12th, 1983, the son of Ioannis Drolias and Theodora Drolia. After completing his work at Ziridis High School, Athens, Greece in 2000, he entered the University of Patras, in Patras, Greece. He received the degree of Diploma in Civil Engineering from the University of Patras in July, 2005. In August, 2005 he entered the Graduate School at the University of Texas at Austin.

Permanent Address: 108B Aspasia street, Cholongos
Athens, 15561, Greece

This thesis was typed by Apostolos Drolias